Investigation of Opuntia Ficus Indica (OFI) Corrosion Inhibiting Potential by Incorporating Fine Aggregate Scoria Gravel as an Enabler of Concrete Internal Curing

Israel Wakuma Habtemariam

A Thesis Submitted to Department of Civil Engineering School of Civil Engineering and Architecture

Presented in Partial Fulfilment of the Requirements of Masters of Science in Civil Engineering (Specialization in Construction Engineering and Management)

Office of Graduate Studies
Adama Science and Technology University

June 2023
Adama, Ethiopia

Investigation of Opuntia Ficus Indica (OFI) Corrosion Inhibiting Potential by Incorporating Fine Aggregate Scoria Gravel as an Enabler of Concrete Internal Curing

By

Israel Wakuma Habtemariam

Advisor: Fikreyesus Demeke (PhD)

Co-Advisor: Tadele Hunde (PhD

A thesis Submitted to Department of Civil Engineering School of Civil Engineering and Architecture

Office of Graduate Studies
Adama Science and Technology University

June 2023
Adama, Ethiopia

DECLARATION

I declare that this thesis/dissertation entitled "**Investigation of Opuntia Ficus Indica (OFI) Corrosion Inhibiting Potential by Incorporating Fine Aggregate Scoria Gravel as an Enabler of Concrete Internal Curing**" is my work and has not been submitted to any university for similar purposes. Proper citations duly recognize the references used in this thesis.

Israel Wakuma _____ _____

Signature Date

RECOMMENDATION OF ADVISOR

We, the advisors of this thesis, hereby certify that we have closely advised/ supervised the student while developing this thesis and read the draft thesis entitled "**Investigation of Opuntia Ficus Indica (OFI) Corrosion Inhibiting Potential by Incorporating Fine Aggregate Scoria Gravel as an Enabler of Concrete Internal Curing**" prepared under our guidance by Israel Wakuma. Therefore, we recommend the submission of the thesis.

Fikreyesus Demeke (PhD) _____ _____

(Major Advisor/Supervisor) Signature Date

Tadele Hunde (PhD) _____ _____

(Co-Advisor/Supervisor) Signature Date

APPROVAL PAGE OF ADVISOR

We hereby certify the recommendation and suggestion given by the thesis review committee are appropriately incorporated into the final thesis entitled “Investigation of Opuntia Ficus Indica (OFI) Corrosion Inhibiting Potential by Incorporating Fine Aggregate Scoria Gravel as an Enabler of Concrete Internal Curing” prepared under our guidance by Israel Wakuma.

Fikreyesus Demeke (PhD) _____ _____

(Major Advisor/Supervisor) Signature Date

Tadele Hunde (PhD) _____ _____

(Co-Advisor/Supervisor) Signature Date

APPROVAL OF BOARD REVIEWERS

We, the undersigned, members of the Board of Examiners of the thesis by Israel Wakuma, have read and evaluated the thesis entitled "**Investigation of Opuntia Ficus Indica (OFI) Corrosion Inhibiting Potential by Incorporating Fine Aggregate Scoria Gravel as an Enabler of Concrete Internal Curing**" and examined the candidate during the open defense. This is, therefore, to certify that the thesis is accepted for partial fulfillment of the requirement of the degree of Master of Science in Construction Engineering and Management.

Chairperson	Signature	Date
Internal Examiner	Signature	Date
External Examiner	Signature	Date

Finally, approval and acceptance of the thesis are contingent upon the submission of its final Copy to the Office of Postgraduate Studies (OPGS) through the Department of Graduate Council (DGC) and School Graduate Committee (SGC).

Department Head	Signature	Date
School Dean	Signature	Date
Office of Post Graduate Studies Dean	Signature	Date

ACKNOWLEDGMENT

I am deeply grateful to Almighty God for providing me with the opportunity, strength, knowledge, and perseverance to conduct my research successfully. I extend my heartfelt thanks to my supervisors, Fikreyesus Demeke (PhD) from the Department of Civil Engineering and Tadele Hunde (PhD) from the Department of Material Science Engineering at ASTU, for their unwavering support, motivation, guidance, and cooperation throughout my research journey. Working under their mentorship has been an invaluable and memorable experience, and I consider myself extremely fortunate to have had such caring and responsive mentors.

I would like to acknowledge ASTU for allowing me to pursue this research, and I sincerely appreciate all the Civil Engineering Department staff members for their continuous support. I am also grateful to the experts who participated in the study for their cooperation, valuable time, and insights into my research problem.

My heartfelt appreciation goes to my research group colleagues and friends, including Eyob Wendowsen, Imran Anwar, Liya Melaku, and others, for their valuable comments, technical discussions, and knowledge exchange throughout my research journey. Our collaboration and the enjoyable moments we shared have significantly contributed to my personal and academic growth.

Lastly, I dedicate this thesis to my parents, Wakuma Habtemariam and Sindu Weldemariam, who have devoted their lives to their children's education. Your unwavering support and emphasis on education have been pivotal to my achievements. You are my heroes and the source of my strength. I am grateful to my determined family, Rahel Wakuma and Natnael Wakuma, for their unconditional love, cooperation, and guidance in shaping my life. Without all of you, this study would not have been possible.

ABSTRACT

Corrosion is a natural process that causes the gradual deterioration of metals and alloys, poses significant challenges in Reinforced concretes. Despite ongoing efforts to develop effective corrosion mitigation methods, there is a demand for environmentally friendly solutions that are user-friendly and readily available. Opuntia ficus indica (OFI), a green corrosion inhibitor, has emerged as a promising option for preventing corrosion and addressing these needs. However, its effectiveness in the construction industry requires further investigation into passive film formation and inhibitory capacity without compromising the properties of concrete. This study aims to investigate the possible use of OFI as a corrosion inhibitor in concrete by incorporating fine aggregate scoria gravel, which facilitate extended hydration through the internal curing effect in concrete. The research seeks to evaluate OFI's ability to inhibit corrosion and its impact on enhancing the corrosion inhibition of the concrete system by supplying a portion of water in the concrete through the fine aggregate scoria gravel internal curing mechanism. To accomplish these goals, a range of experimental and analytical techniques were employed, such as X-ray Diffraction (XRD), Scanning Electron Microscopy (SEM), Fourier Transform Infrared Spectroscopy (FTIR), Electrochemical Impedance Spectroscopy (EIS), and Tafel plot analysis. The results demonstrate that a concrete mixture containing 30% OFI and 5% fine aggregate scoria gravel outperforms other combinations. This blend significantly reduces the corrosion current density from 2.195μA to 0.43μA and increases the polarization resistance from 58.83Ω to 89.1Ω compared to the control mix. It also enhances cement hydration products, evident in XRD peaks. Additionally, OFI promotes crystallization, observed in SEM images, resulting in fewer corrosion pits on the reinforcement surface as examined under an optical microscope. This research adds to the current knowledge by identifying the potential use of OFI in concrete with an internal curing material and examines the formation of oxide hydroxide passive film at the concrete-reinforcement interface. The findings of this study have broad implications, promoting green enviroment and offering natural solutions for corrosion prevention for Reinforced concretes.

Key words/terms: Opuntia ficus indica, Fine aggregate scoria gravel, Internal curing, Green corrosion inhibitor, Corrosion of reinforced concrete

TABLE OF CONTENT

LIST OF FIGURES

LIST OF TABLES

LIST OF ABBREVIATIONS

Abbrevations	Full Name
A	Ampere
C	Capacitance
CE	Counter electrode
CA	Coarse Aggregate
CE	Counter Electrode
Ecorr	Corrosion Potential
F	Frequency
FA	Fine Aggregate
FASG	Fine aggregate scoria gravel
HSD	Honestly Significant Difference
IE	Percentage Corrosion Inhibition Efficiency
J	Current density
LWA	Lightweight aggregate
mv	Mili volt
PH	Potential of Hydrogen
R	Resistance
RE	Reference Electrode
UWCA	Unit Weight of Coarse Aggregate
UWFA	Unit Weight of Fine Aggregate
ω	Angular Frequency
WE	Working Electrode
Z	Impedance

LIST OF ABBREVIATIONS/ ACRONYMS

Acronyms	Full Name
ACI	American Concrete Institute
A^o	Angaston
ANOVA	Analysis of variance
ASTM	American Society for Testing Materials
Asg	Apparent specific gravity
Bsg	Bulk specific gravity
Ecorr	Corrosion Potential
EIS	Electrochemical impedance spectroscopy
FM	Fineness Modulus
FTIR	Fourier Transform Infrared Spectroscopy
HSD	Honestly Significant Difference
ICDD	International Center of Diffraction Data
IE	Percentage Corrosion Inhibition Efficiency
Icorr	Corrosion Current Density
$I_o$sin	Sinusoidal Current
J	Current density
MP	Mega Pascal
OFI	Opuntia-Ficus-Indica
OPC	Ordinary Portland Cement
RC	Reinforced concrete
RP	Polarization Resistance
SEM	Scanning Electron Microscope
SSD	Saturated Surface Dry
TGA	Thermo-Gravimetric Analysis
$V_o$sin	Sinusoidal Voltage
W	Warburg Impedance
XRD	X-Ray Diffraction
βa	Anodic Tafel Coefficient
βc	Cathodic Tafel Coefficient

LIST OF CHEMICAL FORMULAS

Formulas	Name of Chemical Compound	Formulas	Name of Chemical Compound
Fe	Iron	γ-Fe_2O_3	Maghamite
H_2O	Water	α-Fe_2O_3	Hematite
O_2	Oxygen	ROOH	Polysaccharide chain and phenols radical group
OH	Hydroxide		
CO_2	Carbon dioxide	$C_5H_{10}O_5$	Arabinose
FeO	Iron Oxide	H_2N-CH-COOH	Amino acetic acid (Glycine)
SiO_2	Silicon oxide		
Al_2O_3	Aluminum Oxide	$CaCO_3$	Calcium carbonate
CaO	Calcium oxide	C-S-H-A	Friedel's compound (calcium sulfoaluminate hydrate)
MgO	Magnesium oxide		
Na_2O	Sodium dioxide		
K_2O	Potassium oxide	3CaO·Al2O3	Tricalcium aluminate
MnO	Manganese Oxide	CaSO4	Calcium sulfate ettringite
P_2O_5	Diphosphorus	(Ca6(Al	Calcium aluminum
TiO_2	Pentoxide	(OH)6)2(SO4)3·26H2O	Hydroxide sulfate hexadecahydrate
Fe $(OH)_2$	Iron Hydroxide		
Fe_2O_3	Ferric oxide	(C18H33FeO21)	Octadecahydroxy iron (III) carboxylate
Fe_3O_4	Black magnetite		
Fe^{2+}	Ferrous ions	C-S-H	Calcium silicate hydrates
H_2CO_3	Carbonic acid		
$CaSO_4.2H_2O$	Gypsum		
Fe_2O_4	Iron (III) oxide		
Fe $(OH)_3$	Iron (III) hydroxide		
Fe $(OH)_3.3H_2O$	Iron (III) hydroxide trihydrate		

CHAPTER ONE

INTRODUCTION

1.1 Background Of The Study

Concrete is a versatile and widely used construction material known for its strength and durability (Dey et al. 2021). It is comprised of a mixture of cement, aggregates, water, and other additives. Cement is the binding agent that holds the aggregates together, forming a solid and robust material when cured (Gagg 2014). The brittle nature of cement paste and the weak bond between cement paste and aggregates make it susceptible to cracking and failure when subjected to tensile forces (Van Damme 2018; Gagg 2014; Wilby 2013). Concrete structures require reinforcement with steel bars to withstand high tension loads.

Incorporating steel bars into concrete improves the bond between the steel reinforcement and concrete matrix and enhances the overall durability of the structure (Hossain et al. 2013). This reinforcement is crucial because concrete exhibits low tensile strength (Rodrigues et al. 2021). By leveraging the strength and ductility of steel, reinforcing concrete with steel bars minimizes its vulnerability to tension-induced failure (Poursaee, 2016). Reinforcement in concrete structures enhances their load-bearing capacity and overall performance, ensuring long-term durability (Hua et al. 2022). Consequently, reinforced concrete is extensively utilized in various infrastructure projects, including buildings, bridges, and dams (Abd Elrehim et al. 2019).

Since the establishment of ASTM specifications for steel usage in concrete construction in 1911 (Daniyal and Akhtar 2020), reinforced concrete has become one of the most prevalent construction materials globally (Van Damme 2018). However, various environmental factors have caused steel rebars to corrode and render reinforced concrete incapable of sustaining strength to the expected level (Goyal et al. 2018; Singh and Venugopalan 2013). Among all durability-related problems in steel-reinforced concrete structures, the corrosion of steel reinforcement has been recognized as the primary source of deterioration (Poursaee 2016; Zheng et al. 2012).

Corrosion is a natural process that typically begins when corrosion agents such as chloride ions or carbon dioxide from the surrounding environment penetrate the concrete cover and reach the steel surface (Goyal et al. 2018). Various factors, including exposure to marine environments, de-icing salts, high humidity, and acidic substances causes corrosion (Söylev and Richardson 2008). Corrosion of steel reinforcements is a significant and costly deterioration mechanism for reinforced concrete structures, primarily through depassivation

(Goyal et al. 2018). When steel bars corrode, they undergo expansion, resulting in the development of hoop stress. This stress, in turn, leads to spalling, cracking, and a loss of structural integrity as the corroded steel occupies a larger volume (Anitha et al. 2019). In 2014, NACE International initiated a study called "International Measures of Prevention, Application, and Economics of Corrosion Technologies (IMPACT)," which estimated that the global cost of corrosion is $2.5 trillion per year, representing approximately 3.4% of the global GDP in 2013 (Koch 2017). Globally, Corrosion costs account for approximately 3% of the world's Gross Domestic Product (GDP), equivalent to $2.2 trillion (Aslam et al. 2022). Hence, the corrosion of steel reinforcement poses a significant concern from both safety and economic standpoints, as it directly impacts the sustainability of steel-reinforced concrete structures.

For reinforced concrete structures, the cost of Corrosion can be immense. Fortunately, significant progress has been made in developing methods for corrosion protection, such as cathodic protection, corrosion inhibitors, coatings, and corrosion-resistant bars (Goyal et al. 2018; Ma et al. 2022). However, these methods are often Costly and complex to implement. They require specialized skills for installation and maintenance, and in some cases, inhibition capacity is not always reliable over time (Goyal et al. 2018a; Poursaee 2016). As an alternative, natural organic compounds, such as seeds, plants, leaf extracts, and organic compounds, offer a cost-effective, harmless, and environmentally friendly solution (Rani and Basu 2012). In light of this, further research is being conducted to determine whether natural organic compounds can enhance steel corrosion resistance.

Different approaches, such as internal curing, modified mix designs, and higher concrete grades, have been proposed to increase the inhibition capacity of concrete (Venkatesh et al. 2019). Recent research has found that Opuntia ficus indica (OFI), a natural plant growing in arid and semi-arid regions, is an effective corrosion inhibitor (Martinez-Molina et al. 2015; Torres-Acosta and Alejandra Díaz-Cruz 2020). Previous studies (Belviranlı et al. 2019; Martinez-M et al. 2016) have confirmed that its chemical composition of phenolic compounds, polysaccharides, proteins, and amino acids can chelate metal ions and form a protective layer on concrete surfaces. OFI is an environmentally friendly and cost-effective option for inhibiting corrosion, preventing concrete degradation, and extending the service life of concrete (Torres-Acosta and Alejandra Díaz-Cruz 2020). However, Further research is needed to comprehend carbon steel's surface oxide/hydroxide formation with OFI mucilage (Martinez-Molina et al. 2016) and enhance its inhibitory capacity. Replacing part of the water in the concrete with OFI has shown to be effective in corrosion inhibition for concretes, but challenges persist in

removing water and affecting concrete's physical properties as the percentage of OFI increases (Martinez-Molina et al. 2016; Torres-Acosta and Alejandra Díaz-Cruz 2020).

Using internal curing in concrete increases the corrosion resistance of the structure by reducing its permeability and decreasing the amount of water and oxygen that can reach the reinforcing steel (Bentz and Weiss 2011). As a result, the likelihood of corrosion is reduced, thereby extending the lifespan of the concrete structure. Unfortunately, this method often involves using expensive internal curing materials such as (Superabsorbent polymers, expanded shale, and expanded clay) in construction, raising financial concerns for the industry. Studies have shown that fine aggregate scoria gravel can be a viable alternative for lightweight internal curing materials (Alaskar et al. 2021). Considering these findings, the present study delves into the exploration of combining Opuntia ficus indica (OFI) as a natural corrosion inhibitor with incorporating fine aggregate scoria gravel internal curing effect on concrete. This study aims to enhance the performance of OFI as a corrosion inhibitor, addressing the challenges related to inhibition effectiveness in concrete.

1.2 Statement of the Problem

Without Corrosion, Concrete structures would maintain their strength and structural integrity for extended periods, decreasing the necessity for repairs, reconstruction, or replacement (Apostolopoulos and Koutsoukos 2008). Corrosion, however, is an inevitable a natural process that can only be slowed down, not entirely halted, causing the gradual deterioration of concrete structures, as noted by Hansson (2016). The corrosion of steel reinforcements has been identified as a critical and expensive deterioration factor in reinforced concrete structures in research conducted by Broomfield (2003) and Poursaee (2016). Despite the development of various methods such as cathodic protection, corrosion inhibitors, coatings, and corrosion-resistant bars, challenges persist regarding costs, implementation, and expertise within the construction industry (Daniyal and Akhtar 2020; Goyal et al. 2018). Therefore, the construction sector requires corrosion inhibitors that are environmentally friendly, more user-friendly, and easily accessible solutions (Hossain et al. 2021). Due to this reason, Numerous studies have been conducted to explore natural corrosion inhibitors and found promising findings.

Opuntia ficus-indica (OFI) has emerged as a promising candidate since it has garnered attention due to its abundance worldwide (Reda and Atsbha 2019; Torres-Acosta 2007) and its potential as an effective corrosion inhibitor. Studies have shown encouraging results regarding the inhibitory properties of OFI, making it a viable alternative for corrosion inhibition (Martinez-

Molina et al. 2015). However, further studies are necessary to understand carbon steel's surface oxide/hydroxide formation in contact with OFI mucilage (Martinez-Molina et al. 2016). Moreover, the inhibitory capacity of OFI needs to be enhanced to maximize its effectiveness in corrosion inhibition. Based on the findings of the study (Martinez-Molina et al. 2016; Torres-Acosta and Alejandra Díaz-Cruz 2020), it was concluded that replacing a portion of water in the concrete water with OFI proved to be the most effective solution for its implementation. However, challenges remain in removing water, affecting concrete's physical characteristics when the percentage of OFI increases. Replacement in water increased, as observed in previous studies (Torres-Acosta and Alejandra Díaz-Cruz 2020). To overcome this issue and explore the potential of internal curing materials in concrete, this study aims to utilize lightweight scoria gravel as an internal curing material.

Although internal curings in concrete offers benefits, such as improved corrosion resistance and reduced water and oxygen ingress to reinforcing steel, commercially available internal curing agents/materials pose challenges in terms of cost (Rahman et al. 2018), limited availability (Liu et al. 2022), limited guidance, or regulations surrounding the use of internal curing materials (Bentz and Weiss 2011; Concrete Pavement Technology Center 2017), compatibility with other materials for the construction industry (Saravanan et al. 2021) Hence, the quest for natural internal curing alternatives is crucial. Recent studies have shown that scoria gravel, a naturally available aggregate, can be a lightweight internal curing aggregate. These factors motivate the present study to investigate the combination of Opuntia ficus indica (OFI) as a natural corrosion inhibitor and fine aggregate scoria gravel as an internal curing enabler for concrete.

1.3 Aim And Objectives of the Study

1.3.1 General Objective

The aim of this study is to investigate the potential use of Opuntia Ficus Indica (OFI) as a corrosion inhibitor by incorporating fine aggregate scoria gravel for the internal curing effect of concrete.

1.3.2 Specific Objectives

1. To investigate the replacement ratio of scoria gravel for sand in concrete mixes to achieve the desired compressive strength of concrete with an effective internal curing effect at optimal curing time.

2. To investigate the effect of partial replacement of water with opuntia ficus-indica (OFI) on concrete's ability to resist corrosion.
3. To study concrete's physical durability and surface oxide/hydroxide formation on carbon steel when it comes into contact with OFI mucilage.

1.4 Significance of the Study

This research is significant in its critical contribution to addressing solutions for steel reinforcement corrosion in concrete structures. Although various corrosion protection methods have been developed, they often encounter challenges, such as high cost, complexity of implementation, and unreliable long-term performance. Hence, exploring alternative solutions using natural organic compounds is a compelling opportunity, offering cost-effectiveness, environmental friendliness, and harmlessness.

Using Opuntia ficus-indica (OFI) as a corrosion inhibitor in concrete holds promise for extending the service life of the structure. Its chemical composition enables the chelation of metal ions, forming a protective layer on concrete surfaces. In addition, internal curing, which enhances the corrosion resistance of concrete, can be expensive. Therefore, alternative materials, such as scoria gravel, which is lightweight and cost-effective, are being investigated to reduce permeability and minimize steel exposure to water and oxygen.

By harnessing the abundance of these materials, the construction industry can benefit from a cost-effective concrete corrosion inhibitor. Furthermore, implementing this corrosion inhibition technique, which involves a mix of design and procedures similar to the standard control mix, eliminates the need for expertise and maintenance personnel after the structure is built. The use of natural materials also makes this corrosion inhibition technique environmentally friendly.

As a valuable addition to the body of knowledge in the field, this study contributes to the understanding of the effectiveness of Opuntia ficus-indica when combined with the internal curing effect of concrete. Additionally, surface oxide/hydroxide formation on carbon steel in contact with OFI mucilage was investigated using techniques such as electrochemical impedance spectroscopy, X-ray Diffraction (XRD), Scanning Electron Microscopy (SEM), Fourier Transform Infrared Spectroscopy (FTIR), and Thermogravimetric Analysis (TGA). Provides valuable insights. This study serves as a reference for future research in this area.

1.5 Scope of the Study

This study aimed to investigate the effectiveness of Opuntia ficus indica (OFI) as a corrosion inhibitor in C-25 reinforced concrete by utilizing the internal curing effect of fine aggregate scoria gravel. This study focused on measuring the variation in compressive strength at different percentages of scoria gravel to identify its internal curing effect. The study also aimed to assess the efficiency of the OFI in inhibiting corrosion by comparing it to a control mix. An artificial aggressive corrosion environment was created in the laboratory to simulate real-life corrosion conditions within a limited timeframe.

This research primarily focused on analyzing the formation of surface oxide/hydroxide on carbon steel in contact with OFI mucilage. Techniques such as Electrochemical Impedance Spectroscopy (EIS) and Tafel tests were used to gain a deeper understanding of the corrosion inhibition mechanisms of the passive film layer.

Various techniques were used to evaluate the corrosion inhibition efficiency, including X-ray Diffraction (XRD), Scanning Electron Microscopy (SEM), and Fourier Transform Infrared Spectroscopy (FTIR). Furthermore, this study assessed the, including fresh workability, compressive strength, and total void percentage.

1.6 Organization of the Study

This thesis has five chapters, each devoted to a specific purpose. The details of each chapter are as follows.

Chapter One introduces the study, presenting its background, motivation, problem statement, research objectives, scope, and significance. This sets the foundation for the entire study and establishes the context and importance of the research topic.

Chapter Two focuses on the literature review, in which an in-depth exploration of the relevant literature is conducted. It covers topics such as the general concept of corrosion, mechanisms of corrosion in concrete, current challenges in corrosion, and previous studies on natural corrosion inhibitors, including opuntia ficus indica. Furthermore, the chapter discusses the concept of the internal curing mechanism, its functionality, and the diverse approaches employed in utilizing internal curing materials. It also includes a review of previous studies on fine aggregate scoria gravel for implementing the internal curing mechanism. Finally, the chapter pinpoints the existing research gap in accordance with the study objectives.

Chapter Three discusses the research methodology employed in this study. It outlines the overall research methodology and elaborates on the methodologies adopted to achieve each objective. This chapter also presents the material characterization results following relevant standards.

Chapter Four presents' findings and discussions surrounding the efficient utilization of fine aggregate scoria gravel as an internal curing agent and opuntia ficus-indica (OFI) corrosion inhibition capabilities in examined C-25 concrete. The results are compared against a control mixture while exploring the ideal substitution ratio of fine aggregate scoria gravel to sand to attain maximum internal curing effectiveness for examined concrete. Furthermore, the chapter delves into determining the suitable percentage of OFI that can replace the water in concrete mixtures, subsequently improving their corrosion resistance. Additionally, based on the research methodology in chapter three, an analysis of the tested concrete's physical durability and the formation of surface oxides/hydroxides on carbon steel in contact with OFI mucilage is provided.

Chapter Five summarizes the methodology and findings presented in the preceding chapters. The study concludes by highlighting the contributions made to the existing literature, addressing the limitations of the research, and providing suggestions for further research.

1.7 Summary

This chapter introduces the research and presents the background and statement of the problem. The motivation for this research is discussed, highlighting the key issues that need to be addressed. The aim, objectives, scope, and significance of the research are briefly outlined, demonstrating the purpose and relevance of the study. Furthermore, the organization of the thesis is described, explaining how each chapter contributes to achieving the research objectives. The following chapter presents a comprehensive literature review, examines the existing research, and identifies gaps in prior studies.

CHAPTER TWO
LITERATURE REVIEW

2.1 Introduction

This chapter explores reinforcement corrosion and emphasizes its causes, contributing factors, and consequences. Furthermore, it examines methods to prevent corrosion in reinforced concrete and method of analysis of concrete corrosion, including the Techniques for Simulating and accelerating corrosion in laboratory conditions. The purpose of this chapter is to provide an overview of recent research papers dealing with concrete corrosion prevention mechanisms and the challenges encountered in the development of prevention methods studies, as well as to identify gaps related to the topics of this study.

2.1.1 Background Of Reinforced Concrete

Reinforced concrete (RC), a composite material that combines the strength of concrete with the tensile properties of steel, has a rich history dating back to the 19th century. In 1867, a French gardener, Joseph Monier, made an unexpected discovery when he noticed that his flowerpots had become significantly more resilient after iron nails were embedded into the castings (Singh and Venugopalan 2013). This led to a series of advances in concrete technology and the formulation of the American Society for Testing and Materials (ASTM) steel bar specifications in 1910. They released detailed specifications for the following year for steel bars used in concrete (Daniyal and Akhtar 2020b). Subsequent advancements in incorporating reinforcement into concrete have successfully produced reinforced concrete (RC).

2.1.2 Composition Of Reinforced Concrete

Reinforced concrete (RC) is a composite material that combines concrete and steel properties to resist various loading types (Luca Bertolin 2011). Concrete has high compressive strength but low tensile strength, whereas steel has high tensile strength but low compressive strength (Rodrigues et al. 2021). These two materials can withstand tensile, shear, and compressive stresses in a concrete structure by embedding steel bars, rods, or mesh. RC is widely used in civil engineering and construction projects because of its durability, versatility, and cost-effectiveness.

A reinforced concrete structure consists of concrete, aggregates, water, and steel. Cement is a binding agent that hardens and holds the concrete together (Gagg 2014). Aggregates provide bulk and strength to concrete, such as sand, gravel, or crushed stone. Water is essential for the chemical reaction of cement hydration and for the workability of fresh concrete to occur.

Reinforcing steel can be in the form of bars, wires (reinforcing bars), or short fibers (steel fibers) that are uniformly distributed throughout a concrete matrix.

The strength, durability, and ability to withstand various environmental conditions make reinforced concrete an extremely versatile material that can be applied to various construction projects (Dey et al. 2021). Reinforced concrete structures, however, are challenged by corrosion. Corrosion occurs when metal deteriorates due to chemical reactions with the environment. It can compromise the strength and durability of both steel reinforcement and concrete.

2.2 General Concept of Corrosion

Corrosion originated from the Latin verb "corrodere," meaning "to gnaw completely." corrosion is the loss of a metal's surface due to a chemical reaction, electrochemical process, or biochemical process when metals and alloys interact with their surroundings or environment. During this process, metals and alloys are thought to change into their more thermodynamically stable oxides, hydroxides, or carbonates (AL-Lamei et al. 2020). Steel embedded in concrete is usually protected from corrosion due to a thin layer of iron oxide that develops on its surface and remains stable in the alkaline environment of the concrete. It has been demonstrated in multiple studies, including (AL-Lamei et al. 2020; Hossain et al. 2021; Raja et al. 2016; Söylev and Richardson 2008) that chloride intrusion and carbonation are the leading causes of corrosion to RC structures.

2.2.1 Mechanism Of Corrosion

Once the hydration of cement begins, the steel in concrete forms a protective coating on its surface made up of γ-Fe_2O_3, which is firmly attached to the steel with a thickness ranging from 10^{-3} to 10^{-1} μm (Goyal et al. 2018). This coating prevents the movement of ions between the steel and the surrounding concrete, reducing the corrosion rate. The oxide layer keeps the steel from damage and is only stable at high pH values of 12–14 (Broomfield 2003). This layer must be destroyed for corrosion, which happens when carbonation or chloride ions are present. Figure 2.1 and equations 2.1-2.6 can be used to comprehend the corrosion process.

As iron is oxidized at the anode, it is released as ferrous ions into the solution, releasing its electrons [Eq. (2.1)]. The oxidation and reduction reactions at the anode and cathode are called half-cell reactions.

$$Fe \rightarrow Fe^{2+} + 2e^{-} \quad \text{..... Equation 2. 1}$$

The cathode can undergo various reduction reactions depending on the availability of oxygen and the pH of the environment. [Eq. (2.1)]. Illustrates the reaction in the highly alkaline concrete pore containing oxygen that produces hydroxyl ions [Eq. (2.2)].

$$2H_2O + O_2 + 4e^{-} \rightarrow 4OH^{-} \quad \text{..... Equation 2. 2}$$

Iron ions in solution react further with hydroxyl ions to form ferrous hydroxide [Eq. (2.3)].

$$Fe^{2+} + 2OH^{-} \rightarrow Fe(OH)_2 \quad \text{..... Equation 2. 2}$$

When ferrous hydroxide undergoes oxidation, it generates hydrated ferric oxide (commonly known as red-brown rust) [Eq. (2.4)] and hydrated magnetite (also called green rust) [Eq. (2.5)]. Both these substances can further dehydrate into red rust, ferric oxide (Fe2O3), and black magnetite (Fe3O4). In situations where the concrete pore environment has high alkalinity, ferrous hydroxide has the potential to oxidize into gamma ferric oxyhydroxide instead [Eq. (2.6)]. This compound is less permeable and adheres firmly to the steel surface.

$$4Fe(OH)_2 + O_2 \rightarrow 2Fe_2O_3 \cdot H_2O + 2H_2O \quad \text{..... Equation 2. 3}$$

$$6Fe(OH)_2 + O_2 \rightarrow 2Fe_3O_4 \cdot H_2O + 4H_2O \quad \text{..... Equation 2. 4}$$

$$2Fe(OH)_2 + \tfrac{1}{2} O_2 \rightarrow 2\gamma - FeOOH + 2H_2O \quad \text{..... Equation 2. 5}$$

The following diagram (Figure 2.1) shows anodic, cathodic, oxidation, and hydration reactions for corroding steel.

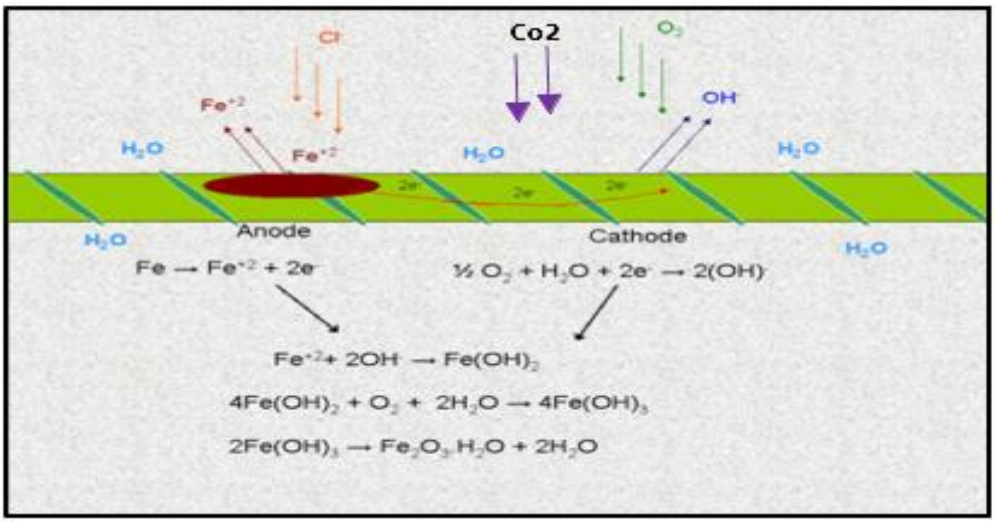

Figure 2.1 Anodic, cathodic, oxidation, and hydration reaction for corroding steel

2.2.2 Chloride-induced Corrosion

When a reinforced concrete structure is exposed to de-icing salts, acidic gases or submerged in seawater, the protective properties of concrete can be compromised (Du et al. 2020; Liang et al. 2021). Aggressive elements like chloride ions and carbon dioxide can infiltrate the concrete, altering its composition and the solution within its pores. As a result, the protective layer around the reinforcement is disturbed, a process known as depassivation (Broomfield 2003). This leads to an accelerated corrosion process, where metallic iron (Fe) at the anode is oxidized to form ferrous ions (Fe2+), as illustrated in Equation (2.1). Initially, this reaction is balanced by the cathodic reduction of dissolved oxygen to hydroxyl ions (OH), as described in Equation (2.2).

The Fe2+ combined with Cl drives to the anode by the corrosion current and forms the H_2O soluble ferrous chloride ($FeCl_2$):

$$Fe^{2+} + 2Cl^- \rightarrow FeCl_2 \quad \text{..... Equation 2. 7}$$

$$FeCl_2 + 2H_2O \rightarrow Fe(OH)_2 + 2HCl \quad \text{..... Equation 2. 8}$$

Some $FeCl_2$ migrates out of the corrosion pit and reacts with the cathodically formed sodium hydroxide (NaOH) to produce a ring of a white precipitate of ferrous hydroxide $Fe(OH)_2$(Du et al. 2020):

$$FeCl_2, + 2NaOH = Fe(OH)_2 + 2NaCl \quad \text{..... Equation 2. 9}$$

After forming, $Fe(OH)_2$ quickly transforms into hydrated ferric oxide (Fe2O3.H2O), commonly known as red-brown rust. Additionally, it can also convert into black magnetite (Fe3O4). Subsequently, green hydrated magnetite (Fe3O4.H2O) is formed. These transformations follow the same reactions mentioned in equations (2.4-2.6) as described by (Liang et al. 2021):

Opening of the pit. This formation prevents the electrolyte trapped within the pit from mixing with the surrounding solution, thus averting local acidification and stopping the replacement of dissolved oxygen within the pit. Combined with a considerable passive reinforcement area, this localized attack can lead to structural damage. Apart from the loss of strength, the expansion forces caused by corrosion products may result in the cracking and spalling of concrete. (Goyal et al. 2018; Prof. Luca Bertolin 2011; Wei et al. 2012).

2.2.3 Carbon-Induced Corrosion

As atmospheric carbon dioxide diffuses into the concrete, it dissolves in the pore solution to form carbonic acid [Eq. (2.10)], which neutralizes alkalis in the pore solution and combines with calcium hydroxide to form calcium carbonate [Eq. (2.11)].

$$CO_2 + H_2O \rightarrow H_2CO_3 \quad \text{Equation 2. 10}$$

$$Ca(OH)_2 + H_2CO_3 \rightarrow CaCO_3 + 2H_2O \quad \text{Equation 2. 11}$$

Carbonation causes the pH value of concrete to decrease (acidic environment), which leads to depassivation and exposure of the steel reinforcement to corrosion. Due to the neutralization of alkalis, carbonation, and diffusion of other acidic gases, such as 2SO and 2NO, the pH of the concrete pore solution decreases. In the case of a pH decrease, reinforcement may lose its passivity and become corroded (Revert et al. 2018; Zhou et al. 2015). The maximum rate of carbonation is observed at 50–70% RH (Goyal et al. 2018b)

2.2.4 Sulphate-Induced Corrosion

Most soil contains some sulfate in the form of gypsum ($CaSO_4.2H_2O$) and additional sulfate in calcium, magnesium, sodium, and potassium (Mehta and Monteiro 2014). Solid sulfate does not significantly harm concrete, but solution sulfate can penetrate concrete pores and react with hydrated cement products. A sulfate attack causes the cement to paste to expand in mortar or concrete. Concrete deterioration occurs because of this subsequent expansion of the solid phase. Calcium sulphoaluminate, or ettringite, is produced within the hydrated cement paste when sulfate salt reacts with the aluminate found in concrete as calcium aluminate hydrate gel (C-A-H). A small amount of alumina can be found in the form of C4AF and a little bit in the form of C3A in cement. Compared to calcium aluminate hydrate, C 4AF exhibits more resistance to sulfate attack (Mehta and Monteiro 2014; Quraishi et al. 2017). Table 2. 1 illustrates the different volumes of rust product that will be formed due to Corrosion of the above causes.

Table 2.1 Volume of different rust products

Corrosion Product	Color	Volume in cm^3
Fe	Earthy	1.3
FeO	Black	1.9
Fe_2O_4	Black	2.1
$Fe(OH)_2$	White	3.8

$Fe(OH)_3$	Brown	4.2
$Fe(OH)3.3H_2O$	Yellow	6.4
Fe_2O_3	Red	2.5

2.3 Factors Affecting Corrosion Rate in Reinforced Concrete Structures

Several factors, including pH, cement type, temperature, and other corrosive substances, influence corrosion reactions in concrete. How they affect the concrete corrosion rate in the subsequent sub-section will be discussed.

2.3.1 Effect Of Concrete Composition

Several factors determine the corrosion rate of concrete, including the water/cement ratio, the concrete's permeability against corrosive chemicals, and the concrete's porosity (Zheng et al. 2012). In theory, a minimum water content of 30% is required for cement hydration reactions; however, for economic reasons, the ratio is kept between 40% and 50% in practice, resulting in more porous concrete. Concrete can be impermeable when air-entraining admixtures (AEA) are added to the mixture, thus creating isolated pores that are not interconnected. Insufficient curing of the concrete is another reason for the porous structure of the concrete (Alaskar et al. 2021). Fresh concrete not cured correctly and exposed to hot and dry conditions will not crystallize appropriately, thus exhibiting a porous structure. Generally, corrosion of concrete steels begins in 80 days for concrete with a corrosion allowance of 50 mm depth and a water/ cement ratio of 0.60 when fully submerged in water, while it begins in 380 days for concrete with a corrosion allowance of 75 mm depth under the same conditions. However, when concrete steel is fully submerged in water and has a corrosion allowance of 50 mm depth and a water/cement ratio of 0.40, Corrosion begins in 800 days. Corrosion can begin earlier when concrete is periodically exposed to wet and dry cycles (Cicek 2017).

2.3.2 Effect Of Oxygen In Concrete

Oxygen plays a critical role in the corrosion process of concrete structures, especially those reinforced with steel. In the presence of moisture, oxygen can cause the iron in reinforcing steel bars to oxidize and form rust (Ahmad 2003). This oxidation process is a leading cause of corrosion in concrete structures, known as steel or rebar corrosion. The concentration of oxygen significantly influences the corrosion rate in concrete. The higher the level of oxygen ingress, the faster the corrosion will progress. When more dissolved oxygen is available in the concrete pores, it accelerates the electrochemical reactions that cause the formation and propagation of rust on the steel surface. This, in turn, leads to cracks and spalling in the concrete, which further

exposes the steel to moisture and oxygen, creating a vicious cycle of degradation (Hussain et al. 2012).

2.3.3 Effect Of Humidity

For corrosion reactions, water is required as a reagent and electrolyte. Consequently, it must reach the surface of the steel bars embedded within the concrete medium, which is highly likely when the concrete structure is submerged in water or exposed to periodic wet and dry cycles (Bertolini et al. 2013). However, corrosion is unlikely to occur in the former case, when the concrete structure is completely submerged in water, since oxygen diffusion through water is very slow, while both need to be present on the steel surface for Corrosion to occur (Cicek 2017).

2.3.4 Effect Of PH

Concrete has one of its unique properties: its high pH levels, which provide an appropriate environment for the steel bars embedded in the solid so that they may passivate and remain passivated (Hansson 2016b). Therefore, corrosion will not occur on concrete as long as reinforced steel is embedded in a passivating film. This essential property characterizes concrete water due to hydrolysis or hydration reactions between clinker compounds within the cement.

2.4 Corrosion-Induced Challenge In Reinforced Concrete

Strength and durability are two crucial characteristics that directly impact the lifespan of concrete structures. As stated by Goyal et al. (2018), significant durability issues are the corrosion of steel reinforcement, which leads to rust formation, cracking, spalling, delamination, and degradation of structures. Premature failure of steel-reinforced concrete structures has been one of the significant problems for the construction industry. The reinforcement used to provide strength to the concrete structure, in most cases, is found to be the main culprit. This is primarily due to the early corrosion of steel reinforcement. Several methods and materials have been developed or are being developed to prevent the Corrosion of reinforcement steel (Daniyal and Akhtar 2020b). The following points will be discussed as the grand societal, economic, technological, and educational challenges related to the Corrosion of steel in RC.

2.4.1 Economic Challenges

Premature degradation not only concerns the safety and quality of human life, but the required repair work also negatively affects the environment due to the increased consumption of energy

and materials. Additionally, the Corrosion of infrastructures causes high costs to society. According to a report published by the Federal Highway Administration in 2001, Corrosion is estimated to cost the United States infrastructure and metal industry and government agencies $276 billion each year (Koch 2017). Around 3% of the world's Gross Domestic Product (GDP) (US $2.2 trillion) is consumed in corrosion costs. In 2014, the finical loss caused by Corrosion was at least RMB 2,127.8 billion yuan in China, accounting for 3.34% of the annual gross national product (GNP). In this regard, Figure 2.2 also compares the expenses of Corrosion to other problems with significant economic effects, like the annual healthcare costs associated with cigarette smoking in the United States of America (Angst 2018).

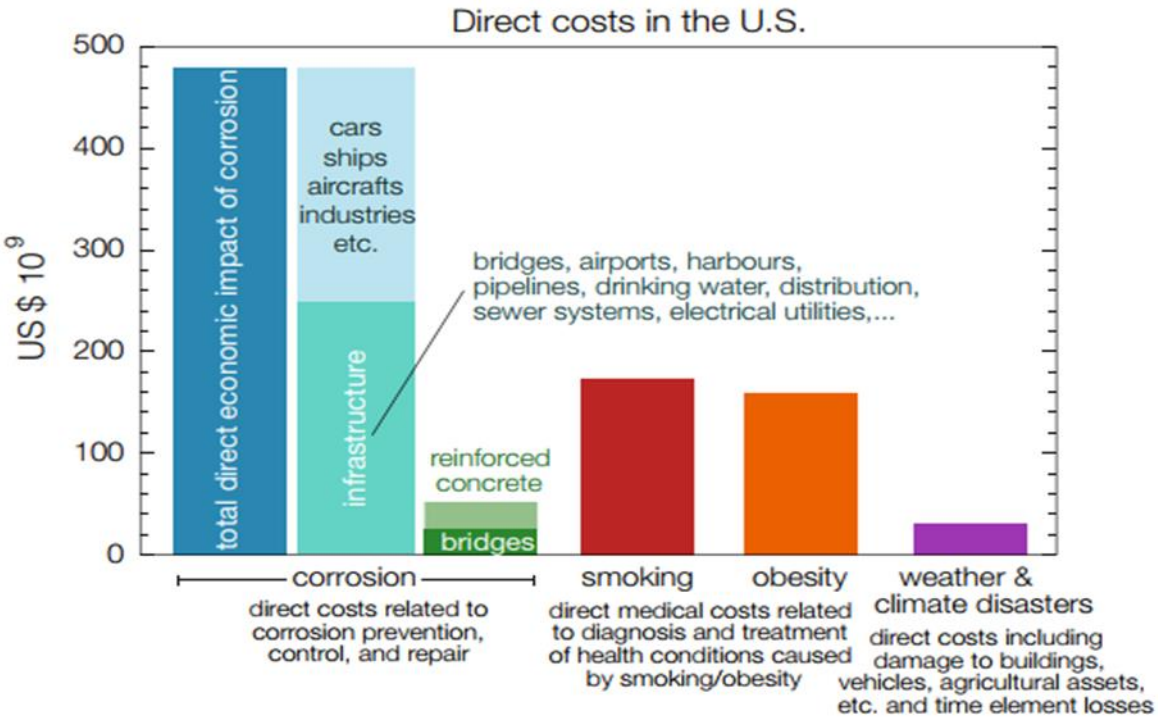

Figure 2.2 Economic Impacts of Corrosion and other significant issues in the USA

2.4.2 Technological Challenge

One of the challenges facing engineers is predicting how a structure will perform in the long term. For existing structures, the main challenge is repairing or replacing them when they need to be replaced. The challenge for new structures is designing them to be durable and sustainable. Due to the complicated and sluggish character of Corrosion, it has been observed (Daniyal and Akhtar 2020a; Li et al. 2021) as a technological challenge as there are no established tests or instruments to evaluate efficient monitoring and inspection techniques for evaluating the Corrosion of steel reinforcement. According to the Angst (2018) study, cost-effective maintenance of existing structures, less conservative decisions, design of repair

interventions, reliable condition assessment, and innovative repair techniques are the significant technological impacts of Corrosion in developed countries. In contrast, problems with the durable design of new structures, reliable, holistic service life modeling (forecasting corrosion), and long-term predictions without practical experience are the issues for developing countries. Figure 2.3 (Angst 2018) shows a figurative description of technological challenges.

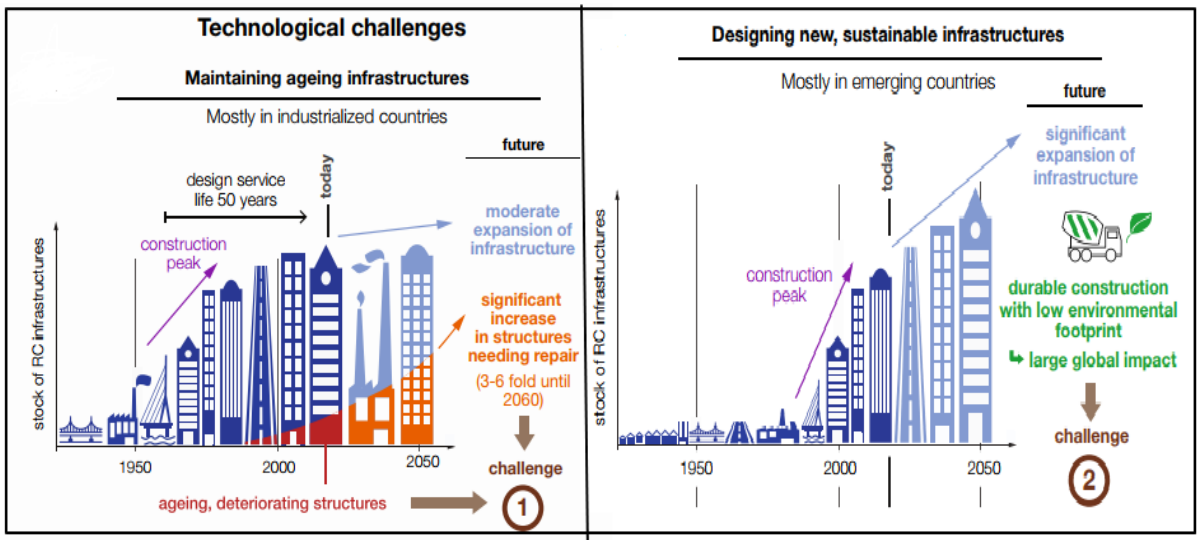

Figure 2.3 Technological challenge of corrosion in developing and developed countries

2.4.3 Environmental Challenge

Several studies (Bentz and Weiss 2011; Bonić et al. 2015; Cadenazzi et al. 2020; Hansson 2016) show RC structure corrosion harms the environment. On the one hand, corrosion results in plant closures, resource waste, product loss or contamination, and air pollution. On the other hand, Corrosion has an indirect impact that increases material consumption, CO_2 emissions in the production of hazardous materials, global warming, and photochemical oxidant creation.

2.5 Prevention Methods For Reinforcement Corrosion

Based on their experience in their field, researchers from various disciplines have attempted to develop additional preventive methods. For instance, metallurgists or material scientists have developed a material that resists corrosion, chemists have developed rebar and metal linings organic coatings, whereas civil engineers developed a better understanding of concrete corrosion control. These efforts have led to many preventive methods differing from each other, though each one is considered the most effective solution for strengthening Corrosion by the respective studies. Studies concerning corrosion prevention methods are categorized into five distinct approaches: corrosion-resistant rebar, Protective coating, corrosion inhibitors, cathodic protection, and natural corrosion inhibitors for providing protection. In the subsequent

discussions, each category will be thoroughly examined, shedding light on the various methodologies and their effectiveness in combating Corrosion.

2.5.1 Corrosion-Resistant Bars

Whenever reinforced concrete is expected to have long-term durability, the reinforcing material must be able to resist Corrosion caused by various environmental and construction work-related corrosion actions, which is why non-metallic reinforcing materials and alloy metals have been developed for the construction industry. This paper categorizes corrosion-resistant bars into two major groups based on their production: alloy rebars and non-metallic rebars.

2.5.1.1 Corrosion-Resistant Alloy Steel Bars

Pure iron is too soft for use as a structural material, but small additions of other elements (Carbon, manganese, or silicon, for instance) can enhance its mechanical properties. An alloy steel is a steel that is alloyed with a variety of elements in total amounts of 1.0% to 50% by weight to improve its mechanical properties (Chen et al. 2005). In order to enhance the corrosion resistance of steel, researchers have conducted studies on alloy steel composed of iron and chromium. Including chromium in these alloys leads to improved resistance against chemical Corrosion, primarily attributed to the passivation process. For passivation to occur and remain stable, the Fe-Cr alloy must contain a minimum chromium content of approximately 11% by weight, above which passivity can occur and below which it is not possible (Liu et al. 2016a). Since the corrosion resistance of alloyed steel bars is determined by the amount of chromium present in the bar, they can be classified into two categories: low alloy rebars and high alloy rebars. For weathering steels, Cr (chromium), Cu (copper), and P (phosphorus) are the main additives used to enhance resistance to electrochemical dissolution in the atmosphere (Sun et al. 2021).

Concerning corrosion resistance and economy, low-Cr steels that belong primarily to the range of low-alloy steels have attracted considerable interest from steel enterprises and scholars (Liu et al. 2016a; Sun et al. 2021; Wang et al. 2014). These steels have been demonstrated to be better than C (carbon) steels in marine environments. A new type of steel rebar, MMFX, containing 9-11% Cr (Mohamed et al. 2013), has been developed to improve steel's corrosion resistance. According to independent tests, MMFX is superior to galvanized and epoxy-coated rebar in corrosion resistance (Liu et al. 2016a). On the other hand, high-alloy rebars belong to the stainless steel category, where alloy additions are greater than 12% (Liu et al. 2016a). For reinforcement purposes, ferritic and austenitic stainless steels have been used. It was observed

by that only austenitic stainless steel (Type 304) was utterly serviceable in high chloride concentrations (3.2% chloride ion equivalent to 5% cement weight), whereas ferritic stainless steels (Types 405 and 430) were affected by the same chloride concentrations. When exposed to a chlorine environment, duplex steel 1.4362 (AISI S2304) and austenitic steel 1.4401 (AISI 316) have excellent corrosion resistance. This is due to the effective protective properties of the passive film, which is enriched with Cr, Ni, and Mo. In addition, steel types containing low Ni but high N and molybdenum contents perform well in an environment containing chlorides. Concrete Society technical report 51 recommends reinforcing austenitic and duplex steels (Goyal et al. 2018a). A comparison of stainless steel with carbon steel and aluminum is shown in Figure 2.4 below (Backhouse and Baddoo 2021).

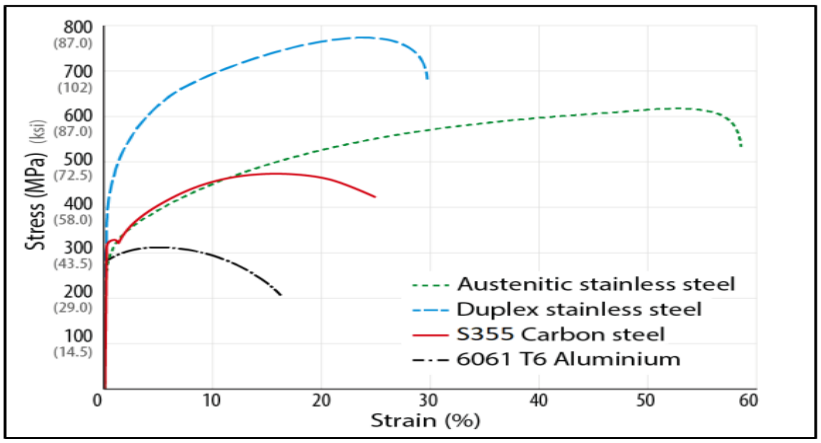

Figure 2.4 Strain characteristics of stainless steel with carbon steel and aluminum

It has been demonstrated by Labiapari et al. (2021); Zengin et al. (2021) that austenitic stainless steel would add between 6 and 16% to the cost of concrete bridges when used as reinforcement. Steel containing three weight percent Cr can increase CO2 corrosion resistance by about 2.5 to 40 while retaining a cost penalty under 1.5 times that of conventional grades C steel (Wang et al. 2014). According to a report by Kepler and Locke (2000), stainless steel was compared to epoxy coating and titanium, as shown in Table 2.2 below

Table 2.2 Reinforcement cost ratio comparison

	Cost of Reinforcement/ cost of black steel	Total cost / total cost with black steel		
		Bridge A	Bridge B	Bridge C
Epoxy-coated	1.4	1.16	1.02	1.00
Stainless Steel	6	1.16	1.13	1.06

Titanium	30.0	1.91	1.74	1.35

Stainless steel rebars exhibit negligible reductions in tensile strength and yield when exposed to 600°C for two hours (Wang et al. 2014). Steel is commonly corroded by pitting Corrosion in concrete, especially when chlorides are present. A welded bar is more likely to experience Corrosion than a non-welded bar.

2.5.1.2 Non-Metallic Reinforcement

A composite material called fiber-reinforced plastic (FRP) consists of fibers and a synthetic polymer matrix. The fibers provide high tensile strength, lightweight, and corrosion resistance to the material. However, the fibers alone cannot handle compression, torsion, or bending loads (Berrocal et al. 2016). Therefore, they are embedded in a resinous matrix that supports and protects them. Generally, they are classified as carbon fiber-reinforced plastic (CFRP), basalt fiber-reinforced plastic (BFRP), aramid fiber-reinforced plastic (AFRP), and glass fiber-reinforced plastic (GFRP) (Siddika et al. 2020). Numerous studies have examined fiber-reinforced plastic as a noncorroding reinforcement in concrete over the last few years.

Furthermore, it was observed that the technology suffers from high cost, poor bonding between concrete and fiber-reinforced polymer rebar, and low ductility of fiber-reinforced polymer (Chung 2000). Basalt and carbon fibers have excellent acidic and alkaline resistance (Goyal et al. 2018a). When exposed to alkaline or acidic environments, glass fibers degrade over time, whereas aramid fibers are sensitive to environmental degradation.

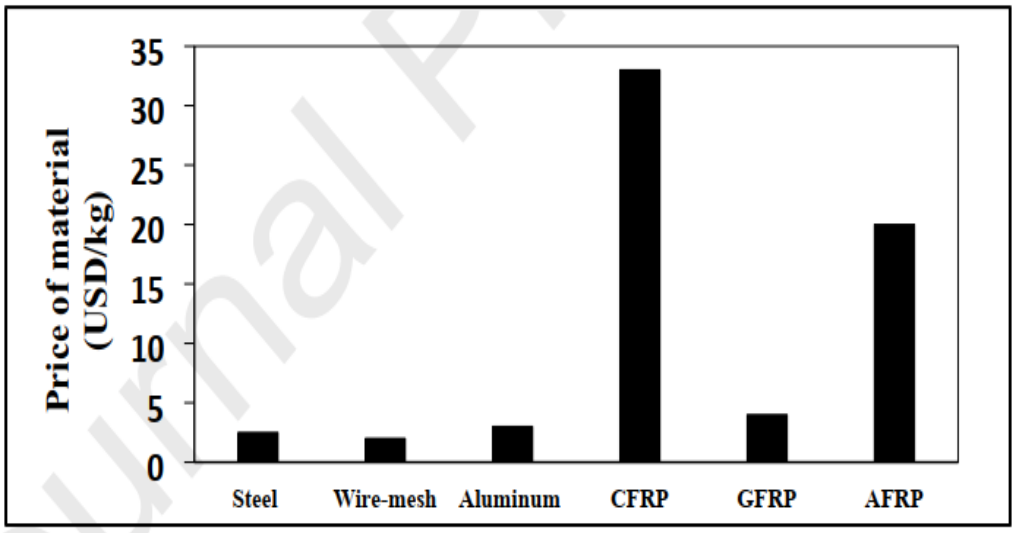

Figure 2.5 A comparison of the prices of different strengthening materials

Strengthening with FRP requires a significant initial investment. FRP is more expensive than conventional strengthening materials, such as steel plates, wire mesh, and aluminum plates. According to recent market trends (Siddika et al. 2020), the prices of the materials used to reinforce RC structures are shown in Figure 2.5.

For a similar amount of CFRP to be used instead of conventional steel plates, the material cost will be approximately 16-17 times higher; this difference is approximately eight times for AFRP (Berrocal et al. 2016). It can be seen from the trend of the price per unit weight of material that strengthening with any FRP material is challenging. Comparatively, AFRP is less expensive than CFRP and GFRP. E-GFRP is the least expensive among them (Mugahed Amran et al. 2018). The cost of carbon fibers is 10-30 times more expensive than that of glass fibers (Ahmed et al. 2020).

2.5.2 Protective Coating

Coatings provide physical barriers to prevent Corrosion. Coatings should demonstrate high adhesion, and their porosity and permeability determine their protection (Deshpande et al. 2014). Various coatings are available to protect rebars in concrete, including metallic, organic, and cementitious coatings. Steel is protected from mechanical damage by these coatings, which are non-reactive in corrosive environments (Goyal et al. 2018).

2.5.2.1 Metallic Coating

Initially, metallic coatings were developed to protect the parent metal (usually mild steel) from Corrosion. Due to these developments, two broad types of coatings have been developed: (I) passive film-forming coatings, such as Si-based coatings and Cr-based coatings, and (ii) sacrificial coatings, such as galvanizing (Goyal et al. 2018). The passive film on the film adheres to the rebar and may break under various conditions, such as service, transportation, and fabrication. This could lead to localized Corrosion in some areas. The parent metal is anodic to the passive film, affecting the corrosion behavior. In contrast, corrosion prevention is based on a sacrificial anode instead of the cathodic underlying parent metal in the second option.

Under normal environmental conditions, only cadmium and zinc can provide galvanic protection to steel (Table 2.3). Consequently, the metal remains protected even if the coating is damaged or breaks during fabrication, transportation, or use (Yeomans 2004, 2016). This has led to extensive research on galvanized steels (Singh and Venugopalan 2013; Yeomans 2004, 2016) compared to other methods such as epoxy and artificial coating.

Copper, nickel, tin, and lead were cathodic to steel in seawater. Lead, tin, cadmium, and zinc were anodic to steel during alkaline solid pH conditions. However, self-corrosion rates were higher at a 9.01 PH value. A coating metal can be selected for a particular environment using these potential values as a guide. By galvanizing concrete, substantial protection is provided against carbonation.

Furthermore, galvanized reinforcement can withstand chloride ion concentrations several times greater than those that cause Corrosion to black steel in concrete (Yeomans 2016). However, compared with other aggressive environments, there are varying opinions regarding zinc's corrosion resistance in concrete environments. For instance, galvanized coatings on steel rebar have several disadvantages, as stated in the Singh and Venugopalan (2013) study: (a) The thickness of the coating cannot be reduced below 50-60 micro mil because this would be too costly and uneconomical; (b) As a result of the formation of powerful galvanic couples, coatings form intermetallic layers that are susceptible to Corrosion; (c) Prolonged exposure to high temperatures during the galvanizing process may adversely affect the mechanical properties of steel rebars, eventually resulting in catastrophic failure; (d) There is a considerable amount of corrosion product (hydrozincite) that forms on the surface of galvanized rebars and which exerts internal stress on the concrete that causes it to crack.

Table 2.3 Different types of coatings for steel rebar

System	Disadvantages
Coating not suitable	
Read lead	Deterioration in alkaline medium
Coal tar enamel	Brittle, Subject to cold flow, sticky
Asphalt	Subject to cold flow
Phenolic	Deterioration in alkaline medium
Urethane	Rigid, brittle, intolerant to poor surface preparation
Neoprene	Poor bond
Aluminium	Rapid Corrosion in the presence of chloride. No electrical insulation effect. Stop.
Coatings Suitable	
Zinc/ cadmium	Rapid Corrosion in the presence of chloride. No electrical insulating effect.
Nickel/Copper	No suitable for chloride exposure, no electrical insulating effect, Galvanic Corrosion.

Epoxy	in Britain. Many formulations will not bend or stretch. Many formations have poor bonds, and only powder epoxy is suitable.

2.5.2.1 Organic Coating

Epoxy coatings on steel are highly effective barriers against aggressive agents, particularly chloride ions, which cannot quickly diffuse through continuous epoxy coatings. Several organic coatings, including epoxy, polyvinyl chloride, polypropylene, phenolic nitrite, and polyurethane, protect against aggressive agents, oxygen, and moisture. A bonded epoxy bar is the most used. It is made by electrostatically applying epoxy powder to a bar that has been thoroughly cleaned and heated (Cicek 2017). Corrosion protection provided by epoxy coatings is excellent, and the coating is not affected when it performs its corrosion protection function (Rahman and Akhtarul Islam 2022). Unlike a metallic coating, the coating has very low permeability to chloride ions, is chemically resistant, and is unaffected by most environmental factors.

Even though epoxy-coated reinforcement is highly corrosion-resistant in most situations, the effectiveness of these coatings in extremely aggressive environments has recently been questioned due to the possibility of damage during transportation and fabrication (Zafeiropoulou et al. 2011). The risk of mechanical and abrasion damage to epoxy-coated reinforcement can be reduced by handling and storing it carefully. Damaged areas of the coating usually need to be recoated. (Kumar 1998) also observed, after inspecting more than thirty bridges, that the corrosion-free service life of these structures is primarily due to the quality of the concrete and the thickness of the cover, not to the use of epoxy-coated rebars.

The Polyurethane Coating process is a viable solution for overcoming the shortfalls of thermosetting polymers such as epoxy. Table 2.4 illustrates the two major types of organic coatings and their durability in different environmental conditions (Møller et al. 2017)

Table 2.4 Comparison between polyurethane and epoxy

Resin	Product name	Application areas
Epoxy	Belzona	Resistance to sulfuric acid and hydrochloric acid.
	Phenoline	Chemical resistant coating
	Corrocoat	Resistant to high concentrations of sulfuric acid
	Envioline	Chemical attacks, corrosion, and leaks

Polyurethane	concoflex Urethane	Primary and secondary containment, highly impermeable, chemically resistant toward a wide range of acid
	Potbrid	Corrosion protection for immersion in acid

The organic coating method has been developed to offer enhanced performance and longer-lasting coatings with improved mechanical properties in both liquid and solid forms (Zhang et al. 2016). These are a build-up of thermal stress in the polymer during curing, poor film-forming capacity, and a marked tendency to form pinholes and pores, causing non-conductivity in the film. Differential shrinkage develops during curing and early weathering in the polymer due to UV radiation, oxygen, heat, and moisture (Zhang et al. 2016). As a result of their high resistance to abrasion and wear, polyurethane coatings are remarkably durable. This is why they are recommended primarily for floors that are subjected to severe stresses that cannot be met by the usual types of floor coverings (Engels et al. 2013).

2.5.3 Corrosion Inhibitors

Corrosion inhibitors are chemicals added in small amounts to water or other liquids or gases to reduce corrosion rates. They work by affecting either the anodic reaction, the cathodic reaction, or both reactions at the same time (Poursaee 2016). Cathodic, anodic, and mixed corrosion inhibitors are based on active inhibitor molecules that retard Corrosion and may be obtained from organic, inorganic, or both compounds. Inorganic inhibitors are oxidizing substances that promote passivity on the surface by adjusting the corrosion potential (Ma et al. 2022). A chromate-based corrosion inhibitor is widely recognized as one of the most effective inorganic corrosion inhibitors in preventing the Corrosion of metals. Unfortunately, hexavalent chromate corrosion inhibitors pose many environmental hazards, and the toxicity of these agents has been well established. Various inorganic inhibitors have been successfully utilized in various corrosive environments to substitute chromate-based inhibitors. For example, nitrate and sulfate-based materials have been successfully used as inorganic inhibitors. Compared to other corrosion prevention measures, these measures are relatively inexpensive and easy to handle (Al-Sabagh et al. 2018; Ma et al. 2022). Because of their inhibition function, inorganic inhibitors are classified as anodic or cathodic.

The anodic inhibitors form an oxide film on the surface of the metal, which causes the metallic surface to shift into the passivation region due to the sizeable anodic shift in corrosion potential. Although the film initially forms at the anode, it may eventually cover the entire metal surface. It is also sometimes called a passivator (Goyal et al. 2018). In general, cathodic inhibitors are

less effective than anodic inhibitors. The cathodic inhibitor prevents diffusion of reducing species to the surface by precipitating on cathodic areas. A cathodic inhibitor indirectly reduces Corrosion by slowing the cathodic reaction itself or by precipitating selectively on cathodic areas to reduce the diffusion of reducing species (Poursaee 2016).

Since organic corrosion inhibitors perform well in various applications, are compatible with various materials, are easy to dissolve, and are relatively nontoxic, they are extensively used in industry. A corrosion inhibitor can be either anodic or cathodic, and its various types are determined by the reaction at the metal's exterior and by its interaction with other ions (Ma et al. 2022). A heteroatom, such as N, S, or O, is present in every organic compound. The heteroatoms significantly inhibit corrosion reactions on metallic materials, particularly copper, iron, and aluminum alloys. These heteroatoms play a vital role in the inhibition process, forming insoluble deposits on the metal's exterior (Ma et al. 2022; Verma et al. 2017; Xhanari and Finšgar 2019). Since organic inhibitors retard mutually cathodic and anodic reactions, their inhibition action is based on the adsorption of inhibitor molecules on the electrolyte/metal interface to form a new insoluble layer (Daoud et al. 2014; Gopiraman et al. 2012). Adsorption may occur physically or chemically. Physical adsorption involves the electrostatic interaction between the surface of the metal and the charged inhibitor molecules, whereas chemical adsorption relies on the interaction between the molecules and substrates chemically (Gowraraju et al. 2017; Yadav et al. 2016). Furthermore, several factors directly affect the effectiveness of inhibition, such as the chemical structure of the organic inhibitors, the concentration, the type of testing electrolyte, the exterior charge, and the circulation of the charge in the molecule. The potential of corrosion inhibitors as a comprehensive method of corrosion protection can be demonstrated in Figure 2.6.

Mixed inhibitors combine anodic and cathodic processes since anodic inhibitors can cause pitting. Combining organic and inorganic constituents may result in excellent compatibility and corrosion inhibition. For instance, Umoren et al. (2019) have examined the adsorptive mechanisms of plant biomaterials in various types of corrosive environments. As a result of this study, it was concluded that plant extracts could inhibit the Corrosion of industrial metals by adsorption, physisorption, or chemisorption. Most of the organic and inorganic compounds containing functional groups such as amines, carbonyls, and alcohols are found to be more effective corrosion inhibitors (Alrefaee et al. 2021; Salehi et al. 2017).

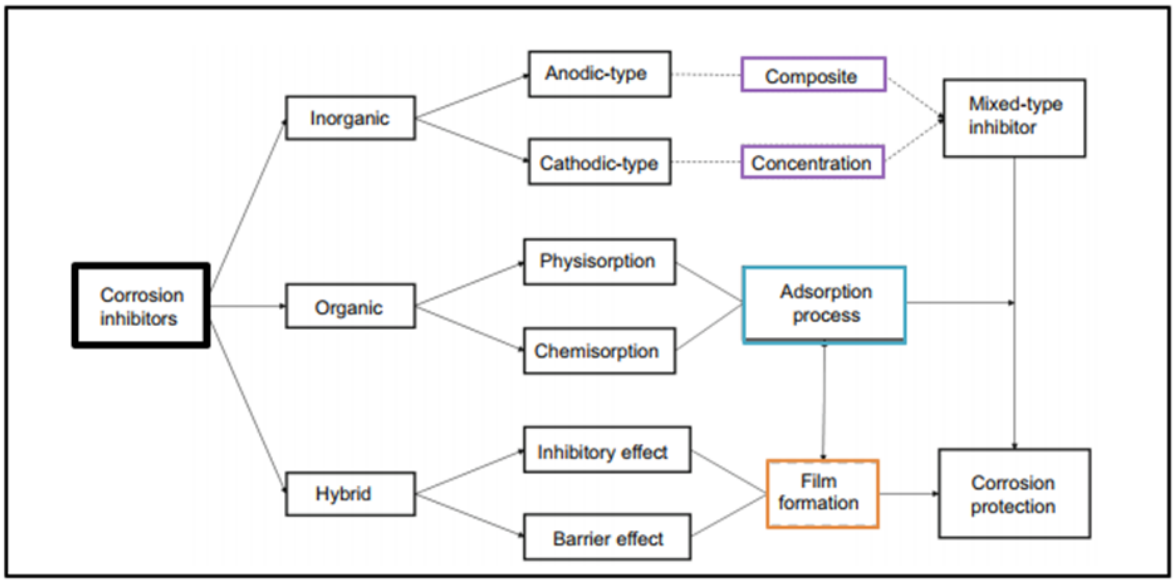

Figure 2.6 An Overview of Corrosion

2.5.4 Cathodic Protection

Cathodic protection is a technique used to prevent Corrosion by applying a negative voltage to the reinforcing steel, which helps reduce the Corrosion rate. It has been demonstrated that cathodic protection can significantly extend the service life of reinforced concrete structures, particularly in aggressive environments (Goyal et al. 2018). Maintenance requirements for cathodic protection include regular system inspection and testing to ensure the applied voltage is within the required range. The cathodic protection can be applied in two ways: sacrificial anode cathodic protection (passive system) and impressed current cathodic protection (driven by an external power supply), and more recently, a hybrid cathodic system that combines the characteristics of both systems has been developed. A process known as sacrificial anode cathodic protection, or SACP, can effectively reduce the Corrosion of concrete structures caused by such factors as the presence of moisture, salt, or other chemical elements in the atmosphere (Hansson 2016a). This process involves connecting a metal sacrificial anode to a concrete structure to protect it from Corrosion. The sacrificial anode attracts corrosion-causing elements away from the concrete, preventing the structure from deteriorating due to Corrosion. This technique is most used on bridges, buildings, and tanks but can also be used on other concrete structures.

According to recent studies, sacrificial anode cathodic protection (SACP) has become a popular method for controlling concrete Corrosion due to its versatility and cost-effectiveness (Byrne et al. 2016). The SACP method is effective in protecting concrete foundations and structures from Corrosion, as it offers a long-term solution with minimal maintenance requirements

(Prasad et al. 2021). This is because the anode has a finite lifespan, meaning that periodic monitoring and replacement of the anode are typically all required (Ma et al. 2022). Furthermore, SACP is relatively inexpensive compared to other methods of concrete corrosion protection, making it a popular choice for many structures (Quraishi et al. 2017).

However, some limitations of SACP should be considered when deciding whether it is an appropriate solution for a given situation. The primary limitation is its limited practical working life (Chen et al. 2009). Anodes are corroded when galvanic current passes through them, eventually needing to be replaced or supplemented (Byrne et al. 2016). Anodes that are significantly degraded can be replaced or augmented with a larger anode, but the replacement may need to be done at intervals of no more than two years (Goyal et al. 2018c). In addition, the anodes generally need to be monitored to ensure they function as expected (Daniyal and Akhtar 2020b). Another limitation is related to maintenance. Sacrificial anodes must be periodically replaced and maintained optimally (Ma et al. 2022). In particular, the anodes need to be cleaned and inspected regularly to ensure they can adequately protect the structure (Prasad et al. 2021). Despite these limitations, sacrificial anodes are generally more cost-effective than concrete Corrosion cathodic protection methods (Prasad et al. 2021). Thus, SACP remains a popular choice for many structures seeking to protect against concrete Corrosion.

Impressed current cathodic protection, on the other hand, is an active system that uses an external power supply to create a protective electrical current on the steel reinforcement. This method is more expensive than sacrificial anode cathodic protection and requires regular maintenance to ensure the proper functioning of the electrical system. However, it can be more effective in highly corrosive environments, such as seawater exposure (Bahekar and Gadve 2017). Nevertheless, cathodic protection effectiveness is highly dependent on several factors, including the system's design, the quality of the materials used, and the condition of the concrete (Poursaee 2016). Furthermore, there are concerns about the potential long-term effects of cathodic protection on concrete since highly alkaline environments can lead to calcium hydroxide formation and subsequent damage to concrete (Bertolini et al. 2013).

2.5.5 Natural Corrosion Inhibitors

A natural corrosion inhibitor is a chemical compound derived from a natural resource, such as plants, fruits, herbs, or biopolymers, which can prevent or reduce metal corrosion in various environments. Abdel-Gaber et al. (2011) consider them green and sustainable alternatives to synthetic inhibitors, which may adversely affect the environment and human health. Plant

extracts are one of the most widely studied sources of natural corrosion inhibitors since they contain various organic molecules that can adsorb on metal surfaces and form protective layers (Venkatesh et al. 2019). Rani and Basu (2012) have reported that garlic, ginger, neem, henna, and papaya are among the plants shown to inhibit the Corrosion of mild steel. Natural products can also be corrosion inhibitors, including amino acids, proteins, ionic liquids, and polyethylene glycol (Abdulrahman et al. 2011; Asaad 2021). Depending on their chemical structure and mode of action, these compounds can act as anodic, cathodic, or mixed inhibitors. Unlike synthetic corrosion inhibitors, natural corrosion inhibitors have several advantages, including low cost, easy availability, biodegradability, and eco-friendliness. However, they also have some limitations, including low stability, poor solubility, and variable efficiency depending on the extraction method and environmental conditions (Hansson 2016a). Among the plants that have raised interest in their potential as green inhibitors is Opuntia Ficus Indica (OFI). The following discussion will focus on Optica Ficus Indica as a natural corrosion inhibitor.

2.5.5.1 Opuntia Ficus Indica (OFI)

Opuntia ficus indica (OFI) is a type of plant that falls under the Cactaceae family and the order Centrospermae (Bayar et al. 2016). It primarily grows in tropical and subtropical regions and is known for its ability to adapt to challenging conditions. Particularly in arid and semi-arid regions, the Opuntia ficus-indica demonstrates remarkable resilience and efficiency, enabling it to thrive in harsh and dry environments (Lefsih et al. 2016). This cactus plant possesses specialized adaptations that enable it to store water and survive extended periods of drought (Bayar et al. 2016). In the United States, within the states of California, Texas, and Florida, and in various countries, Mexico, Chile, Argentina, Morocco, and Italy, the cultivation of opuntia ficus indica (OFI) for commercial purposes (Sáenz et al. 2004). Additionally, studies conducted by Belay and Gebreyohannes (2010) have indicated that Ethiopia is also abundant in OFI.

Three million hectares of OFI are native to Mexico, while approximately 233,000 are cultivated. Ethiopia has 150,000 hectares of cactus lan for human consumption, producing 139,193 tons annually (Sáenz et al. 2004). Ethiopia also has 32,000 hectares of uncultivated cactus land. Various amounts of OFI are found throughout Ethiopia, including abundantly in the Rift Valley (Belay and Gebreyohannes 2010). Figure 2.7 illustrates the abundance of OFI worldwide as stated by ("Map of Opuntia ficus-indica -- Discover Life" n.d.).

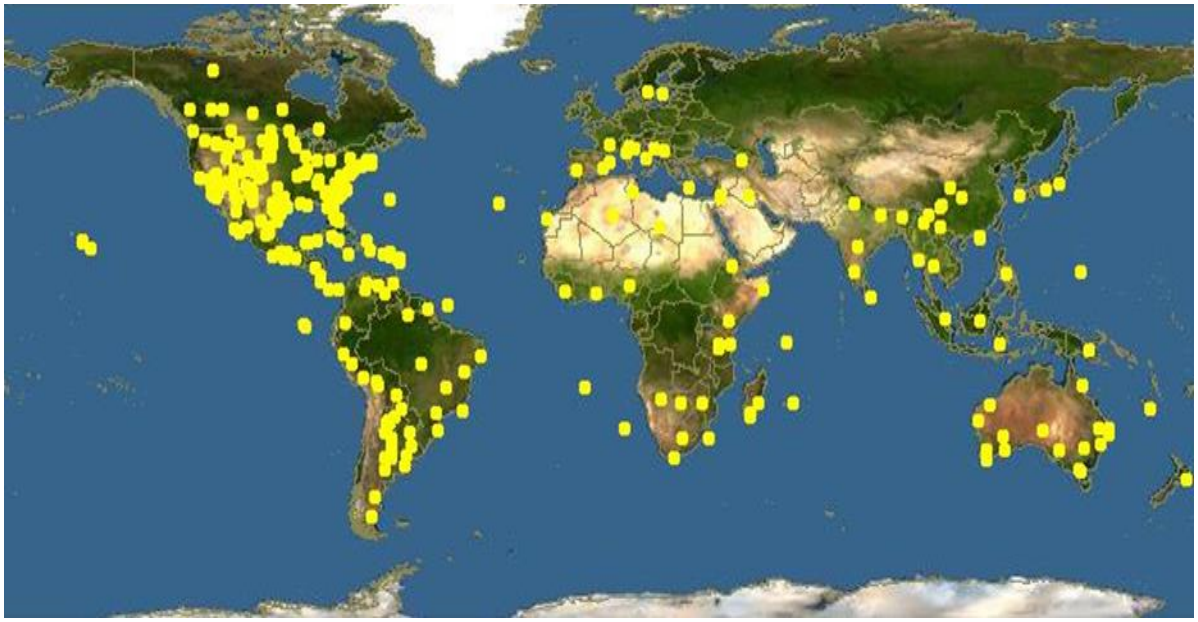

Figure 2.7 Abundancy of OFI in the Globe

OFI cladodes are widely used in various industries due to their beneficial properties. They contain high levels of polysaccharides such as cellulose, hemicellulose, and mucilage, which can form a protective film on the concrete surface, effectively minimizing corrosion1 (Camarena-Rangel et al. 2017). OFI also contains bioactive phenolic compounds like flavonoids, betalains, and phenolic acids, known for their antioxidant properties (García-Barradas et al. 2022). These compounds can help reduce oxidative stress on the concrete and prevent the corrosion process. Additionally, OFI contains proteins and amino acids that can chelate metal ions and form a protective layer on the concrete surface, reducing the electrochemical reactions involved in the corrosion process (Matsuhiro et al. 2006). The presence of minerals such as calcium, potassium, and magnesium in OFI can also contribute to corrosion inhibition by controlling the permeability of concrete and reducing the penetration of corrosive substances like chloride ions (Díaz Blanco et al. 2019a).

The corrosion performance of reinforcing steel in alkaline media was assessed by using dehydrated Opuntia Ficus Indica (Nopal) as an admixture, specifically evaluating the impact of Opuntia-Ficus-Indica (OFI) mucilage Torres-Acosta (2007), and the addition of OFI led to the formation of a denser and more packed oxide/hydroxide surface layer on the steel surface that decreased corrosion activity. This oxide/hydroxide layer growth was confirmed from a microscopic evaluation of the metal surface layer per- formed at the end of the experiment (Torres-Acosta 2007). Mucilage of OFI has also demonstrated good performance as an inhibitor of Corrosion in alkaline solutions, mortar, and concrete that are contaminated with

chlorides (Hernández et al. 2017; López-León et al. 2019; Martinez et al. 2016). During mortar-concrete hardening, this biopolymer interacts with the steel surface to form a more dense and thicker oxide polymer layer, which increases the propagation period when chlorides reach the reinforcing steel. In previous studies, dehydrated OFI and OFI mucilage were shown to inhibit the corrosion of steel in cement-based materials (mortar and concrete) exposed to chloride-laden environments (Martínez-Molina et al. 2015; Torres-Acosta and Alejandra Díaz-Cruz 2020). As the findings of earlier studies, OFI can be used both as corrosion inhibitors and durability enhancers in concrete; however, there are some methodological differences that make them in conflict with each other and also conflict with the theory of corrosion resistance.

Torres-Acosta and González-Calderón (2021) and Martinez et al. (2016) studied the corrosion inhibition of OFI in cement mortar; however, it is difficult to conclude OFI as an efficient Corrosion inhibiting for concrete based on cement mortar. According to Bertolini et al. (2013), in highly alkaline environments, adequate hydration with low permeability is considered mandatory for preventing Corrosion of reinforcement. Martinez-Molina et al. (2015) employ a water/cement ratio of 0.88 and replace OFI in place of water without considering how hydration reacts in concrete. Likewise, Díaz Blanco et al. (2019) and Martinez et al. (2016) follow the same procedure but with a smaller water-cement ratio. A different study conducted by (Torres-Acosta and Alejandra Díaz-Cruz 2020) investigated the durability performance of Opuntia-Ficus-Indica (OFI) in concrete using different forms of nopal mucilage. Specifically, they examined the effects of exudate nopal mucilage (eNm), cooked nopal mucilage (cNm), and dehydrated nopal powder (dNp) for the concrete samples containing eNm and cNm, concentrations of 4%, 8%, 15%, and 30% were used as replacements for water by mass. On the other hand, dNp was added at 1%, 2%, and 4% by mass of cement as replacements for sand. The physical and mechanical properties of the concrete were monitored for both the nopal derivative treatments and the control group (without nopal derivatives) to assess any potential improvements in durability. However, it is essential to note that Torres-Acosta and Alejandra Díaz-Cruz (2020) did not discuss the effectiveness of OFI on the C-S-H reaction. Table 2.5 provides a summary of the percentage addition of OFI in various studies.

Table 2.5 OFI amount used by different studies

Percentage addition of OFI	Aim	References
The dehydrated Nopal material was mixed with saturated calcium hydroxide	Performance of reinforcing steel in alkaline media when dehydrated Opuntia Ficus Indica (OFI) was used as an admixture	(Torres-Acosta 2007)

(SCH) by weight at 0.5, 1.0, and 2.0%.		
1.5,4,8,42,95 % by water replacement	To investigate durability enhancement in a cement-based mortar	(Martinez-Molina et al. 2015)
The natural dehydrated additions, Nopal and Aloe Vera in 0%, 1%,2%, and 4%	Physical characterization of mortar cubes fabricated with botanical (green) dehydrated additions such as Nopal (Opuntia Ficus Indica) and Aloe Vera	(Martínez-Molina et al. 2015)
A CM colloidal dispersion with a 0.5, 1.0, or 1.38 percent concentration (weight/volume) was used. Mucilage was extracted from Opuntia ficus-indica cladodes	experimental results related to the performance of cactus mucilage (CM) and brown seaweed extracts (SEs) to inhibit reinforcing steel bar (rebar) corrosion in saturated calcium hydroxide alkaline solutions (pH ⁄⁄ 12.5).	(Hernández et al. 2017)
4%,8%,42%,95%	determine if a type of cactus mucilage, Opuntia ficus-indica (OFI), may act as a corrosion inhibitor for carbon steel in cement-based materials (mortar) exposed to a chloride-laden environment.	(Martinez-Molina et al. 2016)
Exudate OFI mucilage (eNm), cooked OFI mucilage (cNm), and dehydrated OFI powder (dNp). Concrete containing eNm and cNm was fabricated using 4%, 8%, 15%, and 30% concentrations by water mass replacement. The	to evaluate concrete physical characteristics (i.e., porosity and mechanical resistance) from its durability performance if OFI derivatives were added to the mixture. Three OFI derivatives were evaluated: exudate OFI mucilage (eNm), cooked nopal mucilage (cNm), and dehydrated OFI powder (dNp).	(Torres-Acosta and Alejandra Díaz-Cruz 2020)
1.5%, 4%, 8%, 42%, and 95% by water replacement	to investigate whether the addition of Opuntia ficus-indica (OFI) cactus, a natural/botanical material, enhances the durability of cement-based materials when exposed to CO2-laden environments	(Torres-Acosta and González-Calderón 2021)

c

2.5.6 Concrete Mix Design

Concrete cover refers to the thickness of the concrete that covers the reinforcement. Concrete covers and internal curing are effective techniques used to prevent concrete reinforcement corrazosion. Additional water is added to the mix during curing to provide additional moisture.

Ensuring adequate corrosion protection for reinforcement necessitates the establishment of proper concrete covers. This requirement is a preventive measure against Corrosion, safeguarding reinforced concrete elements' longevity and structural integrity. According to the Building Code Requirements for Structural Concrete (ACI 318) guidelines, specifying a minimum concrete cover for reinforcement is imperative (ACI, 2019). According to ACI, 2019, the thickness of the cover is determined by factors such as the environment in which the structure will be located and the size of the reinforcement. The thicker the cover, the better the protection against Corrosion provided by the reduced exposure to the environment of the reinforcement.

Another method of protecting reinforcement from Corrosion is internal curing. A small amount of water is added to the concrete mix during curing to keep it moist, preventing cracking and improving the finished concrete's quality. Additionally, this extra moisture enhances the protective oxide layer's formation on the reinforcement's surface (Liu et al., 2017). This prevents the penetration of harmful agents such as oxygen and chloride ions, possibly leading to Corrosion. Besides preventing Corrosion, internal curing can also enhance concrete's durability by reducing shrinkage, increasing strength, and improving the quality of the final product (ACI, 2014). It has also been reported that using lightweight aggregates in the concrete mix can enhance the internal curing process by providing a more consistent source of moisture (Alaskar et al. 2021). As a result, concrete covers and internal curing are two essential methods for preventing reinforcement in concrete from corroding.

2.5.7 Analysis of the corrosion protection method effectiveness, cost, durability, and maintenance requirements

This study compares various concrete corrosion protection methods based on their effectiveness, cost, durability, and maintenance requirements. This was accomplished by preparing a table that includes the following comparisons: (1) the corrosion protection method, (2) the effectiveness rating of each method from 1 to 10, with 10 being the most effective, (3) the cost of each method per unit area, and (4) the durability rating of each method on a scale from 1 to 10, with 10 being the most durable as shown in Table 2.8.

Table 2.6 Corrosion protection method analysis

Corrosion Protection Method	Effectiveness (1-10)	Cost (per unit area)	Durability (1z-10)	Maintenance Requirements
Corrosion-resistant alloy steel bars	9	High	9	Low maintenance but may require inspection for signs of corrosion (Liu et al. 2016a)
Non-metallic reinforcement	6	Moderate	7	Minimal maintenance, but may require inspection for signs of corrosion (Ahmed et al. 2020)
Metallic coating	7	Moderate	7	Regular inspection and maintenance are required to ensure coating integrity(Yeomans 2016)
Organic coating	6	Low to moderate	6	Regular inspection and maintenance are required to ensure coating integrity (Zafeiropoulou et al. 2011)
Corrosion inhibitors	5	Low	5	Regular reapplication may be required (Ma et al. 2022)
Cathodic protection	9	High	8	Low maintenance but may require inspection for signs of corrosion (Byrne et al. 2016)
Concrete mix design	6	N/A	7	N/A
Natural corrosion inhibitors	6	Low	6 (vary from type to type	No need for regular inspection need but repeated repair will be there (Asaad 2021)

2.6 Internal Curing for Concrete

Internal curing concrete is a method used in concrete mixture design where additional moisture reservoirs are incorporated into the concrete mixture. These reservoirs can take the form of lightweight aggregates or superabsorbent polymers, and they have the ability to absorb and release water during the curing process (Kevern and Nowasell 2018). Concrete must be cured adequately to achieve the desired strength and performance. Internal curing is a process that provides water to the cementitious matrix of concrete after setting. (aravanan et al. 2021). This

modern twist on effective curing practice has several benefits, including reducing water consumption, improving concrete homogeneity, and reducing surface cracking (Bentz and Weiss 2011). According to Rahman et al. (2018), a conventional method, curing concrete involves creating conditions in which water does not evaporate from the surface, which is to say, curing occurs from the outside to the inside. Conversely, internal curing means curing 'from the inside out' using internal reservoirs (such as lightweight fine aggregates, superabsorbent polymers, or wood fibers).

One of the challenges of standard curing procedures is that water may not penetrate deep enough to form a hydration matrix, which is the main product of the reaction between the silicate phases of Portland cement and water and is primarily responsible for the strength of cement-based materials. This problem has been shown in different studies, especially on high-performance concrete. However, this kind of problem is not observed in internal curing, and a figurative description is shown below in Figure 2.8.

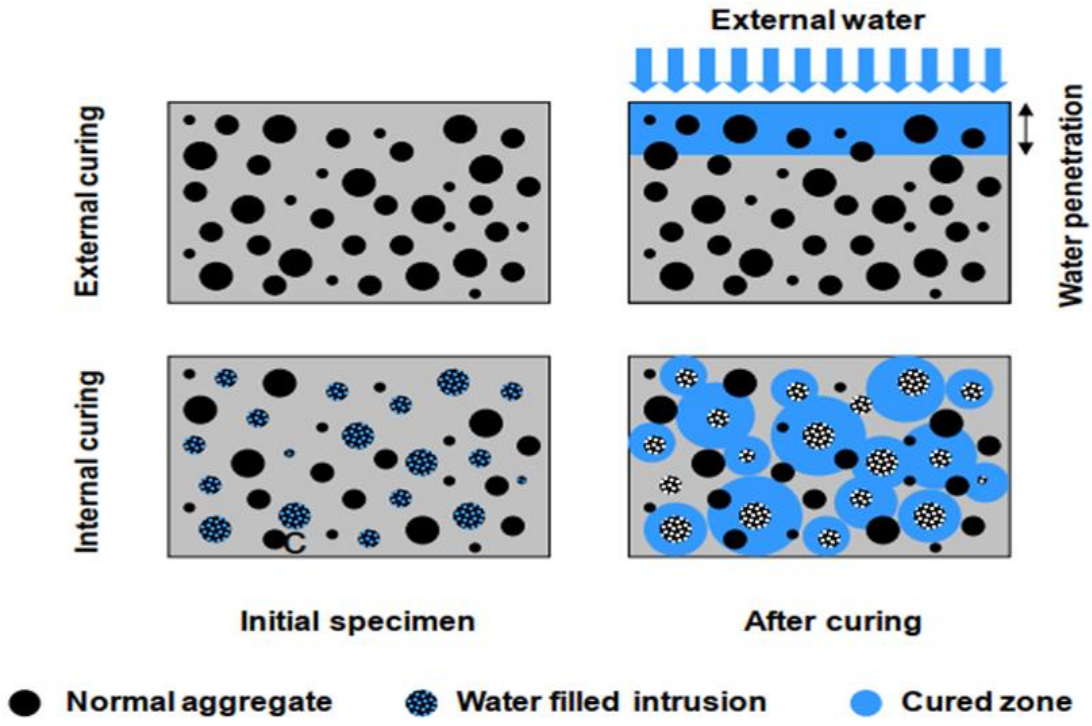

Figure 2.8 Conventional Curing to Internal Curing

It has been determined that different methods for internal curing materials, such as lightweight aggregate, are the most cost-effective for the construction industry (Bentz and Weiss 2011).

2.6.2 Lightweight Aggregate As Internal Curing Material

Concrete is internally cured using lightweight aggregates such as expanded shale, slag, pumice, perlite, and clay to provide additional curing water throughout the concrete mixture (Akhnoukh 2018). The American Concrete Institute defines it as a process of hydrating cement because internal water is available. Additional curing water can be provided throughout the concrete mixture using lightweight aggregate for internal curing. Lightweight aggregate has an increased absorption rate of 10% to 30%, making it ideal for internal curing because of its high absorption rate (Kazemian and Shafei 2022). This process is economical, environmentally friendly, and assists concrete in reaching high-quality standards (Bentz and Weiss 2011). The internal curing of concrete can be accomplished by using water absorbed in clay or expanded shale lightweight aggregates, which replace some of the conventional aggregates in the mixture.

Due to growing demands for environmentally friendly and efficient infrastructures, alternative and sustainable construction materials have gained significant attention in recent years. As a result of its inherent porous structure, low density, and cost-effectiveness, scoria gravel has emerged as a potential candidate for internal curing (Alaskar et al. 2021). An analysis of the existing research on scoria gravel's properties, applications, and performance in concrete mixtures is presented in the next section, which highlights its potential as an effective internal curing agent in the construction industry.

2.6.2 Scoria Gravel As Internal Curing Material

One emerging material for internal curing is scoria gravel, a type of volcanic rock that offers several desirable attributes such as high porosity, low specific gravity, and mechanical stability (Tchamdjou et al. 2017). Scoria gravel is an igneous rock formed by the rapid cooling of basaltic lava, characterized by its high porosity, low density, and vesicular texture (Juimo Tchamdjou et al. 2020). Studies have reported that scoria gravel's physical and mechanical properties make it an attractive alternative to conventional aggregates such as crushed limestone, granite, or sand.

Applications of Scoria Gravel in Concrete Mixtures Researchers have assessed various aspects of scoria gravel's implementation, from pre-wetting methods to various replacement percentages in concrete mixtures. A significant volume of literature has addressed the performance of scoria gravel as an internal curing agent by examining various aspects (Alaskar et al. 2021; Juimo Tchamdjou et al. 2020; Tchamdjou et al. 2017), such as mechanical

properties. A common technique involves pre-soaking scoria gravel to achieve optimal saturation levels to facilitate controlled water release (Alaskar et al. 2021). Studies have shown that replacement percentages ranging from 5% to 15% yield satisfactory results, promoting enhanced mechanical properties while mitigating the risk of autogenous shrinkage.

Mechanical Properties Several studies have reported the positive influence of scoria gravel on concrete mixtures' mechanical properties when utilized as internal curing material (Patel et al. 2014; Rahman et al. 2018). The gradual release of water from saturated scoria particles promotes homogeneous cement hydration, resulting in higher compressive and tensile strength than conventional concrete mixtures. These findings indicate the potential of scoria gravel as a viable alternative to traditional aggregates while providing the advantage of internal curing. Table 2.7 provides a summary of the percentage addition of scoria gravel in concrete as a replacement for sand, serving as both a sand replacement and internal curing material in different studies.

Table 2.7 Percentage amount of scoria gravel used in different studies

Percentage addition	Aim	References
Marble: scoria ratio of 2:1, 1:1, and 1:2 were used, and then the combined level of both marble waste and scoria increased from 33 to 67 to 100%.	To investigate normal strength concrete by partially replacing sand with marble waste and scoria	(Yifru and Mitikie 2020)
Based on the proportion of fine particles present in the coarse volcanic scoria. The groups were categorized as low, average, and high.	To compare coarse volcanic scoria mortars' physical, mechanical, and durability properties with a reference mortar. The investigation focuses on the short-term curing period.	(Tchamdjou et al. 2017)
prewetted coarse and fine LWA at dosages of 5, 10, and 20% by volume of CA and FA, respectively	An experimental investigation was conducted to determine the effect of internal curing of natural light-weight aggregates (LWAs) on the shrinkage, mechanical properties, and durability of high-performance concrete (HPC)	(Alaskar et al. 2021)
Fine aggregate was replaced by Scoria and FAA by volume. Scoria content was varied from 5% to 20% at an increment of 5%, and FAA is fixed at 15%.	to measure the durability of self-compacting concrete with lightweight aggregates	(Saravanan et al. 2021)

cement replacement by 25 and 45% by mass (OPC/NPs mortars) and mortars containing VSA as sand substitution at level of 25, 50, 75 and 100% by mass (VS mortars)	volcanic scoria from 'Djoungo' (Cameroon) as cement and fine aggregate replacement	(Juimo Tchamdjou et al. 2020)
-	a review of LWA as internal curing materials for high-performance cement-based materials	(Ma et al. 2019)

2.6.3 Internal curing uses for Corrosion resistance

Internal curing is a technique that aims to improve the hydration and durability of concrete by providing additional moisture within the concrete matrix. Internal curing can be achieved using porous materials such as lightweight aggregates, superabsorbent polymers, or wood fibers, which can store and release water during curing (Bentz et al., 2017). One of the benefits of internal curing is that it can reduce the risk of Corrosion of steel reinforcement in concrete structures. Corrosion occurs when oxygen and moisture penetrate the concrete cover and reach the steel surface, causing electrochemical reactions that degrade the steel and the surrounding concrete (ACI Committee 222, 2010). Internal curing can prevent or delay Corrosion by reducing the permeability and cracking of concrete and maintaining a high pH level around the steel reinforcement (Sawant et al. 2020).

Using lightweight aggregates allows for the sustained release of water, preventing corrosion agents from entering concrete and reducing concrete permeability (Bentz and Weiss 2011). Research findings indicate that internal curing enhances concrete corrosion resistance, highlighting its potential as a preventative measure to ensure the long-term durability of reinforced concrete structures. Since no free water is available at the concrete and reinforcement interface, corrosion initiation will be delayed, unlike external water curing, since Corrosion requires water and oxygen ions to be removed during the anodic reaction (Nie et al. 2016). The ability of concrete to resist shrinkage at an early age is another advantage of internal curing, which can be used to prevent the intrusion of corrosion-causing materials in concrete.

2.7 Measure Of Corrosion And Corrosion Acceleration In Laboratories

Laboratory assessment of corrosion and corrosion acceleration serves several purposes. Firstly, it allows researchers to study and understand various materials' corrosion mechanisms and behavior in controlled laboratory environments (Broomfield 2003). By subjecting materials to accelerated corrosion tests, such as exposure to corrosive solutions or accelerated aging

conditions, researchers can simulate and study the long-term effects of corrosion in a shorter time frame. This helps evaluate the performance and durability of materials, identify potential corrosion issues, and develop effective corrosion protection strategies. Additionally, laboratory assessments of corrosion provide valuable data for validating and improving corrosion models, designing corrosion-resistant materials, and conducting comparative studies between different materials or corrosion mitigation techniques.

2.7.1 Methods For Measuring Corrosion

Corrosion of concrete is a complex process influenced by various factors such as environmental conditions, concrete composition, and the presence of reinforcing steel (Kwon et al. 2017). Several testing methods are available to assess the corrosion potential and evaluate the corrosion status of concrete structures. These methods enable the detection, monitoring, and evaluation of corrosion-related issues in concrete (Kwon et al. 2017). This section provides an overview of standard corrosion testing techniques and methods, which include macroscopic analysis (concrete crack survey and mass loss measurement), microscopic analysis (XRD, SEM, FTIR, TGA), and electrochemical testing (EIS and Tafel plot) employed in concrete corrosion assessment.

2.7.1.1 Macroscopic Corrosion Analysis

As the name implies, macroscopic concrete corrosion analysis is a technique that evaluates and assesses corrosion-related damage and deterioration to concrete structures at a macroscopic level. These methods focus on the visible signs of Corrosion, such as surface discoloration, cracking, spalling, and general degradation. Several standard macroscopic analysis methods used in concrete corrosion assessment are concrete crack survey and mass loss measurement.

Concrete Crack Survey

A crack survey refers to visually inspecting and mapping cracks on a concrete surface. As a result of this method, insight is gained into the extent and pattern of corrosion-induced cracking, enabling the identification of potential vulnerability areas and the overall condition of the structure (Martinez-Molina et al. 2016).

Mass Loss Measurement

Mass loss measurement is commonly employed in concrete structures to determine the extent of Corrosion and quantify the material loss of reinforcing steel (rebar) (Martinez-Molina et al. 2016). By comparing the original and final masses of rebar, it provides a direct measurement of corrosion-induced deterioration.

2. 7.1.2 Microscopic Corrosion Analysis

In microscopic corrosion analysis for concrete, corrosion phenomena are investigated, corrosion products are identified, and mechanisms of deterioration are understood by examining the concrete at a microscopic level. These techniques provide valuable insights into the localized corrosion processes, microstructural changes, and interaction between the reinforcing steel and the concrete matrix. Several microscopic analysis techniques are commonly used for concrete Corrosion, including XRD, SEM, FTIR, and TGA (Martinez-Molina et al. 2015)

X-ray Diffraction Test (XRD)

XRD is a versatile analytical method for identifying and quantitatively determining various crystalline forms in powder and solid samples (Maldonado and Borthwick 2018). Diffraction occurs as waves interact with a periodic structure whose repeat distance is about the same as the wavelength. When specific geometric requirements are met, X-rays scattered from a crystalline solid can constructively interfere, producing a diffracted beam (Figure 2.9).

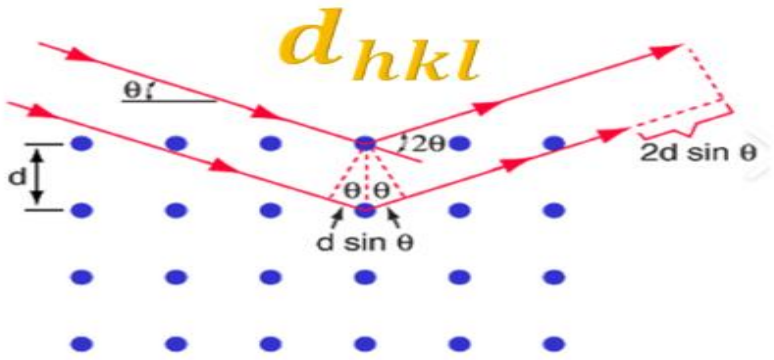

Figure 2.9 XRD Interplanar spacing

The distance between similar atomic planes in a mineral (interatomic spacing), known as d-spacing, is measured in angstroms (Guo et al. 2022). The diffraction angle is theta (θ) and is measured in degrees. For practical reasons, the diffractometer measures an angle twice that of the theta angle, and the measured angle is termed '2-theta (θ)'. The wavelength of the incident X-radiation, symbolized by the Greek letter lambda, is equal to 1.54 Å.

X-ray diffraction (XRD) is a valuable analytical technique widely used to determine the mineralogical composition of materials. In civil engineering, XRD is used to determine the mineralogical composition of concrete, which is one of the primary factors affecting the corrosion of reinforcement bars in concrete structures (Liu et al. 2016). Concrete corrosion is a destructive process that can significantly impact the durability and safety of concrete

structures. Hence, it is crucial to determine the extent of corrosion in concrete structures to take appropriate preventive measures.

XRD analysis can accurately determine the mineralogical composition of concrete, enabling the identification of corrosion products and their impact on the durability of concrete structures. According to a study by Maldonado and Borthwick (2018), the XRD technique was used to determine the mineralogical composition of concrete samples subjected to different corrosion environments, including natural seawater, synthetic seawater, and tap water.

Scanning Electron Microscopy (SEM)

The SEM is a powerful imaging technique capable of providing high-resolution images of the surface morphology of materials (Venkatesh et al. 2022). In corrosion analyses, the SEM can generate images of topography and microstructure changes due to Corrosion. SEM analysis plays a crucial role in several aspects of inhibitor research and corrosion analysis. Firstly, it provides valuable information on how the inhibitor compound adsorbs onto the metal surface, forming a protective film, thus indicating the effectiveness of the inhibitor in minimizing further corrosion. Additionally, SEM is used to analyze the composition and distribution of corrosion products formed on the metal surface during the corrosion process, helping establish a connection between inhibitor performance and the generated corrosion products. Furthermore, SEM enables the study of the impact of different inhibitor concentrations on the corrosion process, aiding in determining the optimal inhibitor concentration for effective corrosion protection. It also facilitates investigating potential synergistic effects between multiple corrosion inhibitors, which can enhance corrosion protection. Finally, SEM analysis helps evaluate the long-term performance of corrosion inhibitors, tracking the degradation of the protective film over time (Ouglova et al. 2006).

Thermogravimetric Analysis (TGA)

TGA is a thermal analysis technique used to study weight changes in materials as a function of temperature (Mannai et al. 2016). In corrosion analysis, TGA is a technique used to examine the mass loss caused by the degradation of material exposed to Corrosion as a function of temperature. In order to determine the thermal stability, degradation temperature, and volatile components associated with the corrosion products of a sample, TGA is subjected to a controlled temperature program. Additionally, TGA provides information regarding the kinetics of corrosion processes and the effectiveness of corrosion inhibitors.

Fourier Transform Infrared Spectroscopy (FTIR)

FTIR is a spectroscopic technique that measures infrared light absorption and transmission by materials (Witkowski and Koniorczyk 2018). It is possible to detect and characterize corrosion products, such as oxides, hydroxides, or carbonates, by analyzing the infrared spectra of corroded samples. In corrosion analysis, FTIR can identify functional groups and chemical bonds in corrosion products (Ahmadi Moghadam et al. 2020). In addition to providing information about the molecular structure, surface functional groups, and chemical changes caused by Corrosion, FTIR can also provide information about the surface.

2.7.1.3 Electrochemistry Measurement

Corrosion is essentially an electrochemical reaction in the context of a reinforcement exposed to an aqueous environment (Goyal et al. 2018). This process oxidizes the metal, and dissolved oxygen or hydrogen ions are simultaneously reduced. Therefore, electrochemical techniques effectively analyze corrosion processes (Srinivasan and Punathil Meethal 2022). Various methods are available to address the Corrosion of metals, either for measuring corrosion rates or understanding the mechanism involved in Corrosion (Koleva et al. 2007). It is possible to study corrosion behavior in metals, alloys, and coatings using traditional electrochemical techniques such as electro-impedance spectroscopy (EIS), linear polarization (LP), and potentiodynamic polarization (PDP).

Electro-Impedance Spectroscopy

Electrochemical Impedance Spectroscopy is widely used to measure and analyze materials' electrochemical behavior, including concrete reinforcement corrosion (Koleva et al. 2007). It is a method of measuring the current response of the material under test by applying a small amplitude AC signal; This AC signal can be used to a range of frequencies, typically from a few millihertz to several megahertz (Dhouibi et al. 2002). As a result of the obtained current response, the system's impedance is calculated at each frequency using the received current response. In EIS, impedance consists of two components: the real part (resistance) and the imaginary part (reactance). By plotting the impedance data on a Nyquist or Bode plot, analysts can analyze the frequency-dependent behavior of the system and extract valuable information about corrosion processes (Ye et al. 2013). EIS is the only method to directly and accurately measure solution resistance, which is necessary to calculate polarization resistance values (Rp). Besides providing detailed information regarding electrode-electrolyte interfaces, EIS can also help explain the formation of porous and nonporous films on surfaces and corrosion reactions (Song 2000).

Electrochemical Impedance Spectroscopy (EIS) utilizes circuit elements for circuit fitting to illustrate various aspects of the electrochemical system under investigation. These elements are essential to comprehend and modeling the impedance response observed during EIS measurements (Harrington and Van Den Driessche 2011). An AC voltage is applied to a system during an EIS experiment, and the resulting current is measured (Song 2000). Based on the results of this measurement, an equivalent circuit model representing the system can be used for analysis. Fitting this model to the data involves adjusting the values of the circuit elements until the model accurately represents the experimental data (Park and Yoo 2003).

As a result, valuable information can be obtained concerning the system under study and its electrochemical behavior. The elements of circuits are: Resistors (R) are fundamental circuit elements representing the system's ohmic resistance (Berradja 2019). They include electrolyte solution, electrode, and other conductive components. A capacitor (C) is also a crucial circuit element (Ye et al. 2013). It represents the capacitance of the double layer formed at the electrode-electrolyte interface, and it is related to charge storage and relaxation at this interface. In electrochemical circuit fitting, the inductor (L) represents inductance, which is seldom significant in most electrochemical processes (Park and Yoo 2003). As an alternative representation of a capacitor, the Constant Phase Element (CPE) is used to account for non-ideal behavior or the distribution of relaxation times in a system (Dhouibi et al. 2002). In addition to describing purely capacitive responses, it can define more complex behaviors. Warburg Element (W) represents diffusion-limited processes within a system, capturing the transport of ions or species from a bulk electrolyte to the electrode surface, thereby facilitating the analysis of mass transport limitations (Park and Yoo 2003). During EIS analysis, these circuit elements contribute to interpreting and understanding the electrochemical system's characteristics and behavior.

Tafel Analysis

Tafel tests are based on the equation describing the relationship between corrosion currents (i_corr) and metal electrodes' corrosion potentials (E_corr). According to the Tafel equation, corrosion currents are proportional to applied potentials, and the slope of the Tafel plot provides information on corrosion kinetics (Li et al. 2018). It is possible to determine corrosion rate and polarization resistance by determining the slopes of the anodic and cathodic Tafels.

Analyzing the Tafel plot obtained from the test makes extracting essential parameters related to concrete Corrosion possible. Tafel slopes provide information regarding corrosion kinetics,

such as corrosion current density and anodic and cathodic reaction rates (Li et al. 2018). The corrosion potential (E_corr) is the temperature at which the anodic and cathodic reactions are balanced, representing corrosion thermodynamics. An essential parameter for assessing the corrosion resistance of reinforcing steel is the polarization resistance derived from the Tafel slopes. The following Table 2.8 shows the summarized corrosion measurement for reinforced concrete.

Table 2.8 Reinforced concrete corrosion measurements.

Type	Name of method	Means of measurement	References
Macroscopic	Mass loss measurement	Measuring the reduction in the mass of reinforcement samples, which indicates the extent of corrosion or degradation	(Torres-Acosta 2007)
	Mortar crack survey	Visually inspecting the concrete surface to identify and quantify any cracks or fissures that may have formed, providing information about the structural integrity.	(Martinez-Molina et al. 2016).
Microscopic	XRD	used to analyze the crystalline structure of materials, including concrete. It helps identify the composition and phases present in the concrete, aiding in assessing its properties.	(Maldonado and Borthwick 2018), (Guo et al. 2022)
	SEM	A high-resolution imaging technique is used to examine the microstructure of concrete. It provides detailed information about the concrete's morphology, composition, and surface characteristics.	Ouglova et al. 2006), (Venkatesh et al. 2022)
	FTIR	A spectroscopic technique that analyzes the infrared absorption spectrum of a material. Concrete analysis, it helps identify the chemical functional groups present and provides information about the concrete's composition and degradation processes.	(Ahmadi Moghadam et al. 2020)., (Witkowski and Koniorczyk 2018)
	TGA	A thermal analysis technique is used to determine the weight changes in a material as a function of temperature. It can be used to analyze concrete's moisture content, decomposition, and other thermal properties.	(Mannai et al. 2016)

Electrochemistry measurement	EIS	Measures the impedance of a concrete sample in response to an applied AC voltage. It provides information about the electrochemical properties, such as corrosion rate.	(Ye et al. 2013), (Dhouibi et al. 2002), (Berradja 2019)
	Tafel plot	Used to determine the corrosion rate and corrosion potential of a material. It involves measuring the current response at different applied potentials, providing insights into the corrosion behavior of concrete.	(Li et al. 2018), (Dhouibi et al. 2002),

2.7.2 Corrosion Acceleration in Laboratories

The term corrosion acceleration in a laboratory refers to the deliberate increase in corrosion rates under controlled experimental conditions (Hong et al. 2020a). Researchers can study and analyze corrosion processes and behaviors in a shorter period than in natural environments. Accelerated tests provide valuable insights into corrosion mechanisms, facilitate the evaluation of various materials and protective coatings, and contribute to developing corrosion prevention strategies (Hong et al. 2020b). This approach, however, has both advantages and limitations.

Accelerated corrosion tests have their limitations when studying corrosion in realistic conditions. These tests cannot fully replicate the actual field conditions, as factors like temperature, humidity, and the presence of other chemicals may not be accurately simulated. Additionally, the relatively short duration of these tests restricts the ability to assess the long-term behavior of concrete structures (Feng et al. 2021b). Furthermore, accelerated corrosion tests often result in higher corrosion rates compared to natural conditions, leading to overestimation of corrosion rates and more conservative predictions regarding the service life of concrete structures (Yuan et al. 2007a).

The main advantage of accelerated corrosion techniques used in concrete research provides several benefits, including saving time, reducing costs, enhancing understanding of corrosion factors, and enabling controlled experiments in laboratory settings. These techniques help researchers obtain results more quickly, optimize resource allocation, gain insights into the causes of corrosion, and study the impact of environmental factors (Hong et al. 2020a; b; Yuan et al. 2007a).

2.7.2.1 Salt Spray Method

Materials are subjected to a continuous or intermittent saltwater mist during salt spray testing, known as salt fog testing or ASTM B117 testing. This method accelerates Corrosion by

exposing the samples to a highly corrosive environment containing chloride ions, which is known to accelerate corrosion processes, especially in metals. In most cases, the samples are placed in a saltwater chamber.

2. 7.2.2 Impressed Current Method

In concrete structures, the impressed current method may also be used to evaluate the corrosion behavior of reinforcing steel. Researchers and engineers can utilize this technique to assess the effectiveness of corrosion protection measures and study corrosion mechanisms related to concrete environments. The impressed current method applies a controlled direct current to the reinforcing steel embedded within concrete. The external current creates anodic polarization potential on the steel surface, simulating electrochemical conditions that promote Corrosion (Hong et al. 2020b; Regina et al. n.d.).

A comprehensive understanding of corrosion prevention strategies and the construction of durable concrete structures is essential. There are numerous applications of the impressed current method for concrete corrosion analysis. With this device, reinforcing steel can be evaluated for corrosion resistance, corrosion inhibitors or protective coatings can be assessed for effectiveness, and concrete mix designs can be compared (Feng et al. 2021b).

2.8 Literature Gap

Numerous studies propose various methods for cost-effective and efficient corrosion protection. However, their effectiveness largely depends on their suitability for particular environments and environmental conditions. The challenge remains to identify corrosion protection strategies for concrete structures that are cost-effective, easily applied, involve readily available materials, and exhibit long-lasting performance. The literature thoroughly examines the challenges and limitations of different corrosion protection methods for reinforced concrete, highlighting the need for cost-effective, environmentally friendly solutions with straightforward implementation and sustained effectiveness.

Design complexity, installation challenges, and limited suitability for certain structures hinder the effectiveness of cathodic protection. Corrosion inhibitors necessitate accurate selection based on materials and environmental conditions, and their efficacy is restricted in highly corrosive environments. Consistent monitoring and modification of inhibitor concentrations are required; however, they provide a cost-effective solution, depending on the cost of raw materials. Reinforcement Coatings face difficulties in surface preparation and application on complicated structures, with restrictions concerning localized corrosion if damaged and limited

protection in harsh environments. Periodic inspection, repair, and reapplication are needed to maintain functionality, while the coating type and application technique determine the cost. Corrosion-resistant bars need proper design, material choice, and production certification. They have higher initial expenses but minimal maintenance due to their inherent resistance, necessitating inspection of areas prone to corrosion. Although they offer savings in maintenance and replacement costs, utilizing premium materials requires a substantial initial investment. To address these challenges, researchers have turned attention to natural corrosion inhibitors. Among these, Opuntia ficus-indica (OFI), a plant widely available worldwide and known for its ability to thrive in harsh environments, has emerged as a promising option.

In the case of using Opuntia ficus-indica (OFI) as a corrosion inhibitor, various methods have been employed, such as exudate OFI mucilage, cooked OFI mucilage, and dehydrated OFI powder (Martinez-Molina et al. 2015, 2016; Torres-Acosta 2007; Torres-Acosta and Alejandra Díaz-Cruz 2020; Torres-Acosta and González-Calderón 2021). Based on its effectiveness and ease of use in concrete inhibition, cooked OFI mucilage is considered the best possible solution (Martinez-Molina et al. 2016; Torres-Acosta and Alejandra Díaz-Cruz 2020; Torres-Acosta and González-Calderón 2021). However, research using cooked OFI mucilage as a partial replacement for water has not considered the potential effects on concrete due to water deficiency, such as autogenous shrinkage and the loss of structural strength over time. Additionally, many studies focus on the addition of OFI to mortar specimens, controlling the slump using a mortar flow table. It has been observed that the mortar achieves a water/cement ratio of 0.88 (Martinez-Molina et al. 2015; Torres-Acosta 2019; Torres-Acosta and González-Calderón 2021), which poses a problem for implementation in concrete mix designs at construction sites. Furthermore, the investigation of the corrosion-inhibiting ability of Opuntia ficus-indica in concrete, including the oxide/hydroxide formation of cooked mucilage, the interaction with steel in concrete, passive film creation capacity, and subsequent hydration products, has not been thoroughly explored.

Although electrochemical impedance spectroscopy (EIS) is a powerful tool for examining the corrosion process, the assumption of the elemental composition in concrete during EIS testing, and the assessment of equivalent circuit models for determining future outcomes in concrete after exposure to corrosive environments, have not been sufficiently investigated. As a result, there is a clear gap in identifying these elements using electrochemical analysis. Furthermore, advanced and easy-to-implement tests, such as precision measurements of reinforcing bars, Fourier Transform Infrared Spectroscopy (FTIR) for material analysis and composition

identification, and Scanning Electron Microscope (SEM) imaging before and after corrosion exposure, have not been conducted in any research investigating the inhibition capacity of OFI corrosion inhibitors. One potential avenue for future investigation involves incorporating internal curing materials into concrete mixtures containing Opuntia ficus-indica as a corrosion inhibitor. While studies have shown that using internal curing materials in concrete promotes effective hydration and can prevent the corrosion of reinforcement, no research has yet examined the implications of using OFI in conjunction with these materials.

2.9 Summary

This chapter encompasses an extensive literature review covering various aspects of corrosion, including the general concept of corrosion, factors influencing corrosion rates in concrete, and different corrosion protection methods. Particular emphasis is placed on the potential of Opuntia ficus-indica as a natural corrosion inhibitor and the mechanism of internal curing in concrete. Additionally, the use of scoria gravel as an internal curing material is explored, along with its benefits in corrosion inhibition. The chapter concludes by highlighting the literature gaps concerning corrosion protection methods and the investigation of Opuntia ficus-indica as a corrosion inhibitor. The subsequent chapter will delve into the methodology employed in this study, aiming to achieve the objectives through experimental and analytical work.

CHAPTER THREE
MATERIALS AND METHODS

3.1 Introduction

The literature review in the previous chapter has discussed various past studies and research gaps in relation to project delivery methods. Based on the identified research gaps, Chapter 1 outlines the research objectives set for this study. This chapter elucidates the methodology adopted to accomplish the study's objectives. This chapter consists of five sections structured to achieve the study's objectives using an experimental and analytical research design.

The first section provides an overview of the materials used in the study for manufacturing plain concrete and reinforced concrete samples. The sources and collection methods of Coarse Aggregate, Fine Aggregate, Fine Aggregate, Scoria Gravel, Cement, Water, Carbon Steel, and Opuntia ficus-indica are presented following the specified guidelines and standards.

In the second section, the study enters phase one of the experimental and analytical work methods. This involves characterizing the materials used to create concrete and reinforced concrete samples, including coarse aggregate, fine aggregate, and water. The results are examined to ensure the collected materials meet the specified standards. Furthermore, the preparation of scoria gravel and Opuntia ficus-indica is explained, and their characterization and test results are outlined for further discussion in the subsequent chapter.

The third section describes phase two of the study, covering concrete mix design, batching, mixing processes, and the specifications of plain and reinforced concrete sample geometries. This section primarily investigates the first objective of determining the internal curing effect of FASG and outlining the methodologies for testing hardened and fresh concrete.

The fourth section outlines phase three of the experimental and analytical work methods, focusing on the morphological study using macroscopic and microscopic analyses. Macroscopic methods such as mortar crack surveys and mass loss measurements are used, alongside microscopic techniques like X-ray diffraction (XRD), Scanning Electron Microscopy (SEM), Fourier Transform Infrared Spectroscopy (FTIR), and optical microscope analysis. The section also covers sample preparation and testing for electrochemistry tests, including electrochemical impedance spectroscopy, Tafel plot analysis, and precision source measurement methods. These methodologies are essential in addressing the study's second and third objectives. The fifth section of this chapter outlines the statistical analysis methods and

software tools used in the study for conducting different tests and justifies the choice of these specific techniques and tools. The following Figure 3.1 shows the framework of the overall research design of the study in graphical form.

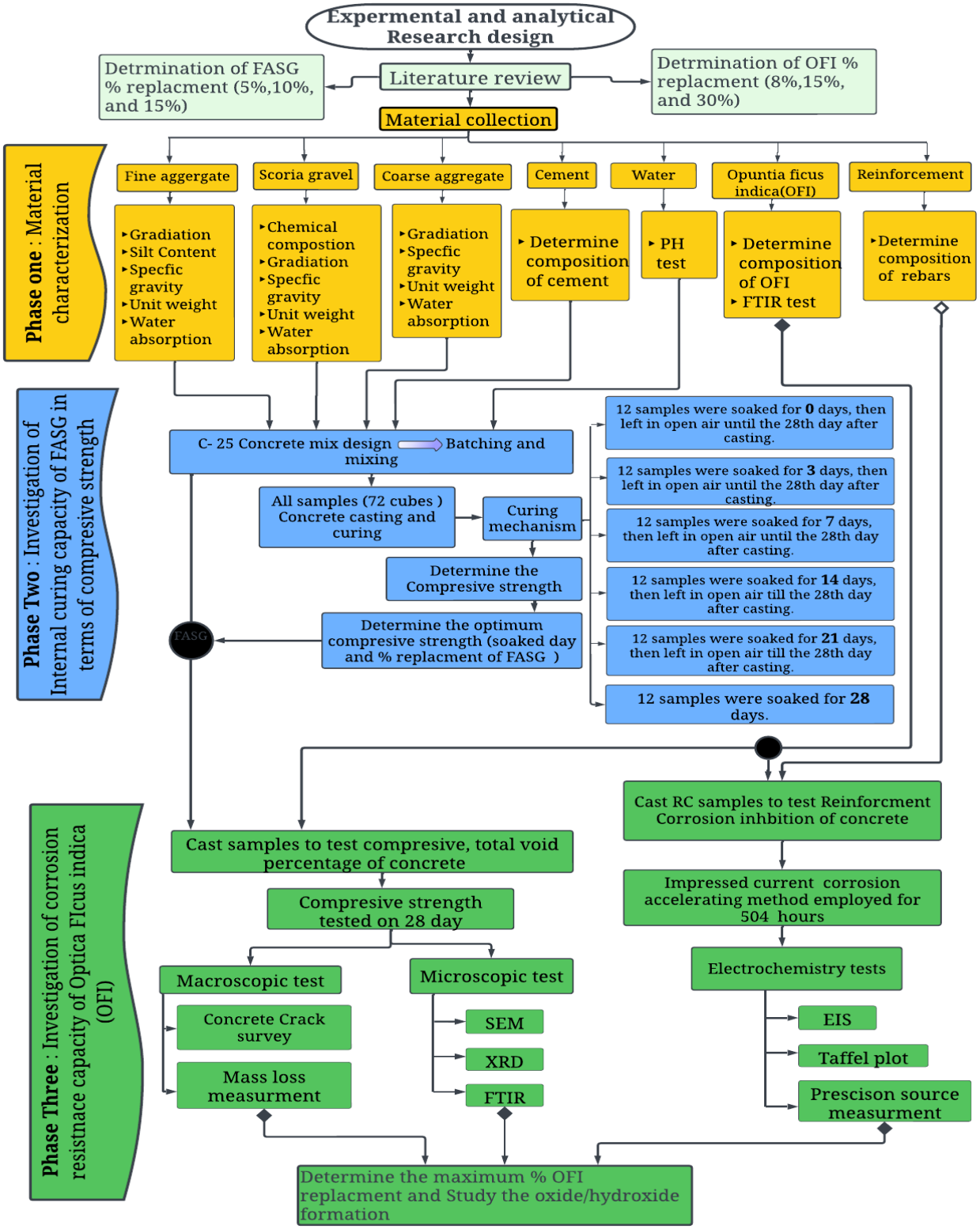

Figure 3.1 Experimental and analytical research design framework

3.2 Materials And Techniques

The following sections comprehensively describe the materials and methods used to investigate corrosion prevention in reinforced Concrete using Opuntia Ficus-Indica with a partial internal curing mechanism. This section describes concisely and informally how the experiment was conducted following relevant standards. It includes descriptions of the materials, equipment, experimental design, sample testing methods, and testing procedures.

3.2.1 Coarse Aggregate

Coarse aggregate is a granular material found in nature and obtained from riverbeds (Sand, gravel) or quarries (crushed rock) consisting of finely divided rock and mineral particles ranging in size from 4.75 mm to 40 mm. This study used crushed gravel coarse aggregate sourced from a nearby quarry site in Adama, Ethiopia. Before use, the aggregate was subjected to a thorough quality assessment as per ASTM C33. This study asses this aggregate to be highly durable and free of any chemicals, clays, silts, or organic matter that could negatively impact its properties.

3.2.2 Fine Aggregate

Fine aggregate is a granular material typically smaller than coarse aggregate, with particle sizes ranging from 0.075mm to 4.75 mm. Find aggregates obtained from natural sources such as riverbeds or manufactured quarries. This study selected locally available river sand from the Metahra region of Ethiopia. The selection was based on the criteria set by the ASTM C 33 standard. Following the standard ensures that the Sand is free of silt, clay, and other organic contaminants. In the present study, the absence of these impurities will be confirmed as an essential condition for using the Sand.

3.2.3 Scoria

Scoria gravel is a pyroclastic material or tephra formed by cooling magma fragments (Tchamdjou et al. 2017) after explosive volcanic eruptions. It forms from lava that contains many gas bubbles, such as water vapor, carbon dioxide, and sulfur dioxide. When the lava cools, these gases expand, forming bubbles within the lava that become trapped and freeze in place, creating a spongy texture in the rock. Due to its unique spongy texture, scoria gravel is an excellent choice for lightweight gravel (Luo et al. 2020; Tchamdjou et al. 2017). Typically, scoria gravel is red or black in areas subjected to recent volcanic activity(Juimo Tchamdjou et al. 2020). This study used dark Scoria sourced locally from Debrezeyit, Ethiopia. The chemical composition and characterization of sand replacement will be assessed using ASTM C330-04.

3.2.4 Cement

Cement is a dense powder made primarily from a calcareous material such as limestone or chalk. Furthermore, Alumina and Silicon are clay or shale from argillaceous material. Despite their excellent mechanical properties and availability, Portland pozzolan cement and ordinary pozzolan cement are the most used types of cement (Elango et al. 2021). During this study, both PPC cement was were obtained from the local market for the phase two study and OPC cement used for the phase one study in Adama, Ethiopia, and stored in a dry, well-ventilated area, according to ASTM C-150 guidelines, which include protecting cement from moisture and atmospheric agent, storing them in an airtight container to prevent humidity exposure and keeping them off the ground and away from the wall to allow the proper air circulation and to avoid moisture buildup. (The research was conducted using the cement available in the market during the study period, without any specific preference for cement type).

3.2.5 Water

Drinkable Water can generally uses for Concrete. It reacts chemically with cement, which will ultimately set and harden. It also acts as a lubricant and makes the concrete work. To select water for this experiment, ASTM C1602 has followed to determine the pH value of water in the range of 6.5-8.5 and to ensure that salt, oil, industrial waste, and alkaline sulfides do not accumulate in large quantities in the water found in Adama science and technology university. Water is used for two primary purposes.

3.2.6 Carbon Steel

Carbon steel is a type of steel primarily alloyed with carbon. The reinforcement bar used in this experiment was Ethiopia Iron Steel Factory's Grade 60 (420) since it is a widely used reinforcement type for C-25 Reinforced structure, with a diameter of 14mm in its original form, without any surface treatments or modifications. The experiment is carried out using this reinforcement bar following ASTM A615 standards.

3.2.7 Opuntia Ficus-Indica (OFI)

This study used Opuntia ficus-indica from Adama town, found in nature on the hills and mountains of Adama town, to obtain cactus mucilage. Cactus mucilage is a thick, sticky substance found in their tissues. It is a viscous, water-soluble substance comprising complex polysaccharides, glycoproteins, and other organic compounds with excellent water retention, a high molecular weight from 2.3×10^4 to 4.3×10^6 g/mol, and poly-electrolyte properties(Martinez-Molina et al. 2016; Torres-Acosta and González-Calderón 2021). It

comprises arabinose, galactose, galacturonic acid, rhamnose, and xylose residues (Hernández et al. 2017)

3.3 Material Characterization: Phase One

This section describes the study's first Phase, which focuses on the ordinary primary materials used in casting regular Concrete: coarse aggregate, cement, fine aggregate, and water. During the evaluation of each material, its characteristics will be explained numerically and graphically to ensure that the materials used meet ASTM standards.

3.3.1 Tests On Coarse Aggregate

In this section, physical tests were conducted on the coarse aggregate. These tests included determining the unit weight, specific gravity, and sieve analysis of the aggregate. No additional tests were performed since the study utilized non-toxic and pure aggregate obtained from a local crushed stone provider.

3.3.1.1 Unit Weight Of Coarse Aggregate Test

The grading, shape, and texture of the aggregate determine the unit weights of coarse aggregate. For this reason, unit weight tests are necessary to ensure that concrete mix designs are optimized for the coarse aggregate used. The study's results, in accordance with ASTM C29, show a range of unit weights for the aggregate, ranging from 1200 to 1750 kg/m^3. Table 3.1 confirms that the selected coarse aggregate met the ASTM criteria.

Table 3.1 Unit weight of coarse aggregate

Indications	Quantity	Calculation
I= Volume of the container	0.01 m^3	UWCA= $\frac{s-N}{I}$
S= Aggregate plus container weight	22.41 Kg	UWCA= $\frac{22.415-5.605}{0.01}$
N= Weight of the empty container	5.605 Kg	UWCA= 1681 kg/m^3

3.3.1.2 Specific Gravity And Water Absorption Test For Coarse Aggregate

The experiment utilized ASTM C127, a standard test method for measuring coarse aggregate specific gravity and absorption. Based on the results obtained and presented in Table 3.2, the bulk specific gravity and saturated-surface-dry bulk specific gravity (SSD) meets the requirements of ASTM C127 water absorption 0.6-6% and SSD with 2.4-2.9 range.

Table 3.2 Specific gravity and water absorption for coarse aggregate results

Description	Amount	Formulas	Calculations
A: weight of oven-dried test sample in air	5 Kg	Bulk specific gravity = $\frac{A}{B-C}$	Bsg= $\frac{5}{5.08-3.3} = 2.80$
B: Weight of SSD sample in air	5.08 Kg	Bulk Specific gravity (SSD) = $\frac{B}{B-C}$	$\mathbf{B_{SSD}}= \frac{5.08}{5.08-3.3} = 2.85$
C: Weight of saturated sample in Water	3.3 Kg	Absorption % = $\frac{B}{B-A}$ X 100	Abn. %$\frac{5.08}{5.08-5}$ x 100 = 1.6%

3.3.1.3 Coarse Aggregate Gradation Test

As part of the ASTM C33 procedure, the experiment utilized apparatus such as a balance, a series of sieves, a shovel, and a sieve brush. A round opening sieve was used to measure the aggregates' particle size distribution to investigate the coarse aggregate's gradation. Table 3.3 illustrates the grading of aggregates and fines modulus, which indicates aggregates' fineness, coarseness, and uniformity. And as per ASTM, fineness modulus lies in the range of 5.5-8

Table 3.3 Sieve analysis calculation for coarse aggregate (astm c33)

Sieve Size (mm)	Weight Retained (g)	Percentage of Retained	Cumulative Percentage Retained	Cumulative Percentage Passing	ASTM C33 Range
20	0	0	0	100	100
19	150	3	3	97	95-100
12.5	1900	38	41	59	4.-80
9.5	1705	34.1	75.1	24.9	20-55
4.75	1235	24.7	99.8	0.2	0-10
Pan	10	0.2	100	0	0
Total	5000				
Total cumulative percentage retained by mass = 718.9					

Fines modulus $= \sum_{sive\ size\ 0.15}^{sive\ size\ 20}(\text{cumulative percentage retained by mass})/100$

= 718.9/100 = 7.189

The gradation curve of the coarse aggregate used was within the ASTM lower and higher-grade requirements, as shown in Figure 3.2.

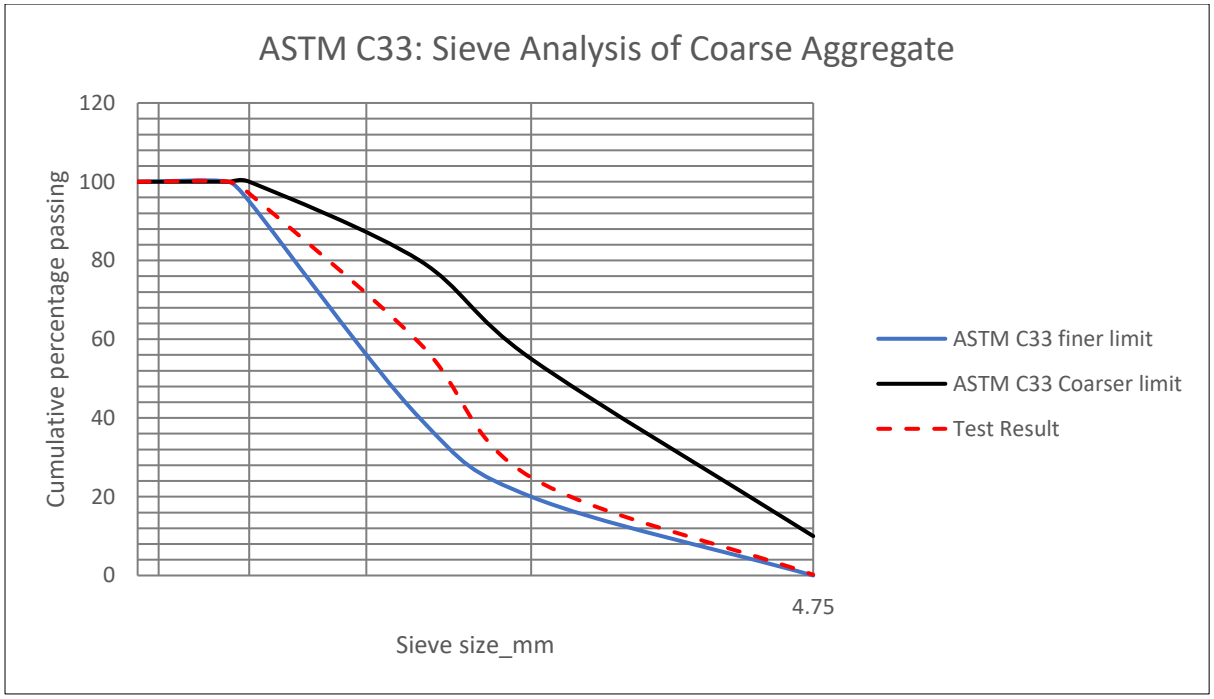

Figure 3.2 Gradation Curve for Coarse Aggregate According to ASTM C33 Range

3.3.2 Tests On Fine Aggregate

This section presents the results of physical tests performed on the fine aggregate, which included assessing its silt content, conducting sieve analysis, and measuring unit weight, specific gravity, and water absorption. These specific tests were chosen within the scope of this study because they provide crucial insights into the fine aggregate's quality, suitability, and behavior when incorporated into concrete mixtures. By analyzing these parameters, the researcher can make informed decisions regarding properly utilizing and proportioning the fine aggregate, thereby ensuring optimal performance and desired outcomes regarding the concrete's strength, workability, and durability.

3.3.2.1 Silt Content Of A Sand

Sand is a common natural resource found in glaciers, rivers, lakes, seas, and windblown deposits. However, these sources often contain impurities like dust, loam, or clay, which are finer than sand. These finer particles can weaken the bond between materials, reducing concrete strength and quality. The silt content was determined according to ASTM C117 to ensure the study's sand met the required standards. The results confirmed that the sand used met ASTM standards, which recommend rejecting sand if the silt content exceeds 6%, as indicated in Table 3.4.

Table 3.4 Silt content of sand

Items	Trial 1	Trial 2	Trial 3	Average
A = Volume of separated layer (ml)	6	6.5	6	6.1667
B = amount of fine aggregate (ml)	300	300	300	300
Silt content (%) == $\frac{A}{B} * 100\%$	2%	2.17%	2%	2.05%

3.3.2.1 Unit Weight Of Fine Aggregate Test

The unit weight of fine aggregate measures how much space it will occupy in concrete. To determine this, the ASTM C29 standard was followed. According to Table 3.5, the unit weight of fine aggregate falls within the range of 1120-1600 kg/m3, which complies with the ASTM C29 standard.

Table 3.5 Unit weight of fine aggregate calculation and result

Indications	Quantity	Calculation
I= Volume of the container	0.01 m^3	UWFA= $\frac{S-N}{I}$
S= Aggregate plus container weight	20.760 Kg	UWFA= $\frac{20.760-5.605}{0.01}$
N= Weight of the empty container	5.605 Kg	UWFA= 1515.5 kg/m^3

3.2.2.2 Specific Gravity And Water Absorption Test For Fine Aggregate

As per ASTM C128-15, the specific gravity of an aggregate is calculated by dividing its mass by the volume of water. On the other hand, absorption refers to the increase in mass of an aggregate due to water present in its pores. The specific gravity range specified in ASTM C128-15 for aggregates is 2.5-3. Based on these criteria, the selected material meets the requirements, ensuring suitability.

Table 3.6 Specific gravity and water absorption for coarse aggregate results

Description	Amount	Formulas	Calculations
A: weight of oven-dried test sample in air	490 g	Bulk specific gravity = $\frac{A}{B+D-C}$	Bsg= $\frac{490}{1507.5+500-1829.9}$ = 2.75
B: Weight of the pycnometer filled with water to the calibration mark	1507.5 g	Bulk Specific gravity (SSD) = $\frac{D}{B+A-C}$	B_{SSD}= $\frac{500}{1507.5+490-1829.9}$ = 2.98

C: weigh of pycnometer filled with sample and water to the calibration mark	1829.9 g	Apparent Specific gravity = $\frac{A}{B+A-C}$.	Asg=$\frac{490}{1507.5+490-1829.9}$ = 2.91
D: Weight of SSD sample in air	500 g	Absorption % = $\frac{B}{B-A} * 100$	Abn = $\frac{500-490}{490} * 100$ = 2.04%

3.3.2.3 Fine Aggregate Gradation Test

The particle size distribution of the fine aggregate was determined using a sieve test method. A fine aggregate sample was weighed and passed through a series of sieves with gradually smaller openings ranging from 4.75 mm to 0.075 mm in diameter. The arrangement of the sieves followed the guidelines of ASTM C33, and the fines modulus of the fine aggregate fell within the range of 2.3-3.1. The results are presented in tabulated form in Table 3.7, where the fines modulus of 2.985 is within the specified range. Additionally, the gradation of the aggregate is graphically represented in Figure 3.3, showing that it falls between the upper and lower limits set by ASTM C33.

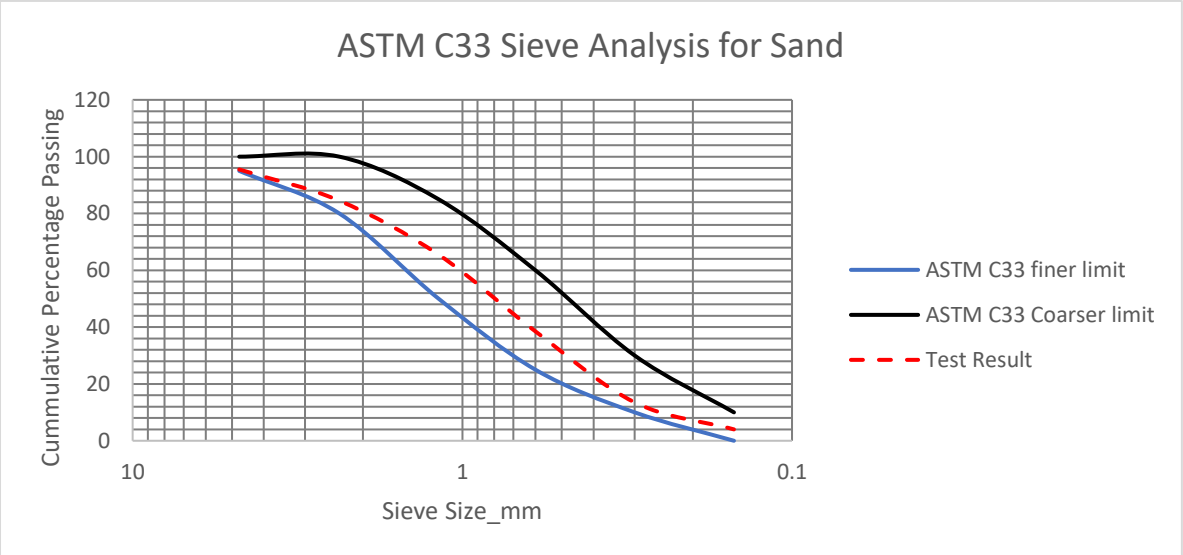

Figure 3.3 Gradation Curve for Fine Aggregate According to ASTM C33

Table 3.7 Sieve analysis of fine aggregate

Sieve Size (mm)	Weight Retained (g)	Percentage of Retained	Cumulative Percentage Retained	Cumulative Percentage Passing	ASTM C33 Range
4.75	45	4.5	4.5	95.5	95-100
2.36	110	11	15.5	84.5	80-100

1.18	190	19	34.5	65.5	50-85
0.6	270	27	61.5	38.5	25-60
0.3	250	25	86.5	13.5	10-30
0.15	95	9.5	96	4	0-10
Pan	40	4	100	0	0
Total	5000				
Total cumulative percentage retained by mass = 298.5					

Fines modulus $= \sum_{sive\ size\ 0.15}^{sive\ size\ 4.75}(\text{cumulative percentage retained by mass})/100$

= 298.5/100 = 2.985

3.3.3 Test On Water

One of the essential components of Concrete is Water, which should be mixed and cured at PH between 6.5 and 8.5 as per ASTM C1602. Concrete's binding properties lose their strength when the pH rises too high, and corrosion occurs when the pH falls below 6. In this study, a PH meter was used to measure the pH of mixing and curing tap water, and the result was 6.89.

3.3.4 Preparation Of Scoria Gravel

Fine scoria aggregate (FASG) particles are initially placed within a container, as shown in Figure 3.4.

Figure 3.4 Preparation of Scoria

Water was added to the container to ensure the particles were completely saturated. The system was then subjected to constant pressure for 24 hours. Following saturation, excess water was removed from the fine scoria aggregate using a sieve and then a towel drying method, as shown in Figure 3.4. A cone test procedure determined the fine scoria aggregates' SSD (Saturated

Surface Dry) condition. A large diameter cone was placed on a plate, and 25 tiny drops of tamper were applied to lightly compact the fine scoria aggregate into the mold. The fine scoria aggregate was placed approximately 0.5 cm above the surface, and the mold was lifted vertically. If slumping was observed, it was concluded that the SSD condition had been met. The same procedure was followed by Alaskar et al. (2021)

3.3.5 Preparation Of Opuntia Ficus Mucilage

This study used fresh, locally available Opuntia Ficus-Indica leaves without spines to extract Opuntia Ficus-Indica mucilage following the method used by Martinez-Molina et al. 2015, (2016; and Torres-Acosta and Alejandra Díaz-Cruz (2020) as shown in Figure 3.5. The OFI mucilage was extracted using the following steps: First, the leaves were meticulously cleaned to ensure that any dust or other residues were eliminated. Then, the leaves were cut into small pieces measuring 2 cm x 2 cm x 2 cm for maximum gel extraction. Next, the cut pieces were mixed with water in a weight ratio of 1:1 (OFI to water) to achieve the desired concentration of mucilage. After preparing the mixture, it was boiled for approximately 45-50 minutes. Finally, the final product (slime and thicket cubes) was drained to obtain only the slime, which was stored in glass containers to prevent decomposition. A Fourier transform infrared (FTIR) test was used to identify the functional group of the Optunia Ficus Indica (OFI) matrix.

Figure 3.5 Preparation of opuntia ficus indica

3.4 Physical Test For Concrete: Phase Two

In this section, the experimental work conducted in the study is presented. It includes the concrete mix design, batching and mixing procedures, specimen geometry, and the types and quantities of materials used. The tests performed on the fresh and hardened concrete, such as workability and compressive strength, are also described. Additionally, the total void percentage test, in accordance with the specified standards and specifications, is presented to assess the quality of the tested specimens.

3.4.1 Concrete Mix Design

The author used the C-25 concrete mix design in this study because it is a widely used type of concrete in the construction sector (Demissew 2022). This study maintained the w/c ratio at 0.491 for all mixes containing 376.78 kg of cement. Eight mixes were prepared, including a control mix, to investigate the potential of scoria gravel as an internal curing material for concrete mixes, as Alaskar et al. (2021) previously studied. As per the findings of the Alaskar study, sand can be replaced with 5%, 10%, and 15% of scoria gravel as a fine aggregate in a concrete mix. Similarly, the current study replaced fine aggregate with 5%, 10%, and 15% scoria gravel in a concrete mix.

In the case of mix design incorporating Opuntia ficus-indica (OFI) in the concrete mix, replacing Water with OFI was carried out at 8%, 15%, and 30%, according to prior research by Martinez-Molina et al. (2015); and Torres-Acosta and Alejandra Díaz-Cruz (2020). A weight substitution of the percentage in place of water is also used to replace the OFI in concrete mix designs. The mix design standard of ACI 211 is followed, and all mix design procedures are presented in Appendix A. The mix ratio is presented in the following Table 3.8

Table 3.8 Mix ratio for C-25 concrete grade

Ingredients	Cement	Fine aggregate	coarse aggregate
Amount/m^3	376.78/376.78	867.2188/376.78	996.0235/376.78
Ratio	1	2.30165	2.64351

3.4.2 Batching and Mixing

Mixing concrete involves combining cement, fine aggregate, coarse aggregate, water, and other elements to produce high-quality and effective concrete. In this study, the concrete ingredients used a mixer to obtain homogeneous, high-quality concrete while following ASTM C-305

throughout the mixing process. The batching cubes and process is presented in Appendix B in figure form.

3.4.3 Specimen Geometry

Two types of specimens were fabricated: 84 concrete cubes (72 concrete cubes to determine of internal curing effect of FASG and 12 concrete samples to test the physical properties of concrete with the combined effect of FASG and OFI) measuring 15 x 15 x 15 cm and 12 reinforced concrete prisms measuring 7 x 7 x 7 cm, as shown in Figure 3.6. Seventy-two cubes were used to characterize the Concrete with and without scoria gravel additions to determine curing days. As part of the second Phase, 12 concrete cubes were used with, and without opuntia, ficus indica additions to characterize the concrete inhibition capability of Concrete in addition to physical characterization, and the concretes tested were subjected to electrochemical characterization using 12 reinforced prisms. One 14 mm diameter reinforcement bar, with a height of 20 cm and a weight of 272 grams, was used to reinforce each prism. The mortar-air interface of each steel bar was coated with corrosion-prevention paint, as described by authors (Martinez-Molina et al. 2016; Torres-Acosta and Alejandra Díaz-Cruz 2020).

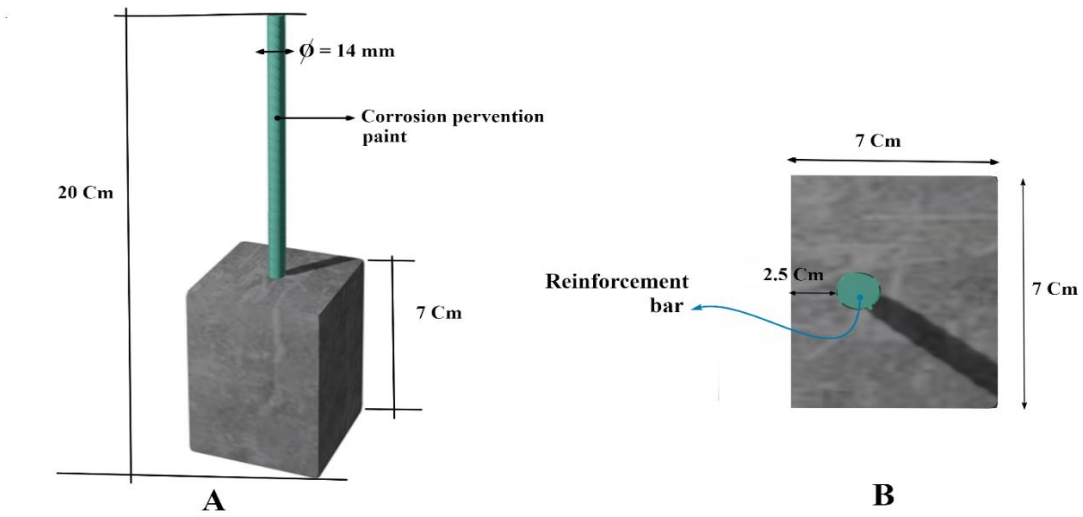

Figure 3.6 A) total view of Reinforced concrete prism, B) top view of the Specimen

3.4.4 Fresh Concrete Test

The slump test was selected following the ASTM C143 standard as the workability test in this research due to its widespread acceptance and simplicity. It is a commonly used and well-established method for evaluating the consistency and flowability of fresh concrete. The test

provides a quick and practical measure of the concrete's workability, allowing for easy comparison and interpretation of the result

3.4.5 Harden Concrete Test

Hardened concrete testing ensures the strength and long-term durability of the concrete used. One of the critical aspects of verifying concrete quality is conducting compressive strength tests on concrete cubes f (Saravanan et al. 2021). In addition, a total void percentage test was performed as part of the durability assessment, specifically after determining the optimal FASG and OFI replacement levels for their respective intended applications. This total void percentage test helps evaluate quantifies all voids in con- crete (macropores, micropores, interconnected, and discrete pores) from an excess of water content during fabrication because of incorporating FASG, or air encapsulated during handling (Torres-Acosta and Alejandra Díaz-Cruz 2020).

3.4.5.1 Compressive Strength Test.

A concrete's compressive strength mainly depends on the water-cement ratio and porosity (Torres-Acosta and Alejandra Díaz-Cruz 2020). This characteristic refers to a concrete's ability to resist axial loads without cracking. This property is assessed according to ASTM C-39. The load is expressed in mega Pascals (MPa) by dividing it by the specimen's cross-sectional area (A). A mechanical compressive strength measuring machine applies a load to the cylinders to achieve rupture. The machine is cleaned, the sample is positioned, and the load is applied at 14 N/mm^2/minute, with a maximum load capacity of 3000 KN. The maximum load is recorded at the point of specimen failure, and the compressive strength is then calculated using the formula: Compressive strength = Load/sample cross-section.

3.3.5.1.1 Compressive Strength Test To Determine Internal Curing Effect Of FASG

As described in the studies (Akhnoukh 2018; Alaskar et al. 2021; Byard et al. 2012; Kazemian and Shafei 2022; Nie et al. 2016), the following method is based on the theoretical approach studied for the internal curing effects. Cement particles react with water during hydration, forming chemical compounds that bind the aggregate. This is particularly apparent in more significant and denser concrete structures where the amount of available water is insufficient for complete hydration, resulting in microcracks and reduced hardness in hardened Concrete. Internal curing involves incorporating lightweight and highly absorbent materials into the concrete mixture. For this study, fine aggregate scoria gravel (FASG) was used. After the concrete cures, the internal curing agents release the stored water, supplying it to the

surrounding cement particles. As a result, the cement particles are supplied with continuous moisture, resulting in complete hydration and less microcrack formation. Consequently, the concrete achieves improved compressive strength, reduced drying shrinkage, and enhanced crack resistance. Due to this assumption, this study investigated FASG's internal curing effects by measuring the replacement percentage and curing day, as described in Table 3.9.

In order to evaluate the internal curing effect of Fine Aggregate Scoria Gravel (FASG), concrete samples were prepared by replacing different weights of sand with FASG at percentages of 5%, 10%, and 15% in the concrete mix. The curing duration for the samples was varied, with subsets of 12 samples, each subjected to different curing periods: 0 days, 3 days, 7 days, 14 days, 21 days, and 28 days. The samples were exposed to standard laboratory conditions throughout the curing process, maintaining a relative humidity of 58 ± 2% and a temperature of 26 degrees Celsius. Once the designated curing period for each sample was completed, they were removed from the soaking tank and placed in the open laboratory environment, marking the initiation of the internal curing process. At the end of the 28-day curing period, the compressive strength test was conducted on all the samples. The variation in compressive strength among the samples was then analyzed to determine the extent of the internal curing effect provided by FASG.

Table 3.9 Assessing the internal curing effect of FASG in concrete mixtures.

Percentage replacement of FASG	Days of Curing					
	0 Days	3 Days	7 Days	14 Days	21 Days	28 Days
0%	3	3	3	3	3	3
5%	3	3	3	3	3	3
10%	3	3	3	3	3	3
15%	3	3	3	3	3	3
Total samples	12	12	12	12	12	12

3.3.5.1.2 Compressive Strength Test To Determine Combined Effect Of FASG And OFI

Once the optimal soaking duration and maximum Fine Aggregate Scoria Gravel (FASG) percentage replacement has been determined, a specific percentage replacement value for FASG will be selected. This chosen percentage will be combined with varying percentages of Opuntia Ficus Indica (OFI), replacing water at 8%, 15%, and 30%. The compressive strength test will be conducted on 12 concrete cube samples with dimensions of 15x15x15 cm. The test

will take place after a 28-day curing period. An automated compressive strength measuring machine will be used, which applies a load to the cubes until they rupture. The machine operates at a 14 N/mm2/minute rate, with a maximum load capacity of 3000 KN. The maximum load at the point of specimen failure will be recorded, and the compressive strength will be calculated using the formula: Compressive strength = Load/sample cross-section.

3.4.5.2 Total void percentage

The presence of voids significantly affects the permeability and durability of concrete. A test was conducted to quantify the total void content in the concrete, including macropores, micropores, interconnected pores, and discrete pores resulting from excess water or trapped air. The measurement followed the procedure outlined in ASTM C-642 [8]. Cylinders were cut into slices with a diameter of 15 cm and a thickness of 4-5 cm. The dry mass of each portion was determined by weighing and then drying it at 100-110°C for a minimum of 24 hours. The mass was measured again after cooling to 20-25°C in a dry environment. If necessary, the drying process was repeated until the mass difference was less than 0.5% of the previous value, and the final mass was labeled A. The specimen was immersed in 21°C water for over 48 hours for the saturated mass after immersion. The mass was measured at regular 24-hour intervals until the change in mass between two intervals was under 0.5%. After removing surface water, the mass was recorded as B. To obtain the saturated mass after boiling, the specimen was immersed in water and boiled for 5 hours, followed by natural cooling for at least 14 hours until reaching 20-25°C. Surface water was removed, and the mass was measured and labeled as C. For the immersed apparent mass, the boiled and immersed specimen was suspended using a wire and weighed in water, labeled as mass D. Based on the result obtained, the following calculation will be made.

Absorption after immersion, % = [(B - A)/A] * 100 Equation 3. 1

Absorption after immersion and boiling, % = [(C - A)/A] * 100 Equation 3. 2

Bulk density, dry = [A/((C - D) * r)] * g1 Equation 3. 3

Bulk density after immersion = [B/((C - D) * r)] * g1 Equation 3. 4

Bulk density after immersion and boiling = [C/((C - D) * r)] * g1 Equation 3. 5

Apparent density = [A/((A - D) * r)] * g2 Equation 3. 6

Volume of permeable pore space (voids), % = [(g2 - g1)/g2] * 100 or [(C - A)/((C - D) * r)] * 100 Equation 3. 7

Where:

A = Mass of oven-dried sample in air, g, B = Mass of surface-dry sample in the air after immersion, (g), C = Mass of surface-dry sample in the air after immersion and boiling, (g), D = Apparent mass of sample in water after immersion and boiling, (g), g1 = Bulk density, dry, Mg/m3, g2 = Apparent density, Mg/m3, and r = Density of water = 1 Mg/m3 = 1 g/cm3.

3.4 Morphological And Electrochemistry Tests: Phase Three

The morphological analysis of Concrete involves assessing the physical and structural properties, particularly the composition, shape, size, and arrangement of the various components that make up Concrete. This section starts by determining the way of corroding the RC samples method employed in this study which is impressed current method. This study employs a variety of techniques for morphological analysis to analyze surface oxide/hydroxide formation on carbon steel when it comes into contact with OFI mucilage, including scanning electron microscopy, X-ray diffraction, and thermogravimetry. These techniques can be applied to visualize and measure concrete components at various scales, from micro to macro. This study uses optical microscopy, mass loss measurement, concrete crack survey, electrochemical tests, specifically EIS and tafel test, and precision source measurement to assess corrosion levels in each concrete mix after exposure to an artificial corroding environment. The following section introduces the impressed current method employed to induce corrosion in reinforced concrete (RC) samples within a controlled laboratory environment.

3.4.1 Accelerate Corrosion Test

In the impressed current method, also known as the galvanostatic method, a constant current is applied from a DC source to the steel embedded in Concrete to cause significant corrosion quickly (Hong et al. 2020a). The IC technique is widely used for accelerating corrosion in RC corrosion tests. Corrosion is induced by electrochemical potential between a steel reinforcement anode and a cathode. In natural corrosion, the current density varies from 0.1 to 10 $\mu A/cm^2$ (Feng et al. 2021a; Hong et al. 2020a). The potential is varied to maintain the current density continuously applied. When using a direct current (DC) power supply for IC testing, the applied current can be up to 100 times higher than the natural current flow, leading to a significant mass loss of the anode, If the specimen is immersed in chloride solutions (Feng et al. 2021a)

The impressed current method accelerates the corrosion of reinforced concrete, including metals, for research and testing purposes (Yuan et al. 2007b). This method involves applying

an external electric current to accelerate corrosion. The impressed current method involves connecting a direct current (DC) power supply to the metal specimen submerged in an electrolyte solution primarily using a chloride environment. The power supply is used as an external source of electrical potential. In this regard, Martinez-Molina et al. (2016); and Torres-Acosta (2007) typically used a concentration of 3–5% NaCl in their studies based on the solubility of NaCl (around 3.5%). Using this concentration range in the laboratory environment is considered safe and appropriate, and most importantly, it is most suitable for real-life applications.

By applying a controlled electrical current through the specimen, the impressed current method creates an electrochemical reaction that mimics the corrosion process by applying a controlled electrical current through the specimen. During the corrosion of the reinforced specimen, the current facilitates the movement of charged ions within the electrolyte solution. Thus, experiments can simulate and study long-term corrosion effects in a shorter period using the arrangement shown in Figure 3.7.

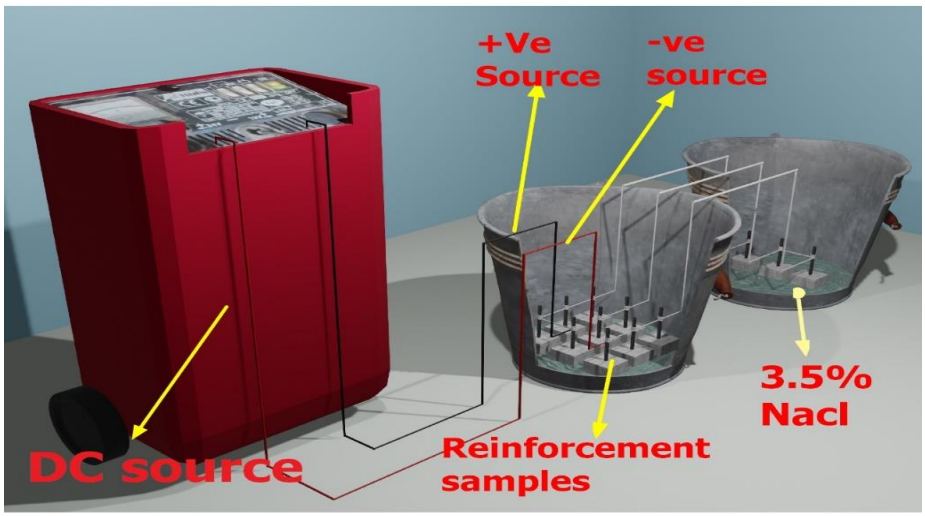

Figure 3.7 Impressed current methods of accelerated corrosion of RC samples

Current density is calculated from the flux (current per surface area of an anode) during the electrode's oxidation-reduction reaction process (Fig. 3.7). The current density resulting from the impressed current method can be determined using equations 3.7 to 3.10. The resistance of the rebar, measured with a Precision Source Measurement, is 0.203476 Ω. The applied DC voltage, read from an ammeter reader, is 9.15 volts. Additionally, for a 20 cm long rebar with a diameter of 14 cm, the surface area is calculated to be 175.84 cm^2. These values can be used to calculate the current density as follows:

Surface Area (A) = 2 πrl Equation 3. 8

= 2*3.14*1.4*20 = 175.84 cm²

Current (I) = $\frac{V}{R}$ Equation 3. 9

= $\frac{9.15}{0.203476}$ = 44.96 A

$J = \frac{I}{A}$ = Equation 3. 10

= $\frac{44.96}{175.84}$= 0.256mA/cm^2

3.4.2 Macroscopic Analysis

3.4.2.1 Mortar Crack Survey

The crack width in concrete structures was studied using a crack microscope, a specialized instrument equipped with an adjustable light source. In addition to being powered by batteries and conveniently carried in a carrying case, this high-definition camera provided precise crack measurement. The eyepiece scale could be rotated 360° to align with the crack direction during detection. Due to its range of 4 mm, division of 0.02 mm, and magnification of x40, the instrument accurately measures crack widths in Concrete. This study assessed crack severity by gathering detailed information and making informed decisions regarding the appropriate repair or reinforcement of cracks.

3.4.2.2 Mass Loss Measurement

After being exposed to a chloride environment, it is crucial to measure the mass loss of rebars in order to assess the corrosion resistance and durability of concrete or reinforcement. This measurement involves subjecting the rebar samples to a corrosive environment, such as immersion in chloride solutions or exposure to environments that simulate real-world conditions. After a specified period, the rebars are removed, cleaned, and weighed to determine the extent of mass loss. This measurement provides insights into the corrosion and deterioration of the rebars resulting from chloride attack.

To ensure standardized and reliable measurement procedures, ASTM G1, which outlines the preparation, cleaning, and evaluation of corrosion test specimens, is followed. Additionally, ASTM G31 provides a guide for conducting laboratory immersion corrosion tests that can be used to determine mass loss.

Following the guidelines in ASTM G 01-03, the rebars from each sample are extracted and cleaned using one of three recommended methods: mechanical, chemical, or electrolytic. This study chose chemical cleaning due to its simplicity and the absence of high current density requirements associated with electrolytic methods. ASTM G 01-03 presents six possible solutions for washing and removing corrosion products from iron. A solution of 200g NaOH, 20g zinc powder, and reagent water (deionized water) was selected.

3.4.3 Microscopic Tests

3.4.3.1 Xray Diffraction Test (XRD)

After 28 days of curing a concrete sample with varying percentages of Optunia ficus indica (OFI), samples were collected from the top, bottom, and middle sections. These samples were exposed to a corrosive environment. Subsequently, the samples were crushed into a fine powder and underwent sieving. X-ray diffraction (XRD) was performed at a specific angle (2θ) to analyze the composition and structural changes. The resulting XRD data was processed using Origin Pro 2022 software, enabling the identification and labeling of the peaks obtained from the XRD analysis. This XRD technique and the accompanying software can provide valuable insights into the crystalline structure and properties of the concrete samples.

This study utilizes Bragg's law, which enables the calculation of the d-spacing between atomic planes responsible for diffraction peaks. The d-spacing values provide crucial information regarding the crystalline size and purity of the material under investigation. By analyzing the diffraction pattern, one can obtain insights into the crystal structure and determine the distance between the lattice planes. These measurements provide essential insights into the size of crystalline domains and the purity level, which are crucial for characterizing and evaluating the quality of the material. In this study, Bagga's law is employed to determine the interplanar spacing, while the Scherrer equation is utilized to determine the maximum d value of the samples. These analyses enable a comprehensive understanding of the structural properties and quality assessment of the material under investigation.

Bragg's law is an equation that relates the angle of diffraction, the wavelength of incident radiation, and the spacing between crystal lattice planes

$$N\lambda = 2d\sin\theta \qquad \text{Equation 3. 11}$$

Where: - n= is an integer representing the diffraction order

λ = is the wavelength of the incident radiation (usually X-rays) in meters

d = is the spacing between the crystal lattice planes, also known as the d-spacing, in meters

θ = is the angle of diffraction between the incident beam and the diffracted beam, measured in radians

The Scherrer Equation estimates the average crystallite size (D) or the maximum d-spacing value of crystalline domains within a material. It is derived from the broadening of the XRD peaks due to the finite size of the crystallites. The Scherrer Equation is expressed as:

$$D = K\lambda / (\beta\cos\theta) \qquad \text{Equation 3. 12}$$

The Scherrer Equation can estimate the average crystallite size or the maximum d-spacing value of crystalline domains within a material. It is derived from the structure factor for a set of equally spaced planes and the determination of the prOFIle near the peak.) where D is the mean size of the ordered (crystalline) domains, K is a dimensionless shape factor, λ is the X-ray wavelength, β is the line broadening at half the maximum intensity (FWHM), and θ is the Bragg angle.

3.4.3.2 Scanning Electron Microscopy (Sem)

In this study, the internal morphology of concrete was examined using SEM. Eight concrete samples were prepared, half containing Opuntia ficus indica (OFI) and the other half representing conventional concrete. Four of these samples were exposed to corrosion-inducing conditions, while the remaining four were conventional concrete samples. The reinforcement was carefully dismantled to obtain a representative sample of the reinforced concrete (RC) exposed to the corrosive environment, and samples were taken from the concrete-reinforcement interface. For the conventional concrete samples, samples were taken from the middle of the concrete after conducting compressive strength tests. These samples, both for RC and conventional concrete, were representative mortar samples, free from cracks, and shaped using sandpaper and scissors. The SEM instrument used for analysis was the JCM-6000Plus, operating at an acceleration voltage of 15.00, with magnifications of 1500.0, 600.0, and 300.0.

3.4.3.3 Fourier Transform Infrared Spectroscopy (FTIR)

FTIR spectrum is one of the most used techniques to analyze the structure of polymers and to Fourier Transform Infrared Spectroscopy (FTIR) is a widely used analytical technique for material characterization (Bayar et al. 2016). It provides valuable information about a substance's molecular composition and chemical structure. An FTIR test exposes a sample to infrared radiation, and the resulting spectrum is analyzed. This spectrum reveals the absorption

and transmission of infrared light by the sample at different wavelengths. Determine their major functional groups. The functional groups and chemical bonds present in the material can be identified by comparing the observed peaks and patterns in the spectrum with known reference spectra (Salehi et al. 2019). FTIR is beneficial for identifying organic compounds, such as polymers, proteins, and organic contaminants (Bayar et al. 2016). FTIR tests were conducted in this experiment to determine the effectiveness of corrosion inhibition in Concrete by analyzing the chemical composition and molecular changes associated with corrosion. The sample-taking methods for opuntia ficus indica and concrete samples are discussed in detail in the following subsections:

3.4.3.3.1 FTIR sample-taking technique OFI

The extracted Opuntia ficus indica (OFI) mucilage must be transformed into powder to analyze the spectrum. Because high temperatures can break down chemical bonds in gel, and exposure to open air can introduce fluctuations in relative humidity and temperature, potentially affecting the composition of the gel, this conversion was performed at a constant temperature. This gel was placed in a plastic jar and dried in an oven at 30 degrees Celsius for a week to maintain consistency. Three separate samples were tested for FTIR to ensure reliable results and minimize any possible discrepancies. From these samples, a representative sample was carefully selected for further analysis.

3.4.3.3.2 FTIR sample-taking technique Concrete

After 28 days of curing a concrete sample with varying percentages of Optunia ficus indica (OFI), including the control group, which is 0% addition, samples were collected from the top, bottom, and middle sections. These samples were exposed to a corrosive environment. Subsequently, the samples were crushed into a fine powder and underwent for FTIR test.

3.4.3.4 Optical Microscope Test

This study examined the outer surface of the rebar carefully to determine whether there was uniform corrosion or pit corrosion. The corrosion test was followed by optical microscopy at a magnification of 500x on all rebar reinforcements (Qiao et al. 2017). In order to represent corrosion, images were captured for all specimens, explicitly focusing on the rebar's middle, upper, and bottom parts (Feliu et al. 1989). The study examined these selected regions to identify and characterize corrosion patterns and gain insight into the extent and nature of corrosion in the rebar samples.

3.4.4 Electrochemical Analysis

An electrochemical test provides valuable information regarding corrosion processes at the metal-concrete interface by comprehensively analyzing Concrete's electrochemical behavior (Özcan 2008; Poupard et al. 2004). As stated in the description of the following method, this study investigates the corrosion inhibition capacity of Opuntia ficus indica by measuring the EIS and Tafel plots on concrete specimens and reinforcement bars with and without the addition of this natural corrosion inhibitor.

3.4.4.1 Electro-Impedance Spectroscopy (Eis)

Electrochemical Impedance Spectroscopy (EIS) was conducted on Concrete with and without the addition of opuntia ficus indica natural corrosion inhibitor and corroded steel reinforcement. In the Electro impedance spectroscopy test, a three-electrode system was utilized to evaluate the behavior of carbon steel and concrete samples. For the case of the carbon steel test, the working electrode is grade 60 carbon steel bars, adhering to the specifications outlined in the accompanying table, and for the case of the concrete specimens were immersed in a standardized kit holder during the experiment. Before conducting the Electrochemical Impedance Spectroscopy (EIS) test, the casted reinforced concrete samples underwent a 504-hour corrosion exposure by applying impressed currents. Within this experimental setup, a mercury/mercury chloride electrode was employed as the reference electrode to ensure a stable potential reference throughout the test. A graphite electrode served as the counter electrode, facilitating the necessary flow of electrons within the system. The electrolyte used was a 3.5% sodium chloride solution, which creates an environment conducive to corrosion. Throughout the test, the experiment consistently maintained the electrolyte temperature at 25°C. Figure 3.8 will show the setup of the study.

3.4.4.2 Set Up Parameters For EIS Test For Concrete Samples

Potential Electrochemical Impedance Spectroscopy (PEIS) was performed in single sine mode with specific parameters. The experiment used a Bio-logic SP-300 device with a grounded electrode connection. The Ewe control range was set from -10.00 V to 10.00 V, and the Ewe I filtering was set at 50 kHz. This methodology has also been used as a standard in different research to perform corrosion measurements using Bio-logic potentiostat equipment (Allahyarzadeh et al. 2017; Ashebir et al. 2022; Garnica-Rodríguez and Rodriguez-Gomez 2014; Ruiz-Garcia et al. 2023; Salasi et al. 2015; Zarazúa-Villalobos et al. 2021)

First, an Open Circuit Voltage measurement provided a reference point for the subsequent measures. The open circuit voltage remained constant for 30 seconds with a rate of change of 1.0 mV per hour. The second technique was Potentio Electrochemical Impedance Spectroscopy (PEIS). The Potentio Electrochemical Impedance Spectroscopy (PEIS) measurements were carried out within the 10 to 100 mHz frequency range, using logarithmic spacing and six points per decade. As per ASTM G3-89, the researchers set the E value at 0.2600 V relative to the reference, resulting in an applied voltage of 10 mV. These specific parameters align with the experimental setup employed by Sun et al.(2021). A total of six cycles were performed during the PEIS measurement, with the applied voltage (Va) set at 10.0 mV and the pulse width (pw) set at 0.10 seconds. The current range (I) was established to auto during the measurement.

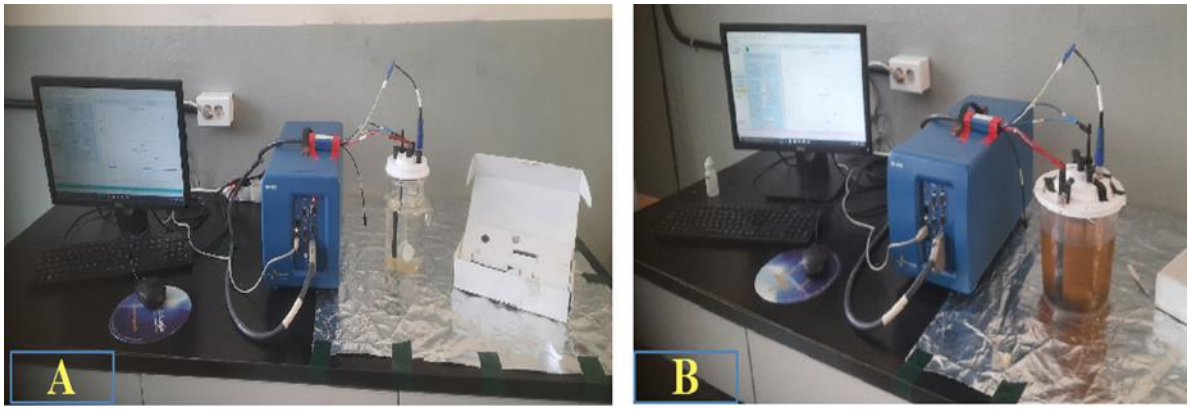

Figure 3.8 A) EIS and tafel test setup for Concrete, B) EIS setup for reinforcement bar

3.4.4.3 Tafel Plot Alanaysis

Potentiodynamic polarization curves show the relationship between potential and log current density, also called corrosion rate. This test allows us to determine the amount of chloride ions that penetrate construction materials and cause deterioration. The blended and control test specimens were cured with 3.5% NaCl solution at room temperature. After curing, a Tafel Plot of each specimen is produced by accelerating with AC over a potential of 10 mV at a frequency of 100 kHz to 10 MHz (Nivin M. Ahmed et al., 2021). During the experiment, three electrodes were used: a reference electrode, a counter electrode, and a working electrode. The electrolyte was 3.5% sodium chloride solution maintained at a temperature of 25°C.

3.4.4.4 Setup For Tafel Analysis

Tafel plots were given a 30-minute duration. The dER/dt (change in E rate with respect to time) was set at 5.0 mV/h, and the dER (change in E) was set at five mV. The dtR (time step) was 1.00 seconds. For the dE/dt scan rate, a value of 1.000 mV/s was utilized. The initial potential (Ei) was set at -0.300 volts, and a reference electrode potential of 0.250 volts indicated the end

potential for this experiment. This same scan rate and voltage window were adopted in related studies (Sun et al. 2021). The investigation recorded the current (I) values and set the step percentage to 25, with a total of 5 steps. The E range for the Tafel plot is set to -2.50 V to 2.50 V, while the current range is set to auto with a minimum and maximum of 10 mA. An 8-bit bandwidth is employed for the experiment.

3.5 Statistical Analysis And Software Uses

3.5.1 Statistical Analysis

In this experiment, a statistical analysis was conducted to determine the results' significance in determining the internal curing effect. The data were analyzed using a two-way ANOVA using Origin pro-2022 software, a statistical method to compare the means of two or more groups exposed to different levels of two independent variables. This analysis allowed for examining the interaction between the two factors and assessing their individual and combined influences on a dependent variable. In this case, the independent variables were the percentage replacement of scoria gravel and the soaking day, while the dependent variable was the 28-day compressive strength of concrete.

After performing the two-way ANOVA, further analysis was conducted using the Tukey HSD test. This post hoc test was employed to compare the means of different groups and determine if there were any significant differences between them. It was applied after obtaining a significant F-statistic in the ANOVA test, which indicated differences among the group means. In this study, the analysis compared the selected maximum replacement of FASG (fine aggregate substitute gravel) and curing day with respect to the other replacement and curing day groups.

1. Data on the Percentage Replacement of scoria gravel, Soaking Day, and 28-day Compressive Strength of Concrete were gathered as shown in Appendix A, Table A.10.
2. Origin Pro 2022 was used as the statistical software package for this study.
3. For this study, the assumptions of normality, homogeneity, and independence of errors were verified using a Q-Q plot and histogram method.
4. Percentage Replacement and Soaking Day were inputted as independent variables, and 28-day Compressive Strength was the dependent variable.
5. The significance level (0.05) was set to determine statistical significance. (Taking into account that the value of p=0.05 was related to the application of the study on reinforced concrete structures, it was essential to note that these structures did not require a highly

sensitive critical error control, unlike bridge structures and other sensitive study areas. Additionally, it was important to recognize that this significance level was widely accepted in numerous fields as a standard threshold for determining the presence of statistically significant effects.)

6. The output was analyzed, including the F-statistic, degrees of freedom, p-value, and effects summary.
7. The results were interpreted, focusing on p-values and interaction effects.
8. Post hoc tests of Tukey's HSD were performed to identify significant factors.
9. The results were presented using tables or graphs as needed.

3.5.1.2 Post Hoc Tests Of Tukey's HSD

Tukey's Honestly Significant Difference (HSD) test is a posthoc test used in two-way ANOVA (Analysis of Variance) to compare the means of different groups and determine whether there are any significant differences between them. It is performed after a significant F-statistic value is obtained in the ANOVA test, indicating differences among the group means (Wong and Cheung 2001). Here is a step-by-step process of how Tukey's HSD works in two-way ANOVA:

1. Two-way ANOVA was conducted to analyze the effects of independent variables on the dependent variable.
2. All possible pairs of group means were listed separately for each factor.
3. The absolute mean difference was calculated for each pair.
4. The HSD value was calculated using a formula with studentized range statistics, mean squared error, and the number of observations:

$$HSD = q * \sqrt{(MSE/n)} \qquad \text{Equation 3.13.}$$

5. The mean difference was compared with the HSD value to determine significant differences.

The results were interpreted to understand the impact of each independent variable on the dependent variable.

3.6 Summary

This chapter presents the methods employed in this study to achieve the objectives outlined in Chapter 1. The next chapter will provide a detailed discussion of the study's results and findings based on the methods described in this chapter.

CHAPTER FOUR

RESULT AND DISCUSSION

4.1 Introduction

The previous chapter provided an overview of the research methodology employed in this study. The present chapter presents the results and discusses the potential utilization of Opuntia ficus-indica (OFI) as a corrosion inhibitor in conjunction with the internal curing effect of Concrete facilitated by lightweight fine aggregate scoria gravel (FASG).

The first section of this chapter delves into the discussion of sub-objective one. It begins by examining the material characterization properties of FASG and OFI. Additionally, it investigates the effects of fine aggregate replacement ratio with FASG and curing time on concrete's compressive strength and density. By the end of this investigation, it transitions to the study's second section. The second section is dedicated to addressing sub-objectives two and three. In this section, the chapter presents the results in relation to the combined effect of FASG and OFI on the compressive strength of Concrete. Furthermore, it discusses the morphological tests conducted.

The third section presents the results and discussions of the macroscopic and microscopic concrete evaluations with varying percentages of OFI. These evaluations specifically focus on corrosion inhibition. The final section of the study carries out an electrochemical analysis of both the concrete and reinforcement bars to measure the effectiveness of corrosion inhibition. This analysis aids in reaching conclusions and making decisions regarding sub-objectives two and three. Additionally, it includes a subsection that highlights the inhibition mechanism of OFI and provides an economic investigation of corrosion inhibitors in concrete mixes.

4.2 Material Test Result And Discussion

The previous chapter explained the research methodology and the characterization and test results of the materials used in ordinary Concrete, including cement, coarse aggregate, fine aggregate, and water. This section of the current chapter will discuss the material characterization of fine aggregate scoria gravel and Opuntia ficus-indica separately in the upcoming topics.

4.2.1 Fine Aggregate Scoria Gravel (FASG) Characterization

This study utilizes fine aggregate scoria gravel (FASG) to replace the fine aggregate portion of Concrete, ensuring its uniform distribution throughout the concrete mix. This approach

prevents the production of lightweight Concrete when FASG replaces coarse aggregate (Ma et al. 2019). Consequently, the tests conducted on the fine aggregate focus on FASG, and the resulting findings are presented below.

4.2.1.1 Chemical Composition Of FASG

ASTM defines standard C294-05 scoria as a dark-colored, coarsely vesicular type containing more or less spherical bubbles. It is a volcanic glass of igneous rock composed wholly of glasses characterized by their texture and internal structure. As a result of their formation process, volcanic scoria consists of crystalline and non-crystalline particles as glassy particles. Because of their chemical and mineral composition, volcanic scoria varies widely in chemical and mineral composition and source. SiO2 and Al_2O_3 are particularly abundant in scoria. It is also rich in other oxides, and the chemical composition of the material tested in the Ethiopian geological survey is shown in Table 4.1. Physically, scoria (lapilli) ejected during basaltic eruptions vary considerably in their vesicularity (Yifru and Mitikie 2020).

Table 4.1 Chemical composition of FASG

Collector's Code	SiO_2	Al_2O_3	Fe_2O_3	CaO	MgO	Na_2O
IW-01	53.00	14.72	10.42	8.06	6.64	2.28
Collector's Code	K_2O	MnO	P_2O_5	TiO_2	H_2O	LOI
IW-01	0.60	0.26	0.49	0.83	1.51	1.92

4.2.1.2 Silt Content Of A FASG

The silt content of FASG, which refers to the presence of fine particles smaller than 75 microns, including clay, silt, and organic matter, can significantly impact the performance and stability of the construction material. To ensure compliance with ASTM standards, this study analyzes the silt content of FASG according to ASTM C117, which specifies a range of 0-6%. The results presented in Table 4.2 demonstrate that the FASG used in the study meets the ASTM standards.

Table 4.2 Silt content of FASG

Items	Trial 1	Trial 2	Trial 3	Average
A = Volume of separated layer (ml)	5	4.5	4.5	4.667
B = amount of fine aggregate (ml)	300	300	300	300
Silt content (%) == $\frac{A}{B} * 100\%$	1.67%	1.5%	1.5%	1.233%

4.2.1.3 Sieve Analysis For FASG

A sieve test method determined the fine aggregate particle size distribution. A FASG sample was weighed and passed through a series of sieves with smaller openings ranging from 4.75 mm to 0.075 mm in diameter. Sieves were arranged in descending order following ASTM C330-04, and the results are presented in tabulated form in Table 4.3 and graphed form in Figure 4.1. The arrangement of the sieves followed the guidelines of ASTM C330-04, and the fines modulus of the fine aggregate fell within the range of 2.3-3.1.

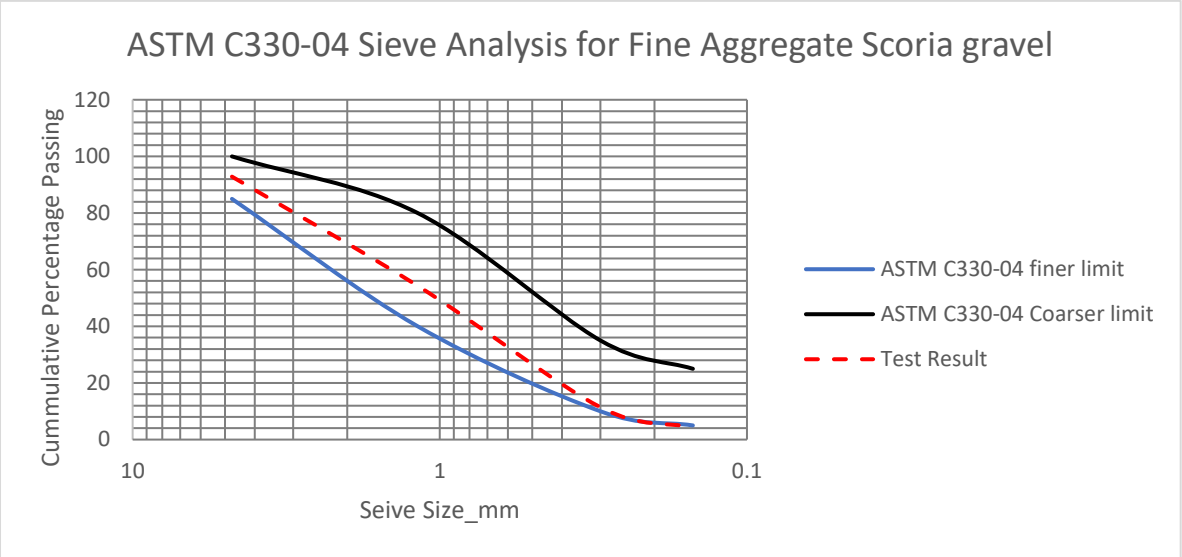

Figure 4.1 Sieve Analysis for Fine Aggregate Scoria Gravel as per ASTM C330-04

Table 4.3 Sieve analysis of FASG as light weight aggregate

Sieve Size (mm)	Weight Retained (g)	Percentage of Retained	Cumulative Percentage Retained	Cumulative Percentage Passing	ASTM C330-04 Range
4.75	25	7.1	7.1	92.9	85-100
1.18	135	38.6	45.7	54.3	40-80
0.3	150	42.9	88.6	11.4	10-35
0.15	25	7.1	95.7	4.3	5-25
Pan	15	4.3	100.0	0.0	0-0
Total	350				
Total cumulative percentage retained by mass = 237.1					

Fines modulus $= \sum_{sive\ size\ 0.15}^{sive\ size\ 4.75}(\text{cumulative percentage retained by mass})/100$

= 298.5/100 = 2.371

Although the FASG used in this study meets the fine lightweight aggregate criteria according to ASTM C330-04, it does not comply with the fine aggregate gradation test specified in ASTM C33. However, FASG was still chosen as a sand replacement to achieve the desired internal curing effect on concrete. The analysis will be based on ASTM C33, the standard used to evaluate the gradation of fine aggregates in concrete to assess the combined effect of gradation. The larger percentage replacement (15%) will be examined to determine if the blending of materials is satisfactory. If the gradation requirements are met at this higher replacement percentage, it can be assumed that the lower replacement percentages (10% and 5%) will also meet the desired criteria. Figure 4.2 illustrates the gradation of the blended material consisting of 15% FASG and sand. The graph demonstrates that the gradation curve of the blended material falls within the upper and lower limits specified by the relevant standards. Furthermore, Table 4.4 presents the fineness modulus values of the blended material, which range between 2.3 and 3.1, aligning with the requirements stated in ASTM C33.

Table 4.4 Sieve analysis FASG as a fine aggregate

Sieve Size (mm)	Weight Retained (g)	Percentage of Retained	Cumulative Percentage Retained	Cumulative Percentage Passing	ASTM C330-04 Range
4.75	30	5	5	95	95-100
2.36	80	13.33	18.33	81.67	80-100
1.18	155	25.83	44.16	55.833	50-80
0.6	95	15.83	60	40	25-60
0.3	115	19.16	79.16	20.83	10-30
0.15	120	20	99.16	0.83	0-10
Pan	5	0.83	100.	0	0-0
Total	600				
Total cumulative percentage retained by mass = 305.83					

Fines modulus $= \sum_{sive\ size\ 0.15}^{sive\ size\ 4.75}$(cumulative percentage retained by mass)/100

= 305.83/100 = 3.058

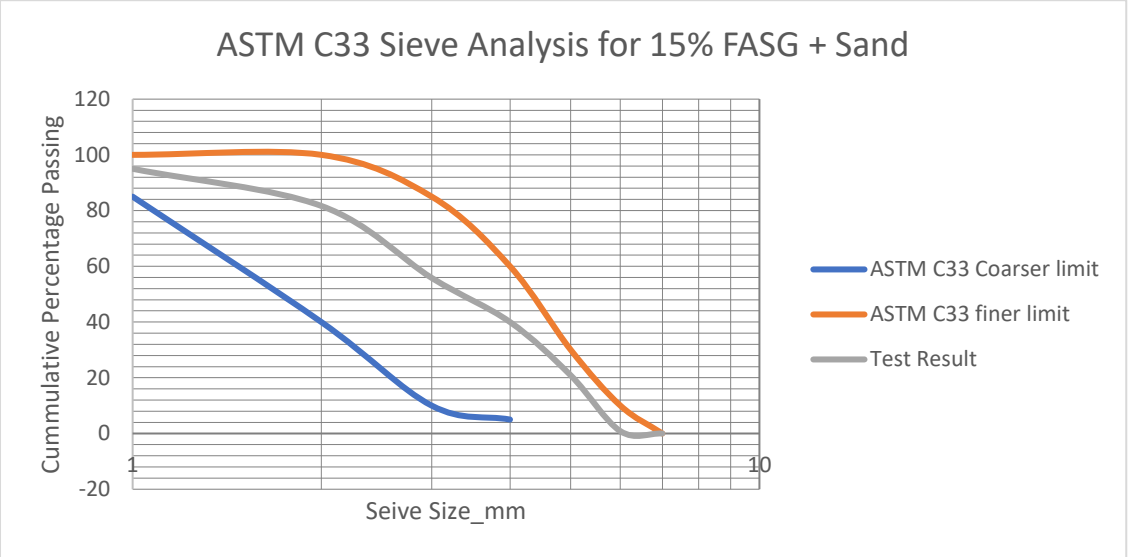

Figure 4.2 Sieve Analysis for Fine Aggregate Scoria Gravel as per ASTM C33

4.2.1.4 Unit Weight Of FASG

This unit weight of fine aggregate indicates how much the aggregate will occupy the concrete. Table 4.5 confirms the ASTM C29 standard, as the unit weight of FASG obtained is 1112 kg/m^3. The bulk density of fine aggregates must be less than 1120 for lightweight structural aggregates, as specified by ASTM C 330

Table 4.5 Unit weight of FASG calculation and result

Indications	Quantity	Calculation
I= Volume of the container	0.005 m^3	UWFA= $\frac{s-N}{I}$
S= Aggregate plus container weight	9.005 Kg	UWFA= $\frac{9.005-3.445}{0.005}$
N= Weight of the empty container	3.445 Kg	UWFA= 1112 kg/m^3

4.2.1.5 Specific Gravity And Water Absorption Test For FASG

Based on ASTM C128-15, The specific gravity of an aggregate is defined as the mass of the aggregate divided by the volume of Water. Absorption refers to the increase in mass of an aggregate caused by the presence of water within its pores. These characteristics were determined for FASG based on ASTM C128-15, confirming that the selected material meets the requirements since it is in the range of 2.5-3, as shown in Table 4.6

Table 4.6 Specific gravity and water absorption for FASG

Description	Amount	Formulas	Calculations
A: weight of oven-dried test sample in air	486 g	Bulk specific gravity = $\frac{A}{B+D-C}$	Bsg= $\frac{486}{1507.5+500-1802.5}$ $= 2.342$
B: Weight of the pycnometer filled with water to the calibration mark	1507.5 g	Bulk Specific gravity (SSD) = $\frac{D}{B+A-C}$	B_{SSD}= $\frac{500}{1507.5+486-1802.5}$ $= 2.61$
C: weigh of pycnometer filled with sample and water to the calibration mark	1802.5 g	Apparent Specific gravity = $\frac{A}{B+A-C}$.	Asg=$\frac{486}{1507.5+486-1802.5}$ $= 2.54$
D: Weight of SSD sample in air E: Weight of soaked aggregate for 24 hours = 540g	500 g	Absorption % = $\frac{E}{E-D} * 100$	Abn = $\frac{540-500}{500} * 100$ =7.40 %

4.2.2 Optunia Ficus Indica (OFI) Characterization

This study focuses on utilizing locally available Optunia ficus indica (OFI) to extract its mucilage and investigate its corrosion inhibition properties in reinforced Concrete and its performance in plain concrete. The previous chapter explains the sample preparation and extraction process. In this discussion, the extracted mucilage material of OFI will be investigated and compared to previous study findings while also analyzing the composition of OFI.

4.2.2.1 Fourier Transform Infrared Spectroscopy (FTIR)

FTIR spectrum is one of the most used techniques to analyze the structure of polymers and to determine their major functional groups (García-Barradas et al. 2022). It provides valuable information about a substance's molecular composition and chemical structure. An FTIR test exposes a sample to infrared radiation, and the resulting spectrum is analyzed. This spectrum reveals the absorption and transmission of infrared light by the sample at different wavelengths. The functional groups and chemical bonds present in the material can be identified by comparing the observed peaks and patterns in the spectrum with known reference spectra (Lefsih et al. 2016). FTIR is beneficial for identifying organic compounds, such as polymers, proteins, and organic contaminants (Bayar et al. 2016). It can be used to assess the quality,

purity, and composition of materials and aid in analysis for distinguishing the inhibition properties of a material.

The following Figure 4.3 shows that the FTIR result of the study represents an infrared spectrum obtained using a JASCO FT/IR-6600typeA spectrometer. It contains valuable information for analysis. The spectrum shows the x-axis as a wavenumber with units of 1/cm, while the y-axis represents transmittance in percentage (%T). The spectrum ranges from 399.1927 cm-1 to 4000.6047 cm-1, with a data interval of 0.964233 cm-1. The data consists of 3736 points, and the transmittance values range from a minimum of 81.17060%T to a maximum of 99.66769%T. These data points include pairs of wavenumber and transmittance values, forming the XYDATA.

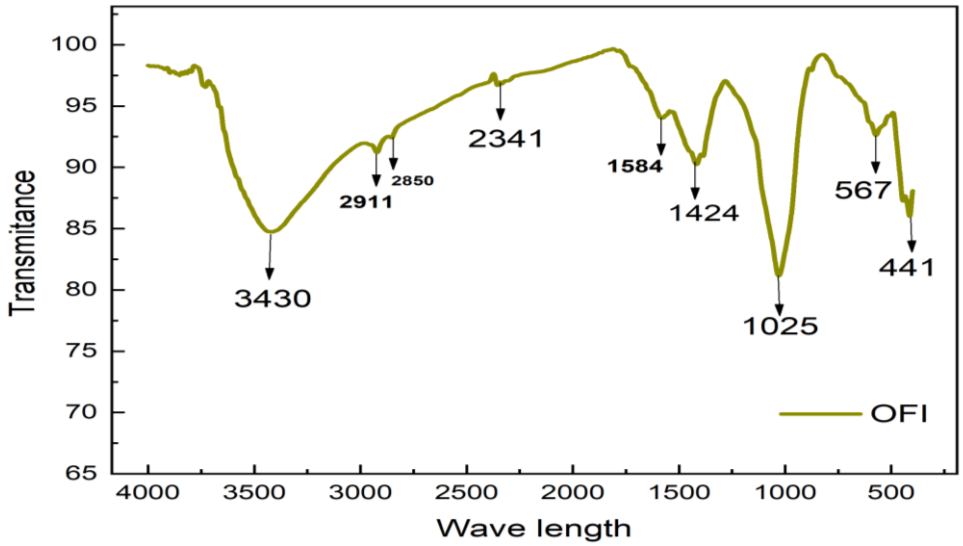

Figure 4.3 FTIR spectra for Optunia Ficus Indica (OFI)

The experimental FTIR spectra of Opuntia ficus indica (OFI) mucilage in powdered form are depicted in Figure 4.3. In the spectrum, the region between 3500-3000 cm^{-1} corresponds to the stretching of hydroxyl groups, according to Bayar et al. (2016); and García-Barradas et al. (2022), which signifies the presence of polysaccharides in the mucilage. According to the Chemistry Libre Texts, reference for FTIR spectra, the peak at 3700-3500 shows the OH stretch of alcohol; the reason for this vibration absorbance on the graph is likely due to the polysaccharide chain and phenols radical group ROOH chains and the wide range of OH stretch that other studies also observed is shows means that there is a strong bond between the OH bond. Also, it is related to the large chain of polysaccharides, such as arabinose ($C_5H_{10}O_5$) and amino acid existence with the H_2N-CH-COOH group. This specific band indicates the binding site for ions and their interaction with water, contributing to the gelling capacity of the mucilage

(Salehi et al. 2019). Additionally, peaks observed at 2911 and 2850 cm^{-1} indicate the symmetric stretching vibrations of the CH group in the methyl ester of galacturonic acid (Gopi et al. 2015). Another study suggests a similar absorption peak can be attributed to a combination of C-H stretches from pyranose CH and glycoside -OCH_2 moieties (Rodríguez-González et al. 2014).

In the FTIR analysis, the bands observed at 1584 cm^{-1} and 1424 cm^{-1} indicate carboxylic acid groups' asymmetric and symmetric stretching vibrations. The degree of esterification refers to how carboxyl groups are esterified in the mucilage (Rodríguez-González et al. 2014). These bands suggest the presence of uronic acid in the mucilage (García-Barradas et al. 2022; Rodríguez-González et al. 2014). In this regard, Contreras-Padilla et al. (2015) stated that the calcium oxalate monohydrate (whewellite) is located at the peak of 1584 $cm^{-1,}$ as shown in Figure 4.3, and corresponds to the antisymmetric and symmetric carboxylate stretching and the OCO deformations. Previous studies by Sáenz et al. (2004), Cárdenas et al. (2008), and Rodríguez-González et al. (2014) have reported that these bands correspond to the ionized form of carboxylic groups, indicating a low degree of esterification in the mucilage molecules.

On the other hand, in the studies conducted by Bayar et al. (2016), García-Barradas et al. (2022), Rodríguez-González et al. (2014), and Sáenz et al. (2004), the mucilage sample used in their respective experiment does not exhibit the characteristic band at 1749 cm-1, which is associated with mucilage having a high degree of esterification. When the esterification level is low, the carboxyl groups remain accessible and can interact with water molecules, resulting in an increased absorption capacity of the mucilage. Consequently, mucilage can form viscous solutions when in contact with water, and the free carboxyl groups can bind with calcium ions and other mucilage molecules to form viscous structural networks. These properties are beneficial for enhancing the formation of passive film layers on steel surfaces in Concrete, thereby promoting corrosion resistance.

Additionally, the band at 1025 cm^{-1} corresponds to the C-O-C groups, characteristic of carbohydrates. In this regard, the study by Lefsih et al. (2016) related this 1025 cm^{-1} peak to the polysaccharide backbone. The 1424 cm^{-1} peak, also in a range of 1450-1375, indicates C-H bending alkanes which sometimes come from the conjugation of alkene. The 1584 peak also lies in the range of 1550-1500, which is representative of the nitro compound as per chemistry.

Magnesium oxide can be detected at the vibrational band in 485 cm-1, which is caused by stretching out of the plane of the Mg-O bond (Contreras-Padilla et al. 2015). Furthermore, the band observed at 1025 cm-1 is attributed to the presence of C-O-C groups, characteristic of

carbohydrates. This peak is also suggested to be related to the polysaccharide backbone, according to Lefsih et al. (2016). The peak at 1424 cm-1, within the range of 1450-1375 cm-1, indicates C-H bending in alkanes. It can sometimes arise from the conjugation of alkenes. The peak at 1584 cm-1, falling within the range of 1550-1500 cm-1, typically represents nitro compounds based on existing literature. Based on the analysis of FTIR data and the similarities observed with previous findings, this study has concluded the composition of OFI. Table 4.7 summarizes these conclusions, which reference similar findings from relevant papers.

Table 4.7 FTIR analysis of opuntia ficus indica (OFI)

Wave number	Frequency Range	Bond	Functional Group	References
3430	3500-3000	O-H	Intermolecular bonded	(Cárdenas et al. 2008; García-Barradas et al. 2022; Waghmare et al. 2022)
2911,2850	2840-3000	C-H	alkane	(Bayar et al. 2016; Lefsih et al. 2016; Venkatesh et al. 2022)
2341	2341	O=C=O	Carbon dioxide	(Gopi et al. 2015)
1584	1580-1650	N-H	amine	(Bayar et al. 2016; Cárdenas et al. 2008;Contreras-Padilla et al. 2015; Lefsih et al. 2016; Rodríguez-González et al. 2014; Venkatesh et al. 2022)
1424	1375-1450	C-H	Alkane (methyl group)	(Ahmadi Moghadam et al. 2020; Gopi et al. 2015; Witkowski and Koniorczyk 2018)

1025	1020-1250	C-N	amine	(Bayar et al. 2016; García-Barradas et al. 2022; Venkatesh et al. 2022)
567	800-400	C-H	Aromatic ring	(Cárdenas et al. 2008; Sáenz et al. 2004; Waghmare et al. 2022)

In addition to the information provided in Table 4.6, various studies have confirmed the presence of polysaccharides within the 3500-3000 cm-1 region. A study by Otálora et al. (2015) further characterized the types of polysaccharides in Opuntia ficus indica. The findings revealed that the mucilage of OFI consists of a complex mixture of polysaccharides, including L-arabinose (24.6%-42%), D-galactose (21%-40.1%), D-xylose (22%-22.2%), L-rhamnose (7%-13.1%), and D-galacturonic acid (8%-12.7%). Waghmare et al. (2022) study also corroborated these results.

4.3 Determining Internal Curing Effect Of Fine Aggregate Scoria Gravel

4.3.1 Workability Test Result For Fresh Concrete Mix

ASTM C143 defines workability as the ability of fresh Concrete to be mixed, transported, flowed, and placed without difficulty. This study examined the workability of Concrete with the addition of fine aggregate scoria gravel (FASG) and conventional Concrete as per ASTM C143 standard. This work examined the level of workability of Concrete with FASG and convectional Concrete using the slump cone test. Table 4.8 and Figure 4.4 illustrate the slump values of blended and control Concrete.

Table 4.8 Slump value of concrete with and without FASG

Addition of FASG	Mean	Standard Deviation	Variance	Minimum	Maximum
0% FASG	45.6	0.77675	0.60333	45	46.5
5% FASG	47.2	0.60828	0.37	46.5	47.6
10% FASG	48.8	0.30551	0.09333	48.6	49.2
15% FASG	49.5	0.5	0.25	49	50

The impact of fine aggregate scoria gravel (FASG) on the workability of Concrete is often overlooked. This could be attributed to the fact that pre-saturated lightweight aggregate (FASG) neither absorbs nor releases water before setting, resulting in a minimal influence on

workability. This observation aligns with the findings of a study Ma et al. (2019). However, it should be noted that excessively rapid mixing can cause the FASG to release water, thereby increasing the workability of the concrete mix. This effect can be observed in the measured slump values. As the proportion of FASG in the mix increases, the workability improves. This can be attributed to the fact that the surface-saturated FASG does not absorb water. Consequently, when FASG is substituted for Sand in the mixture, the Concrete is exposed to higher overall water content.

As shown the Figure 4.4, there is no such mean variation of the slump value within the addition to the addition of FASG, but there is a noticeable workability enhancement as the FASG addition is increased.

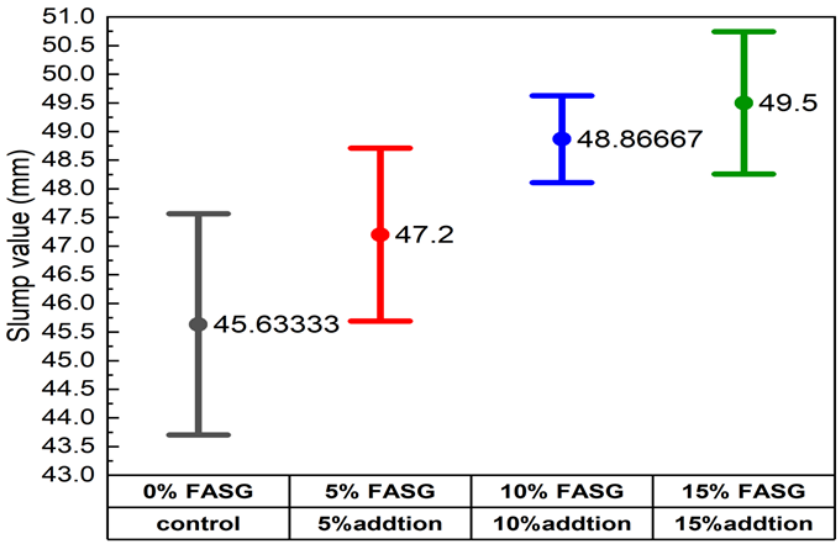

Figure 4.4 Workability of fresh Concrete with and without the addition of FASG

The Tukey's HSD test results (Appendix A, Table 2) indicate that the addition of fine aggregate scoria gravel (FASG) at different percentages has a significant impact on the slump values, except for the comparison between 15% FASG and 10% FASG, where no significant difference was found. In all other pairwise comparisons (0% FASG vs. 5% FASG, 0% FASG vs. 10% FASG, 5% FASG vs. 10% FASG, 0% FASG vs. 15% FASG, and 5% FASG vs. 15% FASG), the mean slump values were significantly higher when FASG was added. These findings suggest that increasing the percentage of FASG leads to increased slump values, indicating a potential effect on the workability or consistency of the studied material.

4.3.2 Compressive Strength Of Concrete Using Fine Aggregate Scoria Gravel (FASG)

This section of the paper presents the findings about the internal curing effects of lightweight fine aggregate scoria gravel (FASG) in the compressive strength of a concrete mixture. The methodology used for this study involves the theoretical approach of pre-soaked FASG releasing stored water after the concrete cures, supplying it to the cement particles, and promoting complete hydration, leading to increased compressive strength as described in various past research papers (Akhnoukh 2018; Alaskar et al. 2021; Byard et al. 2012; Kazemian and Shafei 2022; Nie et al. 2016). Through measuring FASG replacement percentage and curing Day, the current study analyzed these effects on controlled mixtures with varying mix design proportions. It identified that 5% FASG by soaking for 14 days yields higher compressive strength than other variables tested (Figure 4.5). A total of 72 concrete mix cubes were prepared for this study. The cubes were subjected to custom curing periods of 0, 3, 7, 14, 21, and 28 days by soaking them in water. The compressive strength of all samples was tested after 28 days. The results show a noticeable variation in the compressive strength in tabular form (Appendix A4, Table A.10), as depicted in Figure 4.5.

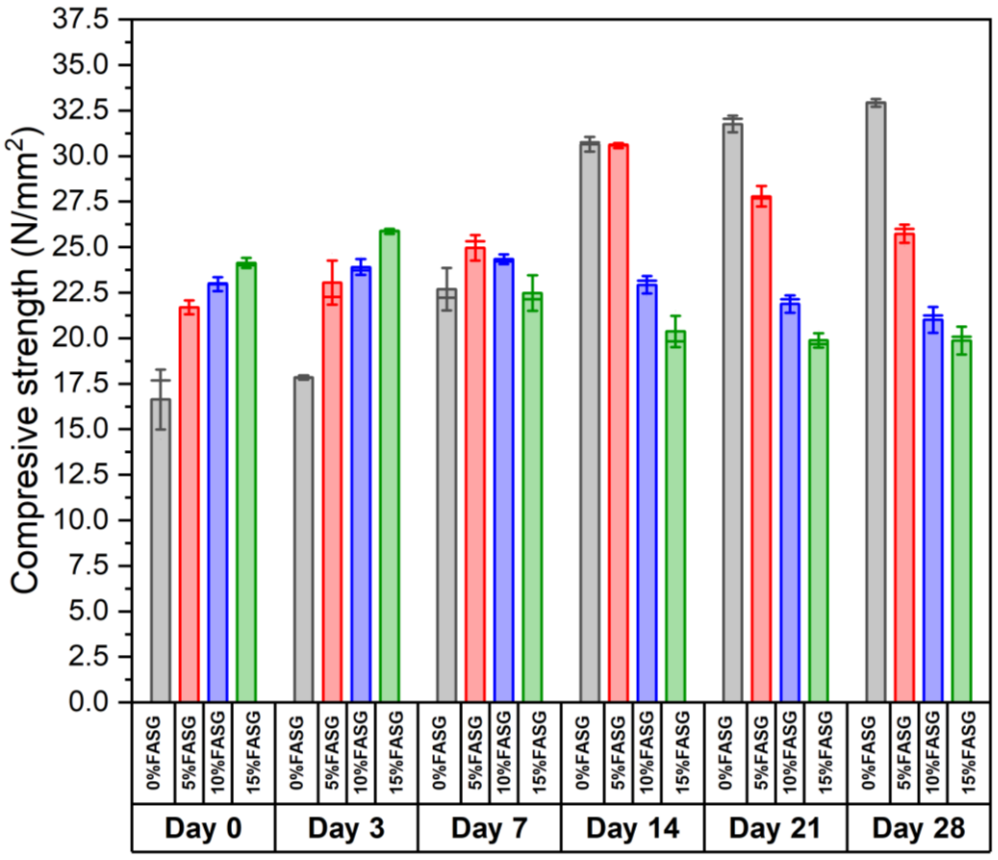

Figure 4.5 28 days compressive strength for different % replacement and Soaking days

The results suggest that the compressive strength of samples with 0% replacement of fine aggregate with FASG increases linearly with more days of curing. This indicates compressive strength for less cured (as the curing time decrease) control samples decreases from right to left in Figure 4.5. This can be attributed to a few factors. Firstly, Concrete needs time to hydrate and, therefore, must undergo curing before reaching its maximum potential in terms of strength. Secondly, since no internal curing material was present in the control group, it did not achieve optimal performance. It can be seen that all replaced samples had higher compressive results than those 0% replacements up until day 7, although there was some deviation afterward.

This study utilized a two-way analysis of variance (ANOVA) to examine the effect of FASG replacement and curing Day on the Compressive strength of Concrete. Before proceeding to two-way ANOVA analysis Q-Q plot Distribution graph is used to analyze the normal distribution of the data (Figure 4.6).

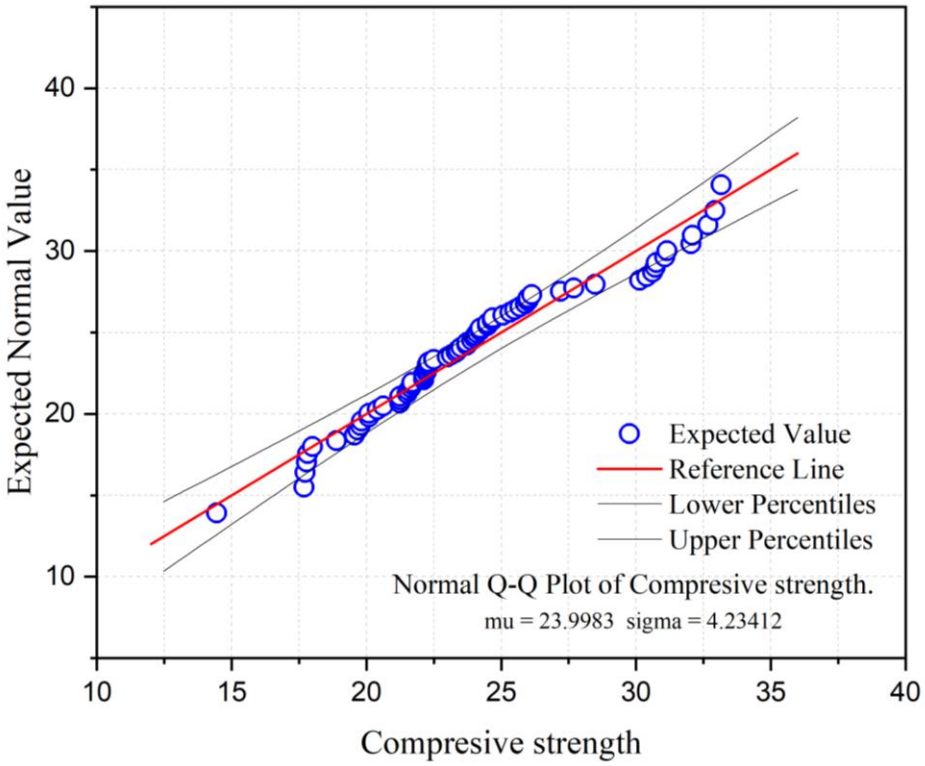

Figure 4.6 Q-Q Plot distrubtion curve

Graph A in a Q-Q plot indicates data points roughly following a straight, diagonal line. It represents data that follows a normal distribution. Accordingly, three hypotheses were formulated:

μ_{01} = varying percentages of FASG used to replace Sand in the concrete mixture will not affect the compressive strength.

μ_{02} = durations for soaking concrete cubes will be insignificant regarding compressive strength

μ_{03} = the combined effect of varying percentages of FASG replacement and different soaking days will not result in a significant difference in the compressive strength of the Concrete.

The result of the Two-way ANOVA analysis in Table 4.9 reveals significant findings. When comparing these p-values to the reference p-value of 0.05, all are much smaller, providing strong evidence of significant effects in the study. Curing Day significantly affects the compressive strength of Concrete, as indicated by the F-value of 69.54457 and a very small p-value of 8.15569E-21. Similarly, %Replacement exhibits a significant impact with an F-value of 106.54893 and a very small p-value of 3.15954E-21, where varying percentages of Fine aggregate scoria gravel (FASG) replacement contribute to differences in compressive strength. The interaction between Curing Day and %Replacement is also significant, with an F-value of 77.99828 and a very small p-value of 1.94256E-28, highlighting the combined influence of different curing durations and FASG replacement percentages. The overall model, encompassing both main effects and their interaction, is highly significant, with an F-value of 79.88451 and an extremely small p-value of 1.00004E-30. Conversely, the error term has an insignificant effect on the dependent variable, with an F-value of 0.65019.

Table 4.9 Two-way ANOVA analysis result

	DF	Sum of Squares	Mean Square	F Value	P Value
Curing Day	5	226.0856	45.21712	69.5445	8.15569E-21
%Replacement	3	207.83086	69.27695	106.548	3.15954E-21
Interaction	15	760.70445	50.71363	77.9982	1.94256E-28
Model	23	1194.6209	51.94004	79.8845	1.00004E-30
Error	48	31.20908	0.65019		
Corrected Total	71	1225.82998			

The percentage replacement and curing day have a significant impact on compressive strength. However, a statistical analysis should be conducted to illustrate the significant differences

between 5% FASG with a 14-day soaking period and other combinations of replacements and days measured. Because of this, this study utilized Tukeys HSD Test and analysis as shown below in Table 4.10.

Table 4.10 Tuke's HSD interaction grouping letter table

Curing Day	%Replacement	Mean	Groups										
Day 28	0	32.91	A										
Day 21	0	31.76	A	B									
Day 14	5	30.57	A	B									
Day 14	0	29.44		B	C								
Day 21	5	27.79			C	D							
Day 28	5	25.73				D	E						
Day 7	5	24.96					E	F					
Day 3	15	24.05					E	F	G				
Day 7	10	23.91					E	F	G				
Day 0	15	23.36					E	F	G	H			
Day 3	10	23.26					E	F	G	H			
Day 3	5	23.05						F	G	H			
Day 14	10	22.93						F	G	H			
Day 7	0	22.69						F	G	H	I		
Day 7	15	22.47						F	G	H	I		
Day 0	10	22.13							G	H	I	J	
Day 21	10	21.88							G	H	I	J	
Day 0	5	21.68							G	H	I	J	
Day 28	10	21.00								H	I	J	
Day 14	15	20.37									I	J	K
Day 21	15	19.88										J	K
Day 28	15	19.86										J	K
Day 3	0	17.85											K	L
Day 0	0	16.63												L

Tukey's HSD analysis, as presented in Table 4.10, indicates that means that do not share a letter are significantly different. As a result, the maximum value obtained for curing day 14 and 5% replacement shows a significant variation compared to all other combinations and interactions in the study. However, there are significantly similar values between the control group and the 21 and 28 days of internal curing. This suggests that the compressive strength of the 5% replacement with FASG has a significant impact and approaches the compressive strength value of the 28-day curing period. The theoretical reasoning behind these results will be discussed in the next section.

4.3.2.1 Analyzing Internal Curing Effect Of FASG On Concrete

The compressive strength of Concrete is influenced by the nature of Fine Aggregate Scoria Gravel (FASG), a lightweight material known for its internal curing effect. The internal curing capacity of FASG was evident in the 10% and 15% replacements, where a maximum

compressive strength was observed after a 7,3 day soaking period, with values of 24.34 MPa and 25.87 MPa, respectively. However, the compressive strength decreased as the curing period increased for Concrete containing 10% and 15% replacements. This can be attributed to the total water absorbed by the FASG. As the current study employed FASG with an absorption capacity of 7.46%, the 5%, 10%, and 15% fine aggregate replacements with FASG allowed the intrusion of 4.33 L, 8.66 L, and 12.99 L of water into one cubic meter of Concrete. This indicates that as the soaking day and the percentage replacement increase, the water-cement ratio in Concrete also increases, resulting in a decrease in compressive strength.

On the other hand, the 15% replacement showed higher compressive strength in the initial 0-3 day soaking period, providing clear evidence of the internal curing effect of FASG. This is further supported by the result of the 10% replacement, which achieved a higher compressive strength of 23.906 MPa at seven days. The study observed a higher compressive strength in the case of a 5% replacement of FASG. This can be attributed to two reasons: first, the replacement ratio of FASG is lower compared to other percentage replacements, and second, the curing period is more extended than other internal curing materials used. In conclusion, this study found that although FASG may not be a perfect internal curing material like expanded clay shale or other materials, it does exhibit a good internal curing effect when partially soaked in Concrete. Specifically, a 14-day soaking period with a 5% replacement of Sand was found to be optimal, resulting in a compressive strength of 30.577 MPa, which is 92.88% similar to the compressive strength of ordinary Concrete soaked for 28 days, which was 32.91 MPa. In this regard, two-way ANOVA findings shown in Table 4.10 exposed as there is no statistically significant difference between the compressive strength of ordinary concrete soaked for 28 days and a 14-day soaking period with a 5% replacement of Sand.

4.4 Compressive Strength Results With The Addition Of OFI

4.4.1 Workability Test Result For Fresh Concrete Mix

The impact of different percentages of Opuntia ficus indica (OFI) addition on the slump of fresh concrete mix is presented in Table 4.11. The Table indicates no significant changes in the slump values across the various mixes.

Table 4.11 Slump value for concrete with ad without addition OFI and 5 % addition of FASG.

OFI percentage	Mean	Standard Deviation	SE of Mean
0% OFI	47.1	0.65574	0.37859
8% OFI	47.73333	0.30551	0.17638

15% OFI	47.86667	0.32146	0.18559
30% OFI	48.73333	0.25166	0.1453

However, a slight increase in the slump value can be observed, which can be attributed to the gel-like structure of OFI, resulting in improved workability of the concrete mix, as observed in Figure 4.7.

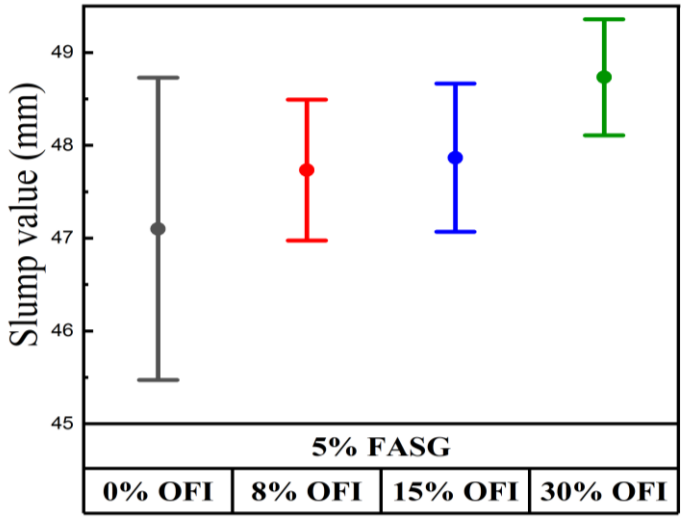

Figure 4.7 Workability of fresh Concrete with and without the addition of FASG

After conducting a one-way ANOVA analysis, the significance of the difference in workability was examined for different percentages of Optunia ficus indica (OFI) addition, as presented in Table 4.12. The results indicate no significant differences in workability between adding 8% OFI and 0% OFI, between adding 15% OFI and 0% OFI, and between adding 15% OFI and 8% OFI. However, a significant difference in workability is observed when comparing the addition of 30% OFI to 0% OFI. The comparisons between 30% OFI and 8% OFI and 30% OFI and 15% OFI show no significant differences. These findings suggest that the workability of concrete is generally unaffected by adding OFI at different percentages, except when adding 30% OFI, which significantly impacts the workability.

Table 4.12 Tukes HSD mean comparison for slump value of mix with OFI and 5% FASG

Interaction	MeanDiff	SEM	q Value	Prob	Alpha	Sig
(8% - 0%)OFI	0.63	0.33912	2.64118	0.31247	0.05	0
(15%- 0% OFI	0.76	0.33912	3.19722	0.1868	0.05	0
(15% - 8%) OFI	0.13	0.33912	0.55604	0.97799	0.05	0
(30% - 0%) OFI	1.63	0.33912	6.81147	0.0058	0.05	1
(30%n- 8%) OFI	1	0.33912	4.17029	0.0715	0.05	0
(30% -15%) OFI	0.86	0.33912	3.61425	0.12438	0.05	0

The findings suggest that incorporating OFI into the concrete mixture does not significantly affect the consistency or flowability, as indicated by the consistent slump values. Nevertheless, the presence of OFI introduces a gel-like structure that enhances the workability of the concrete mix. This improved workability can be beneficial during construction, allowing for easier concrete handling, placement, and finishing.

4.4.2 Compressive Strength Of Concrete

According to the findings outlined in sections 4.3.2 and 4.3.3.1, adding 5% Fine Aggregate Scoria gravel (FASG) represents the optimal replacement level required to achieve the desired compressive strength of concrete with an effective internal curing effect. The Two-way ANOVA and Tukey HSD post hoc results further support this conclusion. Building upon these results, the current study aims to explore the impact of incorporating Opuntia ficus indica (OFI) in addition to the 5% FASG replacement, specifically focusing on its effect on the compressive strength of concrete. In this regard, Figure 4.8 presents the relationship between OFI content and the corresponding compressive strength values.

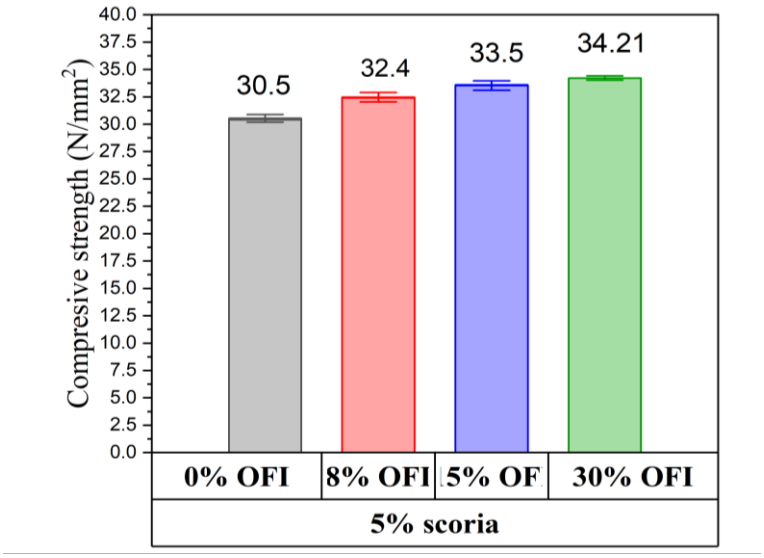

Figure 4.8 28 days compressive strength with and without the addition of OFI and 5% FASG

As depicted in this figure, a clear upward trend indicates that as the amount of OFI increases, the concrete's compressive strength also increases, which exposes that OFI may possess reinforcing properties that enhance the concrete mixture's compressive strength. In order to determine the statistical significance of the addition of OFI (One Factor of Interest) from sample to sample, a one-way ANOVA with Tukey's post hoc analysis was conducted, as shown in Table 4.13.

Table 4.13 Tukes HSD mean comparison for 28 days of compressive strength with and without the addition of OFI and 5% FASG

Interaction	MeanDiff	SEM	q Value	Prob	α	Sig
(8% - 0%) OFI	0.6	0.22016	3.85407	0.09	0.05	0
(15% - 0%) OFI	1.5	0.22016	9.63518	6.19E-4	0.05	1
(15% - 8%) OFI	0.9	0.22016	5.78111	0.014	0.05	1
(30% - 0%)OFI	2.51667	0.22016	16.16569	1.43E-5	0.05	1
(30% - 8%) OFI	1.91667	0.22016	12.31162	1.12E-4	0.05	1
(30% - 15%) OFI	1.01667	0.22016	6.53051	0.0074	0.05	1

Comparing the 8% OFI sample with the 0% OFI sample, a mean difference of 0.6 is observed, suggesting a potential compressive strength increase when OFI is applied. However, this difference does not reach statistical significance at the predetermined alpha level of 0.05. Moving to the comparison between 15% OFI and 0% OFI, a more substantial mean difference of 1.5 is found. This difference is statistically significant, as indicated by the associated p-value of 6.191E-4, which is smaller than the predetermined alpha value. Therefore, applying 15% OFI appears to have a noticeable effect on increasing the compressive strength compared to the absence of OFI. Further analysis between the 15% OFI and 8% OFI samples demonstrates a mean difference of 0.9. Although statistically significant at the alpha level of 0.05, this difference is smaller than the 15% OFI versus 0% OFI comparison. Examining the highest level of OFI, the 30% OFI sample compared to the 0% OFI sample exhibits a significant mean difference of 2.51667. The p-value of 1.43919E-5 confirms the statistical significance, indicating a substantial increase in compressive strength when applying a 30% OFI approach. Furthermore, the comparisons between the 30% OFI and 8% OFI samples and between the 30% OFI and 15% OFI samples yield statistically significant mean differences of 1.91667 and 1.01667, respectively. These findings suggest that increasing the OFI level from 8% to 30% or from 15% to 30% leads to further improvements in compressive strength.

4.5 Macroscopic Analysis Test Result

4.5.1 Mortar Crack Survey Tests

Surface cracks on Reinforcement concrete samples were visually examined after the corrosion exposure period of 504 hours. Crack widths were measured using a crack microscope equipped with adjustable lighting for accuracy. Figure 4.9 demonstrates the observed cracks on the concrete samples, showing a distinct difference in crack occurrence between the 0% OFI replacement sample and samples with increasing OFI additions. The 0% OFI replacement sample displayed significant cracks, while crack occurrence gradually decreased with higher OFI incorporation.

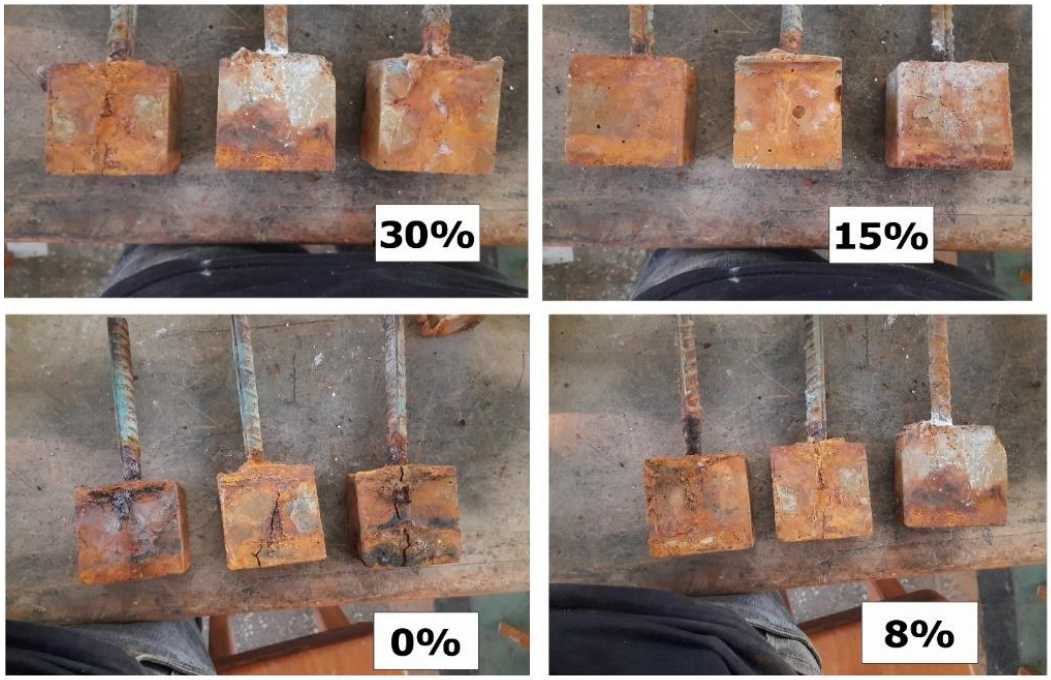

Figure 4.9 RC samples After the Corrosion exposure period

Additionally, Figure 4.10 presents the cumulative fraction of crack width against the maximum crack width recorded for each specific OFI addition percentage, providing a comprehensive understanding of crack behavior.

The concrete samples exhibited hairline cracks with a width of 0.01mm, displaying a non-uniform pattern throughout. Upon examining the crack widths across different samples, the maximum crack width of 0.35mm was observed in the sample with 0% replacement of Opuntia Ficus Indica (OFI), while the minimum crack width of 0.09 mm was observed in the sample with 30% OFI replacement. The 8% and 15% OFI replacement samples had crack widths of 0.18mm and 0.15 mm, respectively. These findings indicate that the concrete can withstand

corrosion-induced cracks in the reinforcement bar, with increased resistance observed as OFI content is added. The appearance of cracks on the mortar surface due to corrosion propagation suggests a potential trend where the addition of slime increases the time it takes for corrosion-induced surface cracks to appear. A previous study also observed similar findings (Martinez-Molina et al. 2016).

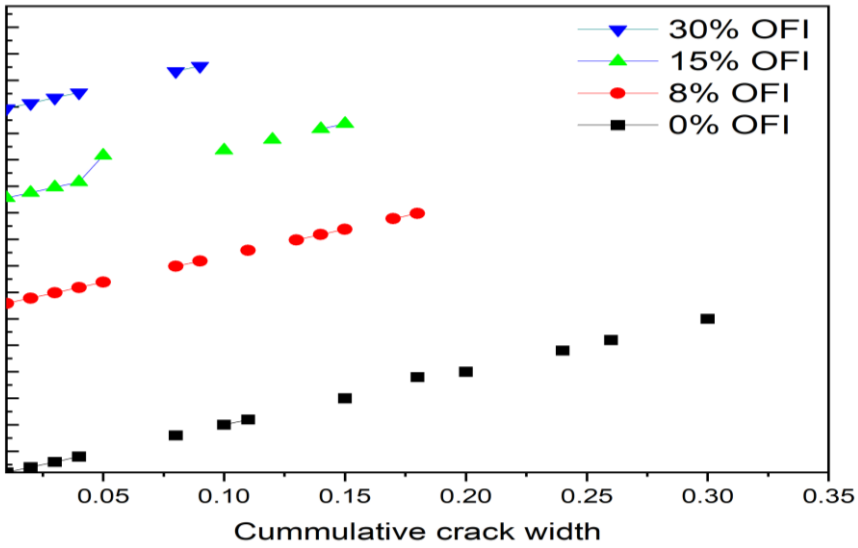

Figure 4.10 Concrete Crack Survey For all RC samples

4.6 Morphological Investigation Analysis

In the previous section, the maximum replacement ratio of 5% fine aggregate scoria gravel (FASG) was identified to achieve the desired internal curing effect. Fresh and hardened concrete samples were tested with and without adding Opuntia ficus indica (OFI). Further, mortar cracks in the reinforcement samples were examined following a specific exposure period.

In this subsection, we will discuss the morphological properties of concrete using X-ray Diffraction (XRD), Fourier Transform Infrared Spectroscopy (FTIR), Scanning Electron Microscopy (SEM), and Thermogravimetric Analysis (TGA). These tests will be conducted on standard concrete cubes and reinforced concrete (RC) samples exposed to a corrosive environment. The results obtained from these analyses will provide insights into the concrete's structural characteristics and chemical composition, allowing us to assess the effects of corrosion on the RC samples.

4.6.1 X-Ray Diffraction (XRD) Analysis

X-ray diffraction (XRD) is crucial for characterizing and examining crystalline materials. This technique offers insights into materials' atomic structure, crystallography, and phase compositions (Bunaciu et al. 2015). This study used this analysis method to explore the oxide/hydroxide formation in concrete samples with and without adding Optunia ficus indica (OFI) in reinforced concrete and standard plain concrete samples. In addition to this, this study seeks to identify the development of crystalline structures, as well as to determine the size of the crystalline according to X-ray diffraction analysis.

The experiment involved X-ray diffraction (XRD) analysis using a Shimadzu XRD 7000 machine. The measurement conditions were set: the X-ray tube had a copper (Cu) target, operated at 40 kV voltage and 30 mA current. The slits used in the analysis included a divergence slit set at 1.0000 degrees and a receiving slit with a width of 0.300 nm. The scanning was performed along the Theta-2Theta drive axis, covering an angle range from 10.00 to 80.00 degrees. A continuous scan mode was used with a scan speed of 3.00 degrees per minute and a sampling pitch of 0.200 degrees between data points. Prior to the scan, a pre-set time of 0.40 seconds was allowed. The obtained XRD data was then processed and analyzed using Origin Pro 2022 software, which facilitated the visualization of peaks and provided tools for further analysis of the generated graphs. By utilizing the Shimadzu XRD 7000 machine, specific measurement conditions, and the Origin Pro 2022 software, the experiment aimed to study the crystalline structure and phase composition of the samples under investigation.

4.6.1.1 Phase Assemblages In Cement Hydration

The X-ray diffraction (XRD) analysis revealed the presence of various crystalline phases. Figure 4.11 shows the XRD peaks of the reinforced concrete (RC) samples with and without adding Optunia ficus indica (OFI). The peaks corresponding to the formation of calcium silicate hydrate (CSH) gel were observed at 2θ angles of 28°, 29.6°, 29.54°, 39.36°, 29.46°, 39.54°, and 29.56°, which are consistent with the hkl values of 006, 221, 221, 131, 221, 131, and 221, respectively (ICDD card number 033-0306). Portlandite (calcium hydroxide) crystals were identified by peaks at 2θ angles of 18.08°, 29.26°, 47.26°, 47.38°, 35.44°, and 51.04°, corresponding to hkl values of 001, 100, 023, 102, 011, and 110 (ICDD card number 004-0733). The addition of OFI at concentrations of 15% and 8% resulted in the formation of calcite (calcium carbonate), observed at 2θ angles of 29.46°, 26.76°, and 49.54°, corresponding to hkl values of 104, 012, and 024 (ICDD card number 005-0586). Interestingly, the RC sample with a 30% OFI replacement exhibited peaks at 2θ angles of 26.74°, 27.86°, 39.56°, and 43.2°,

indicating the presence of calcium oxide (CaO) (ICDD card number 028-0775). Quartz peaks were detected in all RC samples except for the 8% OFI addition, with angles of 21.96°, 22.02°, and 20.94° corresponding to hkl values 100 (ICDD card number 01-085-0335).). Etringites peaks were detected in all RC samples, with angles of 9.2° corresponding to hkl values 101 (ICDD card number 00-033-0301).

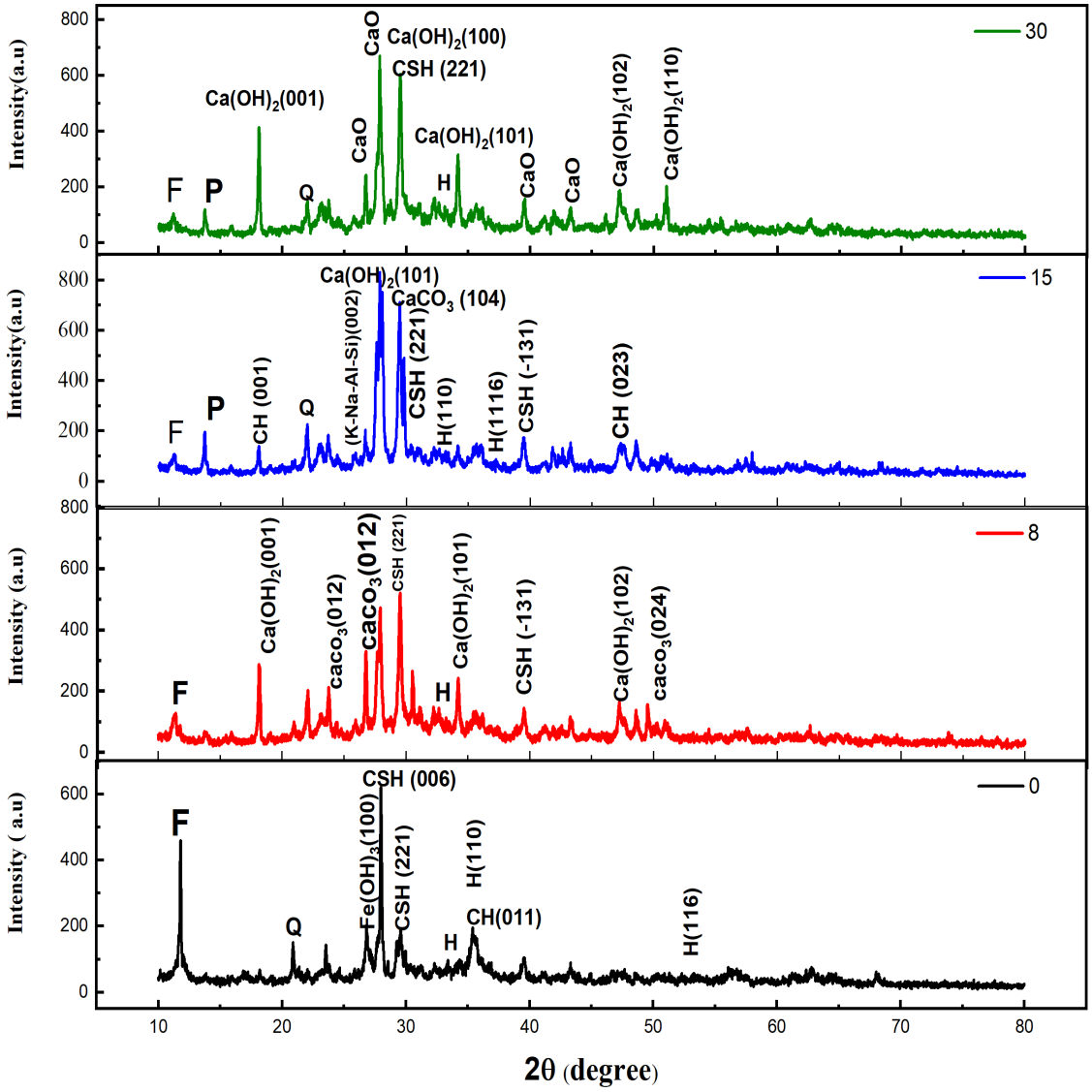

Figure 4.11 XRD pattern for RC concrete sample

The presence of CSH in all OFI addition samples demonstrates that incorporating OFI into concrete positively impacts compressive strength, which is also confirmed by this study in section 4.4.1. The presence of CH (calcium hydroxide) in all samples suggests that the hydration process occurs in all samples and is a suitable indicator of high pH value in concrete. The presence of CaOH in concrete hydration might confirm the inhibition capacity of OFI and support the internal curing effect of concrete.

The presence of calcite in the 8% and 15% replacement samples, but not in the 30% or 0% sample, can be attributed to the absence of OFI in the 0% samples, which lack the content of calcite naturally found in OFI. At 30% OFI replacement, a higher amount of CaO is observed instead of calcite. This is because the increased replacement level enhances the reactivity of the remaining cementitious material, resulting in a higher rate of hydration and the formation of more CaO. In this case, the formation of CaO surpasses the formation of calcite as there is insufficient time for CaO to react with CO2 and precipitate as calcite.

In the absence of calcium carbonate, the integrity of the passive film layer likely remains more stable, provided no other substance would cause its deterioration. This implies that the absence of CaCO3 typically results in improved corrosion resistance for concrete on passive film layers for protection. Consequently, 30% replacement appears optimal for enhancing concrete's corrosion resistance, as forming more CaO during concrete hydration signifies its essential role in cement. However, calcium oxide does not react with water independently during hydration. Instead, it combines with other compounds to create calcium silicates, aluminates, and ferrites, the primary hydration products responsible for concrete's strength and durability.

The presence of K-Na-Al-Si minerals in concrete is mainly attributed to the composition of unknown minerals, which lead to alkali aggregate reactions; this study did not investigate any further analysis on this scenario, but its insight that for an unknown reason, the observation of K-Na-AI-Si make 15% addition is not a favorable choice so far.

4.6.1.2 Phase Assemblages In Corrosion Formation

The X-ray diffraction (XRD) analysis demonstrated varying crystalline phases related to corrosion products and different salt and polysaccharide chain groups. The observations of corrosion by-products and Friedel's salt are connected to the impressed current technique employed to speed up the corrosion in reinforced samples and the functional group of OFI, which also contributes to the polysaccharides. Friedel's salt, alternatively known as Friedel's compound or C-S-H-A (calcium sulfoaluminate hydrate), exhibited XRD diffraction reflections at 2θ 11.78^{o}, 11.44 ^{o}, 11.3 ^{o}, and 11.6 ^{o} for 0%, 8%, 15%, and 30% OFI addition mixes, corresponding to reference card number ICDD 31-0245, as shown in Figure 4.11. Hematite (α-Fe_2O_3), symbolized as H in the XRD Figure 4.11, was reflected at 33.2 ^{o}, 35.7 ^{o}, 54.09 ^{o} with hkl (104,110,116), corresponding to the ICDD reference card number 00-033-0664. Furthermore, some reflections associated with adding OFI to the concrete mix were

observed in 15% and 30% replacements in amorphous peaks, such as β-D-Galactose ($C_6H_{12}O_6$), with reference card number 00-009-0620.

The presence of Friedel's salt in the peak can be related to the methodology used in this study to accelerate the corrosion test, which is the impressed current method while immersing the concrete samples in sodium chloride solutions. Using the impressed current method accelerates the corrosion process by increasing the availability of chloride ions at the concrete surface, promoting Friedel's salt formation. This method induces an electrochemical reaction that releases additional chloride ions, reacting with the hydrated cement phases in the concrete. Sodium chloride in the solution acts as a source of chloride ions that cause the formation of Friedel's salt due to their reactions with calcium and aluminum-containing cement phases.

Friedel's salt is formed in concrete when aluminate phases in cement react with sulfate ions in the presence of water. The reaction is referred to as the ettringite-formation reaction and can be represented by the following equation:

$$3CaO{\cdot}Al_2O_3 + 3CaSO_4 + 32H_2O \rightarrow Ca_6(Al(OH)_6)_2(SO4)_3{\cdot}26H_2O$$

In this reaction, tricalcium aluminate (3CaO·Al2O3) present in cement reacts with gypsum (calcium sulfate, CaSO4) and water to form ettringite (Ca6(Al(OH)6)2(SO4)3·26H2O), which subsequently converts to Friedel's salt under certain conditions.

Friedel's salt in concrete can cause cracking as it creates larger crystalline structures within the cement matrix, increasing the crystalline size. This can result in the expansion and cracking of the concrete due to its larger volume than the original compounds. In addition, Friedel's salt is a significant indicator of corrosion and its potential consequences since it forms due to chloride reactions and can also act as a storage for chloride ions, contributing to concrete corrosion. The XRD graph shows that the intensity peak of Friedel's salt decreases as the percentage of OFI addition in concrete increases. This is related to the ability of OFI to form a mucilage structure in the concrete, closing its pores and preventing the availability of chloride ions. Furthermore, adequate hydration reduces the availability of calcium and aluminum – the primary ingredients for Friedel's salt formation – leading to decreased cracking, as discussed earlier in the XRD peak analysis discussion.

The intensity of the Fredles slat observation, denoted as F, in the XRD peak intensity decreases as the percentage of OFI increases. This indicates that the amount of chloride ingress is reduced as the proportion of OFI increases, demonstrating the capability of OFI to block the

pores and enhance the concrete's interlocking capacity. Torres-Acosta and Alejandra Díaz-Cruz (2020) ‘s findings confirm this scenario. Furthermore, the increased hydration production of Portlandite and CaO aids the concrete in resisting the ingress of chloride ions, leading to the formation of a more robust passive film. This improved film formation prevents cracks and other factors from deteriorating the concretes.

This study compared the crystal formation of different samples using Burgers' law and Scherrer's equation. Burgers' law measured the interplanar spacing, while Scherrer's equation estimated the maximum crystalline size for each sample. Table 4.14 shows the analysis results of the three highest-intensity peaks for the corroded XRD samples.

Table 4.14 Crystalline size determination for XRD peaks

OFI addition	2θ	d (A^o)	FWH	D=λ*k/βcosθ
0% addition	28.02	3.82	0.1213	67.54
	11.87	7.45	0.1313	60.86
	26.86	3.32	0.189	43.24
8% addition	29.55	3.02	0.2533	32.45
	27.95	3.19	0.24	34.13
	18.21	4.87	0.2	40.25
15 % addition	27.87	3.20	0.6706	12.21
	29.48	3.03	0.3215	25.56
	22.02	4.03	0.282	28.71
30% addition	27.90	3.20	0.2084	39.30
	29.53	3.02	0.2359	34.84
	18.16	4.88	0.189	42.59

The table above provides significant findings regarding the samples' crystalline size and interplanar spacing. The results indicate that the sample without any addition (0% addition) exhibits the largest crystalline size, with a D value of 67.54. This sample also shows the highest interplanar spacing, with a value of 7.45. Based on visual observations and the XRD analysis of hydration products, it can be inferred that impurities, such as corroded particles and Friedel's salt formation, contribute to this sample's observed larger crystalline size.

On the other hand, among the samples with varying additions, the highest crystalline size (D value of 42.59) is observed in the sample with a 30% addition. Furthermore, the table

demonstrates a similar interplanar spacing (d) arrangement in all the concrete samples. This indicates that adding opuntia ficus indica (OFI) influences crystalline size formation while maintaining a consistent interplanar spacing pattern. This indicates that samples have larger crystalline sizes, further reaffirming their improved formation of hydration products and increased corrosion resistance.

Based on both visual and macroscopic investigations, the 30% addition of OFI is deemed desirable, demonstrating the maximum enhancement as a replacement material in the previous analysis.

4.6.1.3 Phase Assemblages in Optunia ficus indica (OFI)

Due to the complex composition of Opuntia ficus indica (OFI), which includes various polysaccharides and aromatic C-H chains, as described in section 4.2.2, it is challenging to precisely determine the characterization and compound effect of OFI in concrete samples. However, the XRD peaks reveal some amorphous peaks associated with the impact of the OFI phenolic compound group, and minor peaks like ' D-Galactose, with corresponding card number ICDD 00-009-0620, which has the molecular formula C6H12O6' have also been observed. Although it is difficult to identify the presence of OFI samples in XRD diffraction graphs, the probable peaks are increasingly observed in samples with higher additions of 15% and 30%. As illustrated in graph "P," the addition of OFI positively influences the compound's effect, as the compressive and hydration product in the analysis suggests.

Phenolic compounds are recognized for their ability to form complexes with metal ions. This complexation can inhibit the metal ions from interacting with other materials, decreasing the onset of corrosion mechanisms. Consequently, phenolic compounds in Opuntia ficus-indica can safeguard the reinforcement steel bars within concrete against corrosive conditions (Martinez-Molina et al. 2016). This situation can be substantiated by the peak identification in XRD data, which shows the existence of iron gluconate (C18H33FeO21) with reference card number 00-005-0257.

In order to examine the impact and inclusion of Opuntia Ficus Indica (OFI) in concrete samples, this study also compared conventional plain concrete samples (0% addition) with 30% OFI addition. The results, as depicted in Figure 4.12, revealed specific peaks at 2θ angles of 27.94°, 29.58°, and 37.78°, which corresponded to the formation of calcium silicate hydrate (CSH) gel. These angles align with the hkl values of 006, 221, and 011 for the concrete samples without OFI addition (0%). Additionally, a peak was observed at 27.9° with the hkl value of

310 for the concrete samples with 30% OFI addition, as per the (ICDD card number 033-0306). Furthermore, the presence of Portlandite (calcium hydroxide) crystals was identified through peaks at 2θ angles of 47.8°, corresponding to the hkl value of 023, for the concrete samples without OFI addition. For the concrete samples with 30% OFI addition, peaks were observed at 18.14° and 34.16°, which correlated to the hkl values of 001 and 101, respectively, as shown in (ICDD card number 004-0733). These findings highlight a clear variation and impact on the concrete samples due to the inclusion of OFI.

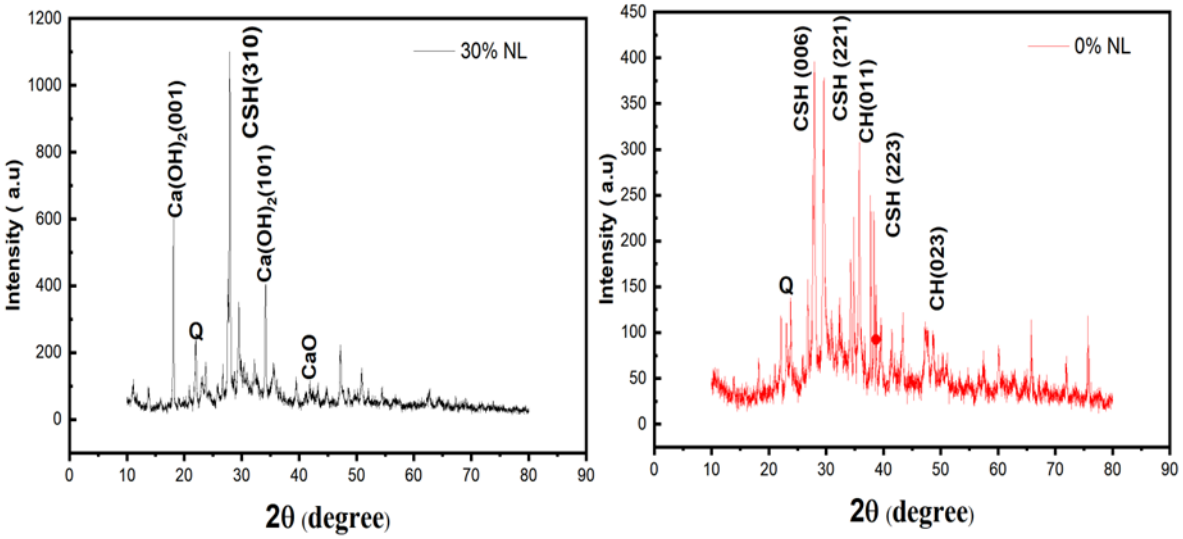

Figure 4.12 XRD for 0% and 30% convectional concrete sample

In this study, XRD analysis has proven to be a valuable method for identifying the various crystalline phases present in a sample and determining their abundance and crystallographic properties. However, this technique does not directly reveal the sample's morphology, texture, or surface characteristics. Alternatively, SEM analysis employs an electron beam to produce high-resolution images of the sample's surface, providing insights into topography, texture, grain size, and elemental distribution. This approach also effectively identifies surface defects, fractures, and contaminants. The subsequent discussion will explore this study's findings obtained through SEM analysis.

4.6.2 Scanning Electron Microscope Test Result

Scanning Electron Microscopy analysis is essential for studying materials' surface morphology, elemental composition, and microstructure at high magnifications. In this study, SEM was employed to investigate the microstructure and phase characteristics of concrete, specifically focusing on the effects of corrosion. By comparing concrete samples with and without the addition of Opuntia ficus-indica (OFI) and examining the exposed concrete subjected to

corrosion alongside conventional concrete samples, changes in the concrete's microstructure, including cement paste degradation and the formation of new phases, were observed.

The provided Scanning Electron Microscope (SEM) data pertains to a corroded concrete sample. The SEM instrument used for analysis is the JCM-6000Plus, with an acceleration voltage of 15.00 and a magnification of 1500.0,600.0, and 300.0. The SEM signal used is Secondary Electron Detection (SED). The SEM images' field of view is 79.5 um x 58.8 um. The micron bar calibration is 322.0, and the micron marker is 20um. The SEM imaging type is designated as type 1. The results obtained are illustrated in Figure 4.13 and Figure 4.14, as shown below.

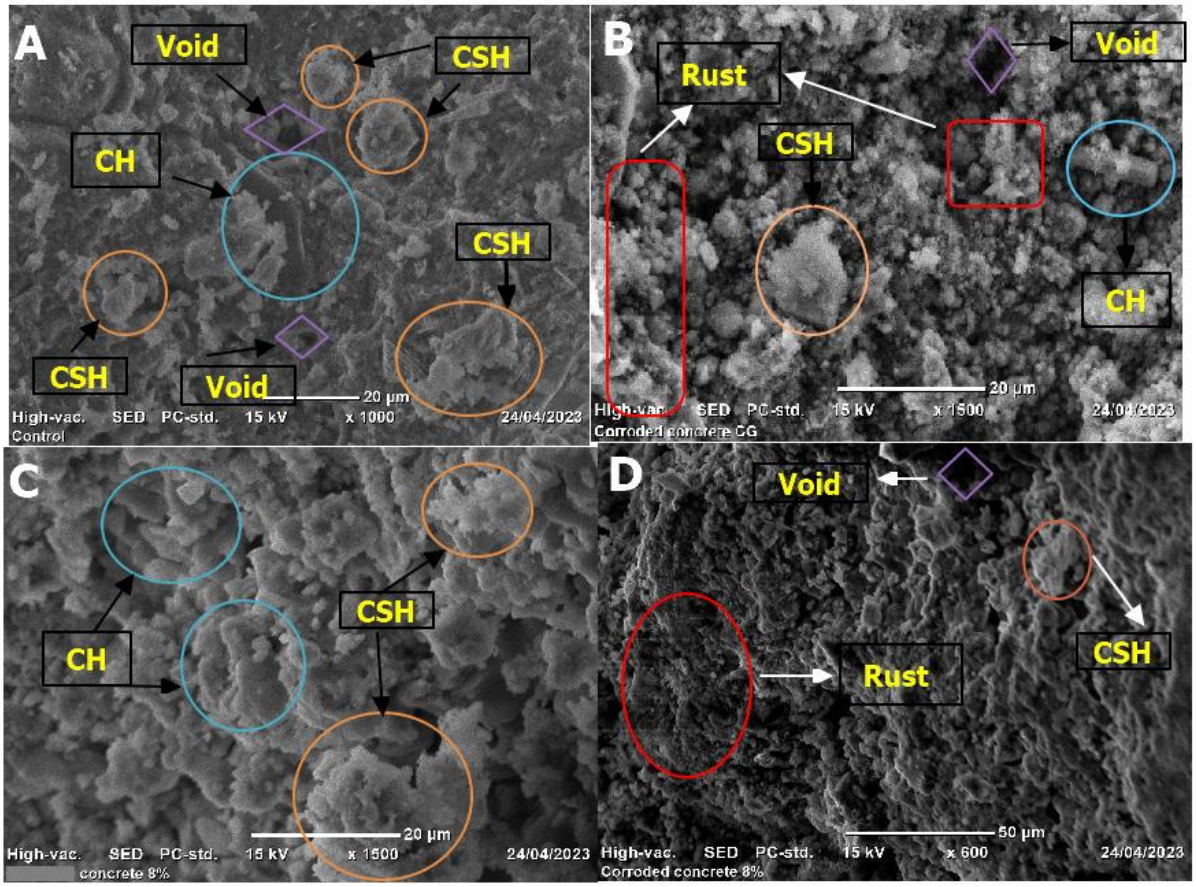

Figure 4.13 SEM Image of (A & C,0%& 8% conventional concrete), (B&D ,0%& 8% Corroded concrete)

As depicted in Figure 4.13, the addition of Opuntia ficus-indica (OFI) in the concrete mixture resulted in the observation of clear and white crystalline calcium silicate hydrate (CSH). Additionally, a snow-like structure of rust product was detected. These findings align with previous studies conducted by Ouglova et al. (2006), confirming the presence of these specific crystalline and rust formations in the concrete samples.

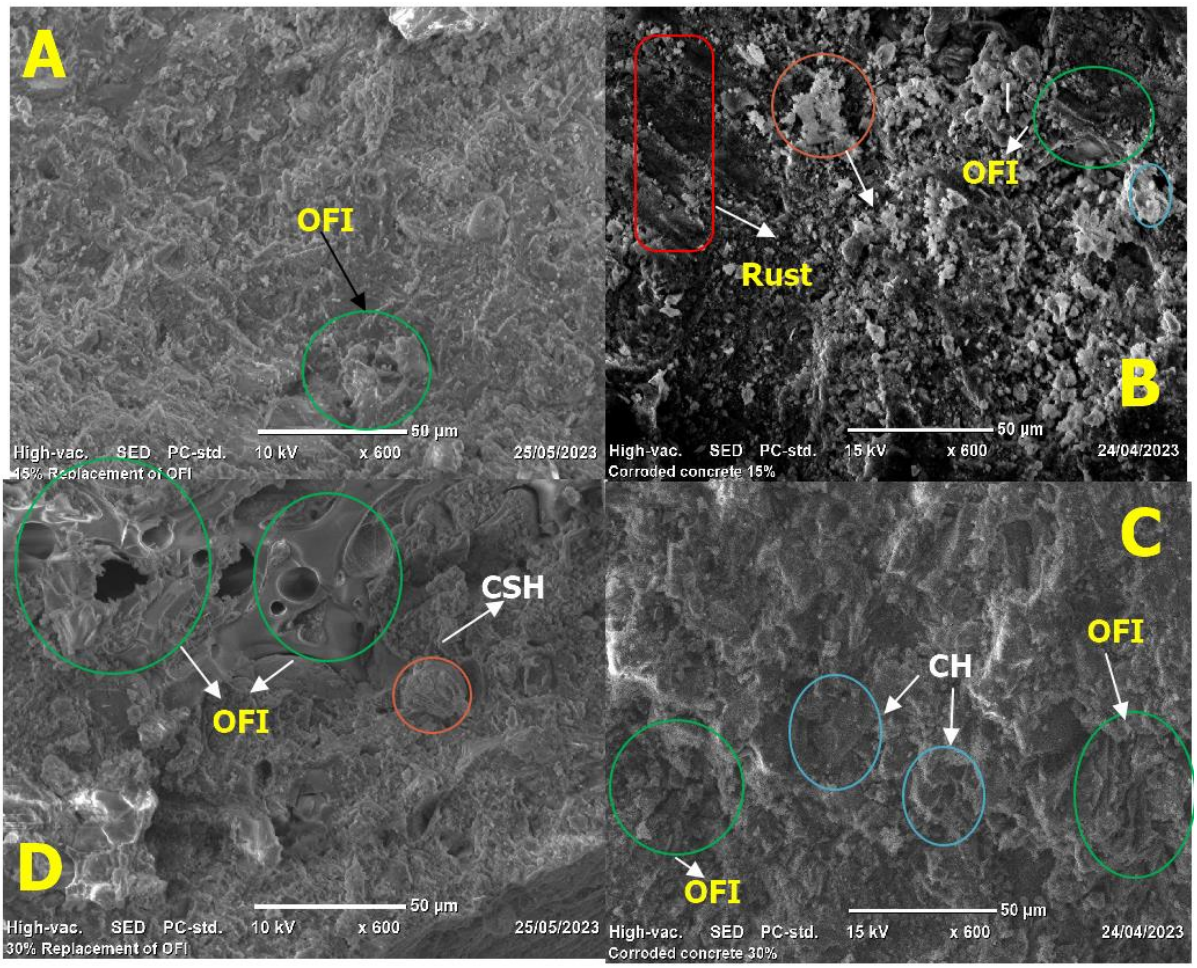

Figure 4.14 SEM Image of (A & D,15%& 30% conventional concrete), (B&C ,15%& 30% Corroded concrete)

In this study, the SEM analysis revealed important observations. As shown in Figure 4.14, the presence of Opuntia ficus-indica (OFI) in the concrete samples resulted in a mud-like structure (Torres-Acosta 2007). Furthermore, it was observed that the amount of OFI presence in the concrete reinforcement interface increased as the percentage of its addition increased. The SEM analysis also clearly identified the presence of crystalline structures and a passive protective coating within the concrete. These findings are consistent with previous reports by Torres-Acosta and Alejandra Díaz-Cruz (2020), further supporting the significance of the crystalline structure and a passive protective coating observation.

In this study, SEM analysis was instrumental in identifying the presence of rust products in the concrete samples. The XRD analysis initially detected amorphous peaks associated with corrosion products. Fourier Transform Infrared Spectroscopy (FTIR) was utilized to gain further insights into these corrosion products. FTIR analysis allowed for determining corrosion

products by examining the characteristic peaks corresponding to different functional groups. The subsequent discussion will provide a detailed exploration of these findings.

4.6.3 Fourier Transform Infrared Spectroscopy (FTIR) Test Result

FTIR (Fourier Transform Infrared Spectroscopy) is a powerful analytical technique used to obtain information about a sample's molecular structure and composition by measuring the absorption of infrared light by the sample's various chemical constituents. This method can be used for various applications, including analyzing organic and inorganic materials (Bayar et al. 2016). FTIR tests were conducted in this experiment to determine the effectiveness of corrosion inhibition in Concrete by analyzing the chemical composition and molecular changes associated with corrosion. Moreover, the output is illustrated in Figure 4.15, as shown below.

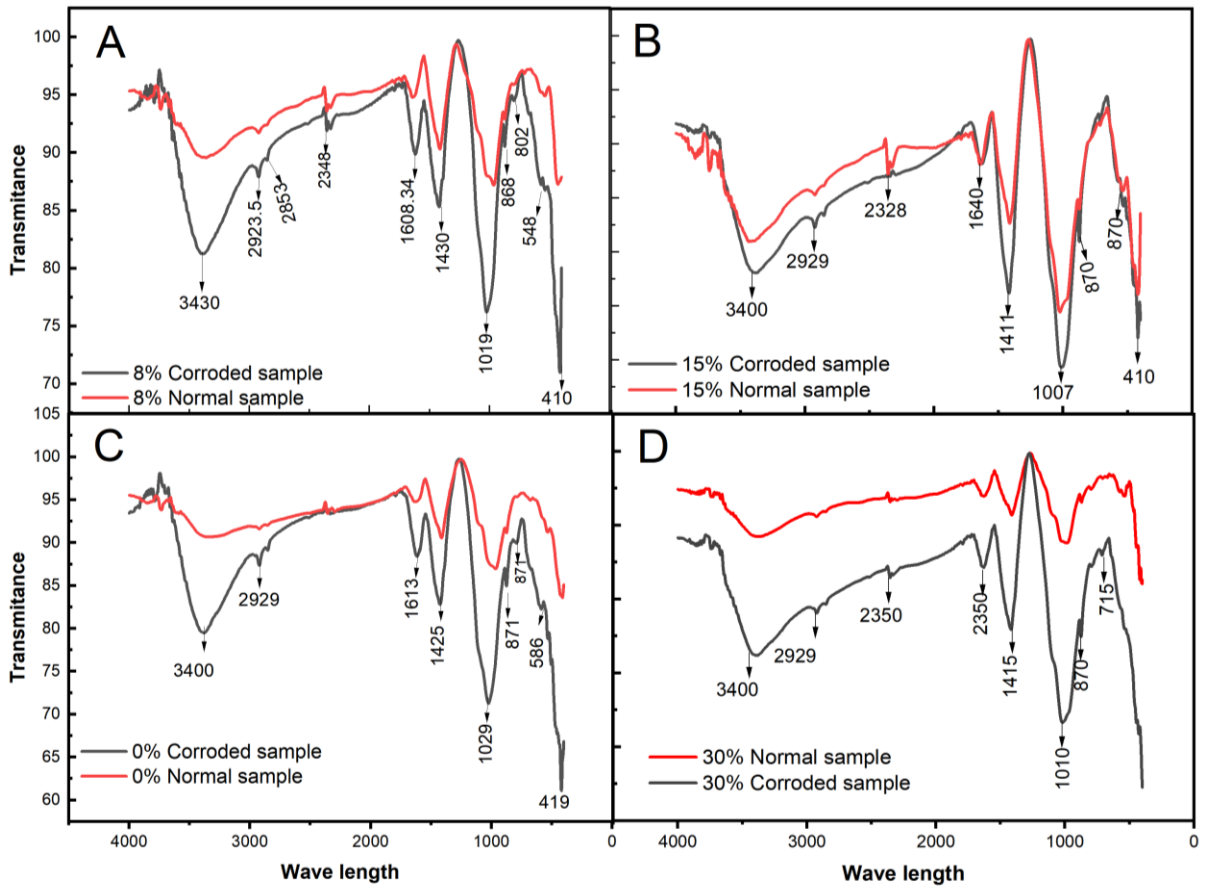

Figure 4.15 FTIR analysis for concrete in 0%,8%,15%, and 30% addition OFI for RC and plain concrete samples

As shown in Figure 4.15, this study tested the FTIR analysis for RC samples subject to corrosive environments using the impressed current method alongside plain concrete samples to analyze their morphology. All the graphs displayed in Figure 4.15 share similar peaks,

ranging from 3400 - 870 cm^{-1}, except for the peak number, which is not visible in graph C (0% addition of OFI Corroded and Convectional samples).

These peaks represent various elements present in concrete samples, such as O-H stretching vibrations found in water molecules or hydroxyl groups at 3400 cm^{-1}, which could be attributed to absorbed or adsorbed water, or hydroxyl groups present within the cement hydration products, such as calcium silicate hydrates (C-S-H) and calcium hydroxide. The presence of C-H stretching vibrations found in organic compounds, specifically in the methylene (CH2) groups, is indicated by the peaks at 2928.5 cm^{-1} and 2853 cm^{-1}. In concrete, this could be due to organic additives (OFI) (Bayar et al. 2016; García-Barradas et al. 2022), and the impurities possibly result from the degradation reinforcement in concrete. The peak at 2348 cm^{-1} might be linked to the presence of CO2 gas, which, in concrete, can be due to carbonation, a chemical reaction where calcium hydroxide reacts with atmospheric CO2 to form calcium carbonate.

The peak observed at 1608.34 cm^{-1} is linked to the bending vibration of water molecules or the stretching vibrations of C=O in carbonate species, such as calcium carbonate, which may form during carbonation. The peak at 1429 cm^{-1} is typically associated with the asymmetric stretching vibrations of $CO3^{2-}$ in carbonate compounds, suggesting the presence of calcium carbonate in the concrete. This can result from carbonation or be a part of the initial cement composition (e.g., limestone). Furthermore, the peaks at 1019 cm^{-1} and 868 cm^{-1} might be ascribed to the Si-O-Si stretching vibrations in the silicate framework of the C-S-H gel, a vital component of hydrated cement paste in concrete.

The presence of a peak at 802 cm-1 could potentially be linked to the existence of aromatic compounds or unsaturated aliphatic hydrocarbons. This may result from phenolic compounds found within the Opuntia ficus-indica extract (Cárdenas et al. 2008; Sáenz et al. 2004; Waghmare et al. 2022). Additionally, peaks observed at 548 and 410 cm-1 could be connected to metal-oxygen (M-O) vibrations or other inorganic substances in the corrosion products.

This study has observed that FTIR graphs of corroded and normal concrete samples have similar peaks and wavelengths, as they share similar chemical compounds. However, the lower transmittance observed in the corroded sample is mainly due to corrosion by-products that lead to higher absorption of infrared light at specific wavelengths. The transmittance value is lower in concrete with a 30% OFI addition. This observation can be related to the findings of the study in section 44, which show that the crystalline size of concrete samples with 30% OFI is more significant than any other addition. This also explains that although the 0% OFI addition

concrete samples have the largest crystalline size, the higher transmittance can be attributed to the larger interplanar spacing between atoms, indicating the porosity of the material and the presence of voids between atoms in the crystalline arrangement. Furthermore, the gel-like structure observed in the SEM analysis discussion 4.6.2 is another reason for the concrete's stable crystalline structure, contributing to the lower transmittance. This is related to forming a passive layer, which has increased in thickness from the expected 10^-3 nm. This thicker layer helps maintain the concrete's crystalline structure and capacity for concrete to resist corrosion and results in lower transmittance.

Given that the morphological analysis alone cannot accurately determine the extent of corrosion in concrete, this study will further investigate concrete's direct corrosion inhibition capacity through electrochemical analysis. In the upcoming discussion, electrochemical Impedance Spectroscopy (EIS) and Tafel plot techniques will be employed to measure and evaluate the concrete's corrosion resistance properties. These methods will provide valuable insights into the effectiveness of corrosion inhibition in the concrete samples under investigation

4.7 Electrochemistry Analysis

The Electrochemical test evaluates the performance of reinforced concrete samples exposed to an artificial corrosive environment over 504 hours. After exposure, samples are subjected to destructive tests that separately analyze the reinforcement bar and Concrete. Rust on the bar is evaluated through Electroimpedance Spectroscopy to determine which concrete mix is most effective at protecting against corrosion. The Tafel technique is employed to determine the corrosion inhibition efficiency of the concrete sample, and electro-impedance spectroscopy is applied to determine the corrosion resistance capacity of the concrete sample. Which is discussed in the section as follows.

4.7.1 Electro-Impedance Spectroscopy Test

Electrochemical impedance spectroscopy (EIS) is a powerful and widely used technique to study the electrochemical processes and mechanisms of corrosion inhibitors in Concrete. In addition, it is a highly reliable technique for monitoring corrosion and is an ideal means of providing kinetic information regarding corrosion reactions on electrodes (Harrington and Van Den Driessche 2011; Özcan 2008; Poupard et al. 2004). Due to this reason, EIS offers valuable information about the performance of Opuntia ficus-indica as a corrosion inhibitor for

reinforced Concrete. It determines the effectiveness of the plant extract in reducing corrosion rates and protecting the reinforcement steel bars inside the Concrete.

4.7.1.1 Electro-Impedance Spectroscopy Test For Carbon Steel

A three-electrode system was utilized to evaluate the behavior of carbon steel. The working electrode is grade 60 carbon steel bars, adhering to the specifications outlined in Table 4.15.

Table 4.15 Composition of selected reinforcement for the experiment

C	Si	Mn	P	S	Cr	Mo	Ni
0.178	0.228	0.632	<0.0030	0.025	0.063	0.019	0.113
Cu	Al	Co	Nb	Ti	V	W	Fe
0.314	<0.0030	0.011	<0.0050	<0.0030	0.00071	<0.030	98.37

Within this experimental setup, a Mercury/mercury chloride electrode was employed as the reference electrode to ensure a stable potential reference throughout the test. A graphite electrode served as the counter electrode, facilitating the necessary flow of electrons within the system. The electrolyte used was a 3.5% sodium chloride solution, which creates an environment conducive to corrosion. Figure 4.16 illustrates the arrangement of the setup.

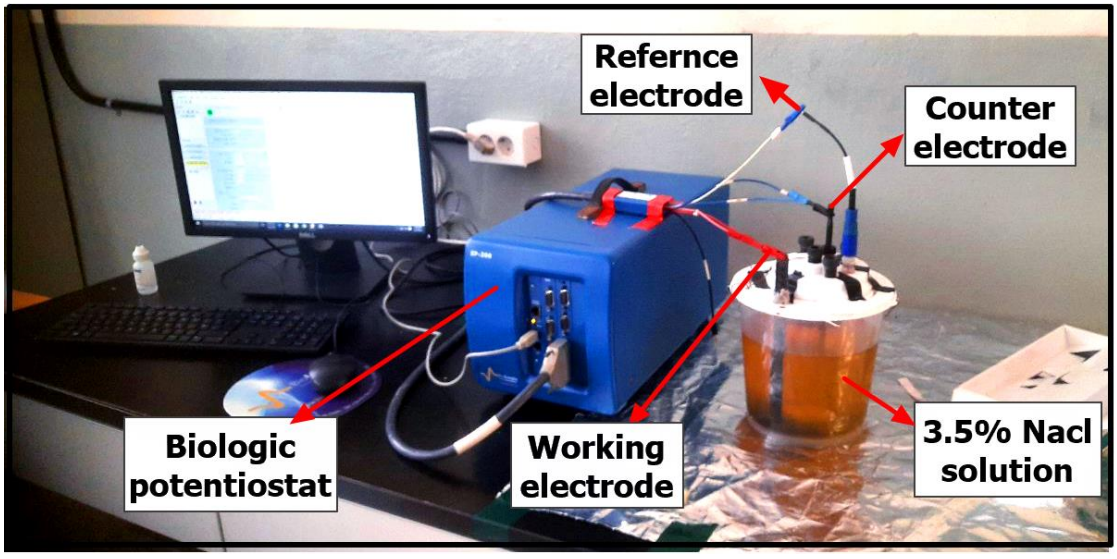

Figure 4.16 EIS measurement Apparunts setup for reinforcement sample

The Potentio Electrochemical Impedance Spectroscopy (PEIS) measurements were carried out within the 100 to 100 mHz frequency range $f = \frac{\omega}{2\pi}$, using logarithmic spacing and six points per decade. As per ASTM G3-89, the researchers set the E value at 0.2600 V relative to the

reference, resulting in an applied small sinusoidal voltage of 10 mV $v(t) = Vosin(\omega t)$. The steady-state current response, $It = Iosin(\omega t + \theta)$, is measured, which has a phase difference of θ from the applied voltage. The impedance, $Z = \frac{\Delta E}{\Delta I}$, is then measured using Ohm's law (Sohail et al. 2020). These specific parameters also align with the experimental setup employed by Sun et al.(2021).

4.7.1.1.1 Niqust Impedance

Nyquist plots are shown in Figure 4.17 for the studied rebar after the active corrosion state inside chloride-contaminated Concrete and without adding opuntia ficus indica concrete.

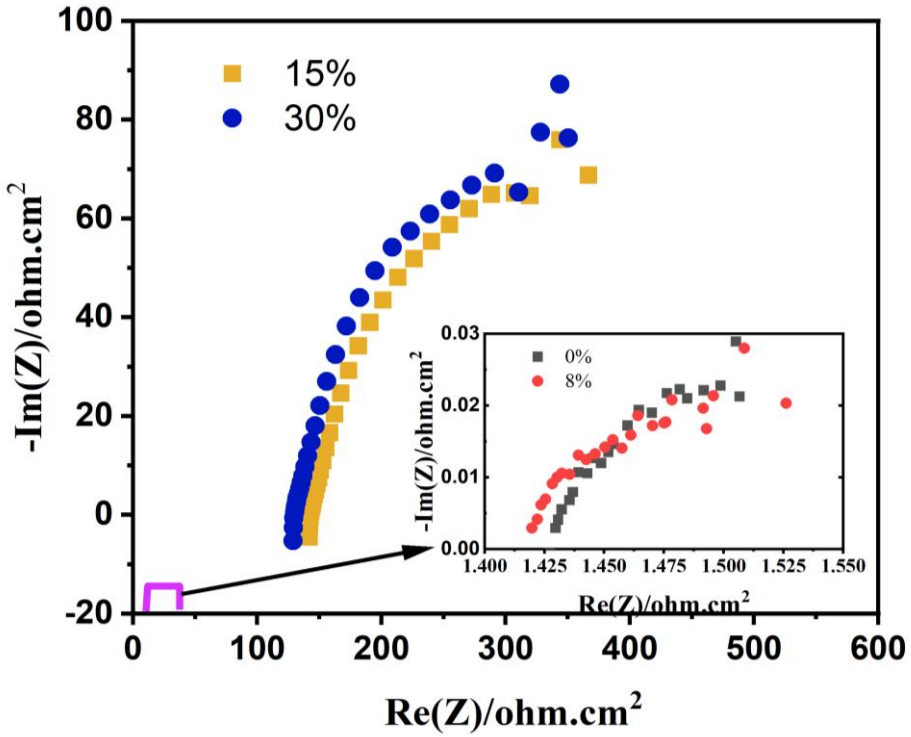

Figure 4.17 A Nyquist plot is for reinforced bars cast in Concrete with and without OFI addition.

The 15% and 30% OFI concrete addition showed similar behavior. Compared with 0% addition, 8% addition does not appear to affect significantly concretes. Figure 4.17 illustrates the frequency ranges of each capacitive arc. Despite corrosion rebar offering less corrosion resistance than standard rebar, the electrochemical impedance spectrum space was within an acceptable range because the reinforced Concrete had been exposed to chloride-containing corrosive environments before the EIS tests. 0% and 8% of the OFI additions were severely corroded, which resulted in reduced electrical resistance. In this case, the Nyquist plot gets closer to zero than with passive rebars, dry Concrete, and chloride-free Concrete. Several other

researchers obtained similar space spectrums. In this regard, Hu et al. (2013) and Sohail et al. (2020) observed similar Nyquist plot ranges. Based on the physical impedance phenomenon of RC, proposed equivalent circuit models, shown in Figure 4.18, were fitted against the experimental results to assess the active corrosion of rebar in Concrete after 504 days of conditioning in a chloride solution.

4.7.1.1.2 Bode impedance

Figure 4.18 illustrates the corrosion inhibition effect of OFI in Concrete using a Bode diagram of steel behavior in 3.5 wt.% NaCl and the impedance module |Z| against frequency. A single time constant can be observed at short time lapses (0.5 h). The single time constant appears as a straight line with a slope close to -1 at medium-low frequencies, followed by a straight line parallel to the x-axis at high frequencies. A plateau in the impedance magnitude was observed at low frequencies, indicating a stable and consistent value for R1 (Park and Yoo 2003). Accordingly, the lowest log /Z/ values were observed for 30%,15%,8%, and 0% OFI additions, respectively, indicating that a lower value will lead to higher polarization resistance. This shows that the electrolyte used in our corrosion testing exhibits good conductivity and provides a low-resistance path for current flow.

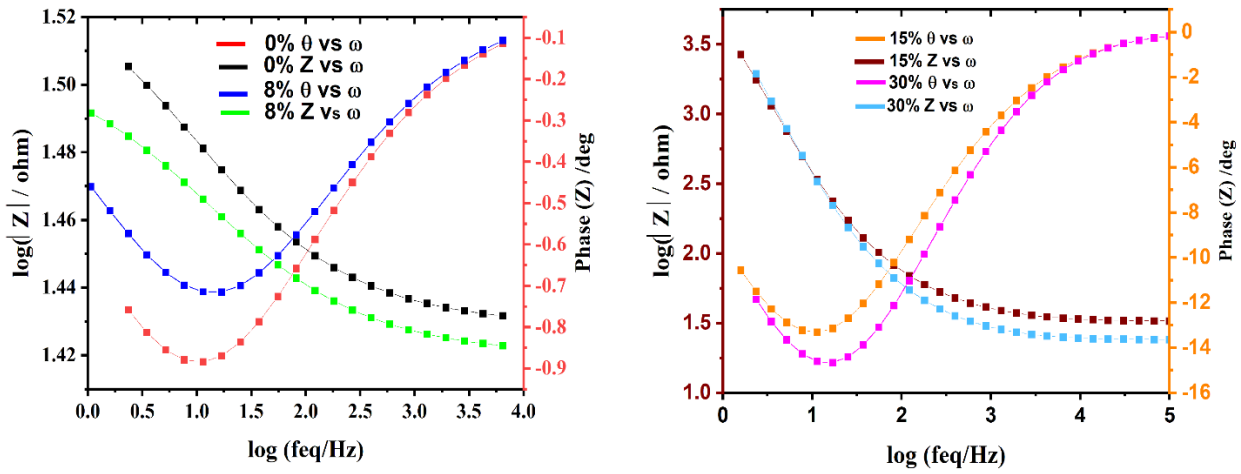

Figure 4.18 Bode impedance curve for investigated Carbon steel reinforcement sample

Figure 4.18 shows the angle phase evolution to the frequency logarithm with and without OFI reinforcement bars. The curves show a constant time with a maximum point at short exposure times. This behavior has been attributed to semi-infinite diffusion phenomena at pores, tangential electrolyte penetration in the interphase metal, and distribution of relaxation times due to heterogeneous electrolyte penetration (Koleva et al. 2007). According to the theta vs. Frequency diagram (Figure 4.18), an increase in the concentration of OFI mucilage in the test

solution is observed to increase the negative value of the phase angle at high frequencies. More negative phase angles corresponded to more capacitive electrochemical behavior (Khaled and Hackerman 2003). Increasing the concentration of mucilage resulted in an enhanced capacitive response, suggesting more inhibitory behavior.

4.7.1.1.3 Equivalent circuit

The Randel's-modified circuit selected for this study is shown in Figure 4.19 and comprises series-parallel resistors and an impedance element. In EIS, this element represents the resistance and capacitance of the electrolyte at the metal-electrolyte interface. R1 (resistance of solution) and C1 (capacitance) are connected in series. The electrolyte resistance is associated with the ionic conductivity of the resolution, whereas the double-layer capacitance is associated with the electrical charge separation at the metal surface. The potential resistance (R2) is connected in parallel with the series combination of R1 and C1, which relates to corrosion.

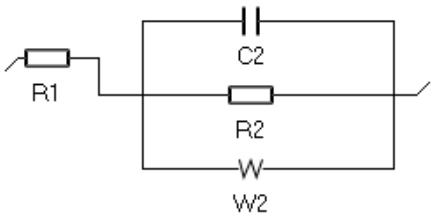

Figure 4.19 Modified Randles circuit.

Corrosion resistance describes the resistance to current flow due to corrosion reactions occurring on a metal surface. The magnitude of R2 indicates the extent of corrosion of corroded rebar. It is based on electron transfer kinetics between the rusty rebar and the electrolyte. The resistor R3 represents the resistance offered by corrosion-damaged rebar during EIS measurement. Because corroded rebar can significantly affect the electrochemical behavior of a system (Hu et al. 2013), it is an essential component to consider, and t is conceived in conjunction with Warburg impedance and in parallel with R2. Warburg impedance (W3) describes diffusion-controlled processes in the electrolyte solution, such as the diffusion of chloride ions in the NaCl solution towards the corroded rebar. The average values of the impedance parameters obtained by fitting the model are shown in Table 4.16.

Table 4.16 Average value of electro-impedance parameters

Samples (rebar)	R1 ($Ohm.cm^2$)	C2 (F)	R2 ($Ohm.cm^2$)	S2 ($Ohm.s^{-1/2}$)

0% addition of OFI	1.429	$2.829e^{-9}$	0.1107	0.607
8% addition of OFI	1.42	$3.138e^{-9}$	0.08848	0.5694
15% addition of OFI	1.513	what	3.169	10.21
30% addition of OFI	1.379	$0.2639e^{-3}$	3.433	11.53

Regarding resistance polarization, the R2 value was 0.11107, 0.08848, 3.169, and 3.433, respectively. Although R2 of 30% addition was higher than those of the other steel rebar, these values suggest a minor corrosion current was going through 30% addition. These currents were generated by corrosion of the electrical connections. In the case of 0% addition,8% addition, 15% addition, and 30% addition, the double layer capacitance was found to be 2.829e-9 F, 3.138e-9 F, 0.223e-3F, and 0.2639e-3F. The higher capacitance of the double layer in the case of 0% and 8% indicates that iron ions have deposited on the steel surface, and corrosion is more severe than 15% and 30% additions. In 15% addition and 30% addition of OFI, the Warburg impedance coefficient was lower than 0% addition and 8% addition. Thus, species diffusion within the system appears more restricted or hindered at these levels. These results related to factors such as the inhibiting ability of OFI and making the rebars contain thicker diffusion layers, a higher viscosity, or a reduced diffusion coefficient.

4.7.1.2 Electro-Impedance Spectroscopy Test For Concrete

A three-electrode system was utilized to evaluate the behavior of concretes. The working electrode is plain Concrete with a connection to the standard kit. Within this experimental setup, a mercury/mercury chloride electrode was employed as the reference electrode to ensure a stable potential reference throughout the test. A graphite electrode served as the counter electrode, facilitating the necessary flow of electrons within the system. The electrolyte used was a 3.5% sodium chloride solution, which creates an environment conducive to corrosion. Figure 4.2 illustrates the arrangement of the setup. The Potentio Electrochemical Impedance Spectroscopy (PEIS) measurements were carried out within the 100 to 100 mHz frequency range $f = \frac{\omega}{2\pi}$, using logarithmic spacing and six points per decade. As per ASTM G3-89, the researchers set the E value at 0.2600 V relative to the reference, resulting in an applied small sinusoidal voltage of 10 mV $v(t) = Vosin(\omega t)$. The steady-state current response, $It = Iosin(\omega t + \theta)$, is measured, which has a phase difference of θ from the applied voltage. The

impedance, $Z = \frac{\Delta E}{\Delta I}$, is then measured using Ohm's law (Sohail et al. 2020). These specific parameters also align with the experimental setup employed by Sun et al.(2021).

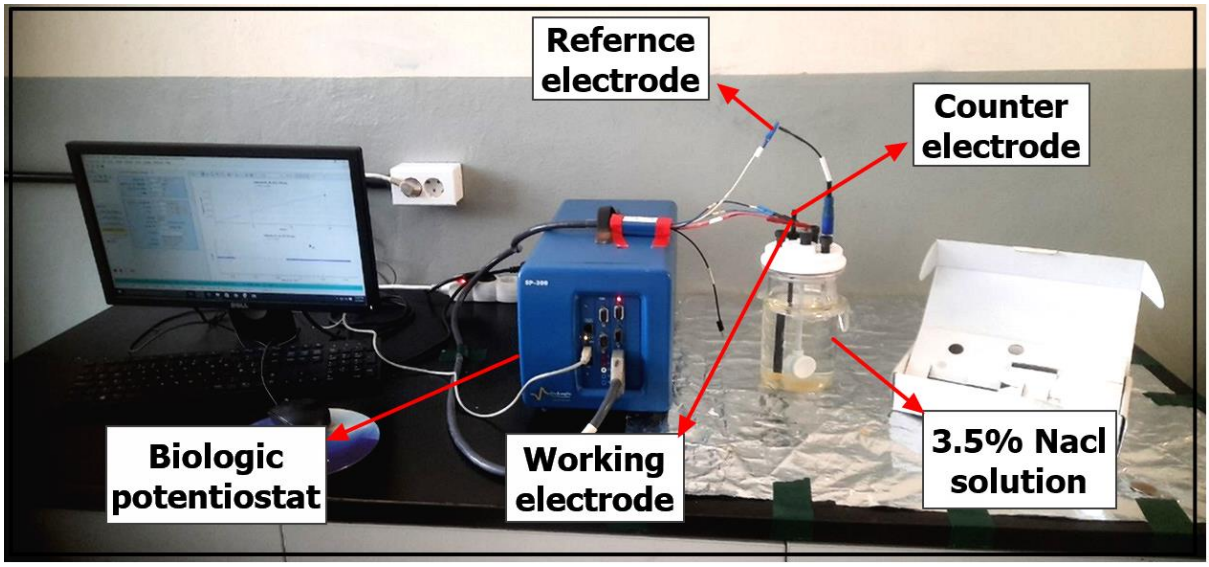

Figure 4.20 EIS measurement Apparunts setup for Concrete sample

4.7.1.2.2 Niqust Impedance

A Nyquist diagram of Concrete with various concentrations of Opuntia ficus-indica is presented in Figure 21.

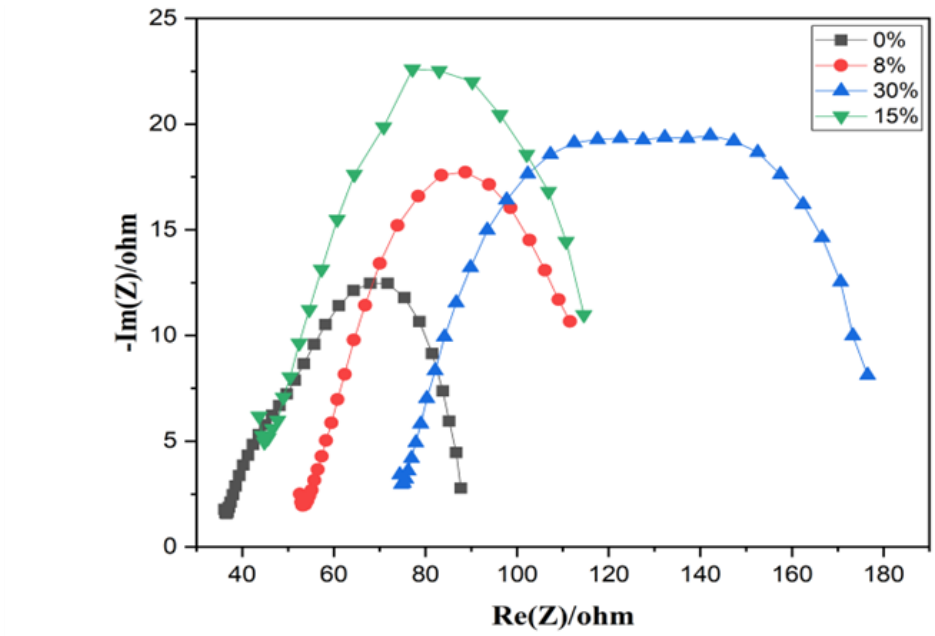

Figure 4.21 Z-fitted Nyquist diagram for all concrete samples

The data indicate a single, capacitive-like, depressed semicircle with its center on the real axis, which suggests a charge transfer controlled process, and this does not change when Opuntia

ficus-indica is added. With an increase in inhibitor concentration up to 15% or 30%, the semicircle diameter increased, reaching its maximum value when 15% Opuntia ficus-indica was added, resulting in the lowest corrosion rate. When inhibitor concentrations were lower than 15%, the semicircle diameter decreased, reaching its lowest value and having the highest corrosion rate.

The electrochemical parameters shown in Table 4.13 support the use of Nyquist diagrams. A 15% Opuntia ficus-indica concentration provided the most outstanding inhibitor efficiency, as validated by the highest charge transfer resistance value (R2). Note that at 15% OFI, the solution exhibits a more substantial resistance value than observed at the other concentrations. It may be caused by dissolving corrosion products into the solution, increasing the solution's resistance, or decreasing its conductivity. Cdl, the double-layer capacitance value, decreases with the addition of Opuntia ficus-indica and reaches its lowest value with OFI. Due to the absorption of Opuntia ficus-indica and the replacement of water molecules on concrete-steel surfaces, this occurs. Table 4.17 shows the results of using the same equivalent circuit discussed in section 4.7.2.1.3.

Table 4.17 Average value of electro-impedance parameters

Samples (Concrete)	R1 (Ohm)	C2 (F)	R2 (Ohm)	S2 (Ohm.$s^{-1/2}$)
0% addition of OFI	36.16	$0.114e^{-12}$	58.83	458.7
8% addition of OFI	51.83	$0.2178\ e^{-12}$	79.03	597.8
15% addition of OFI	73.03	$0.1064\ e^{-12}$	106.5	1260
30% addition of OFI	43.09	$9.545e^{-6}$	89.1	595.9

4.7.1.2.3 Bode impedance

The Bode diagrams in Figure 4.22 illustrate the concrete polarization and solution resistance across a frequency range. All graphs representing various OFI additions exhibit higher log/Z/ values in the low-frequency region than those at high frequencies. It suggests that the curves accurately depict the nature of the system. The corrosion inhibition capability can also be deduced from the Bode plots by examining the peak variations. Lower log/Z/ values indicate the solution resistance (R1), while higher peaks represent the polarization resistance values (R2 + R1). Compared with 0% OFI addition, the 15% and 30% OFI additions display a more significant peak variation at both low and high frequencies, demonstrating the effectiveness of incorporating OFI into the system.

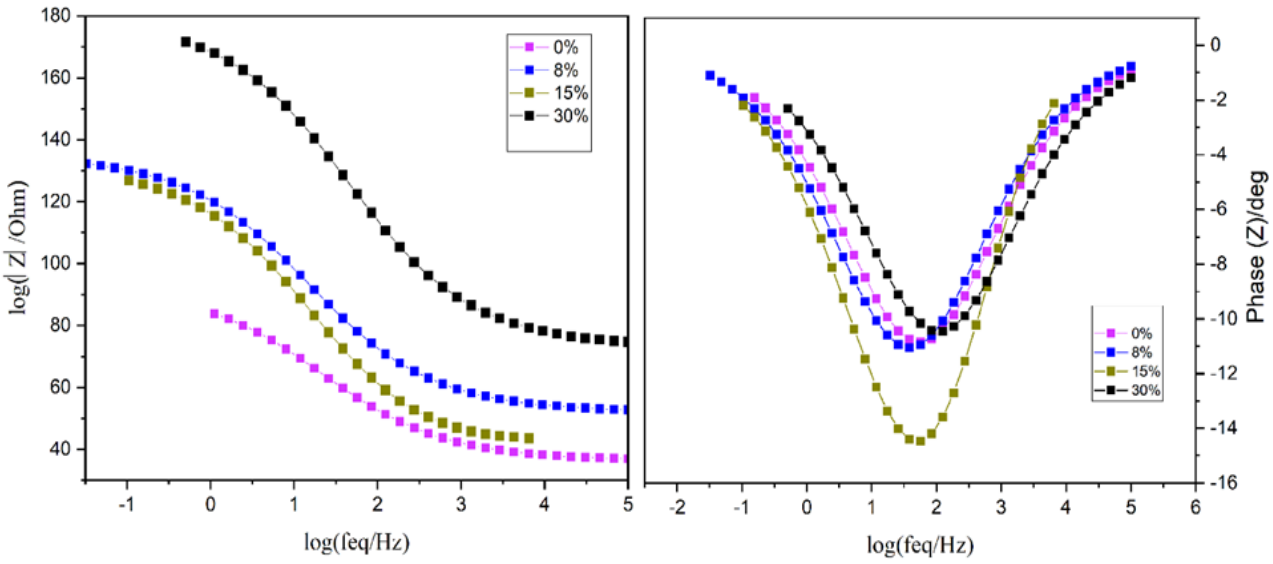

Figure 4.22 Bode impedance graph log /Z/ vs. Log feq/Hz and log (feq/Hz) vs. Phase (Z)/deg

4.7.2 Tafel Test

4.7.2.1 Tafle Test Setup And Parameters

The electrochemical testing utilized the biologic SP-300 potentiostat device for conducting the Tafel analysis. This experiment used a standard electrode connection and electrode material that contained electrolytes. The experimental setup included two techniques: Technique 1 focused on measuring the Open Circuit Voltage, and Technique 2 focused on generating a Tafel plot. In Technique 1, the applied potential (Ewe) was controlled between -2.50 V and 2.50 V. The potential (Ewe) and current (I) signals were filtered at 5 Hz. Safety limits were provided to prevent the experiment from starting in case of E overload, and the channel configuration was grounded.

Tafel plots were given a 30-minute duration. The dER/dt (change in E rate with respect to time) was set at 5.0 mV/h, and the dER (change in E) was set at 5 mV. The dtR (time step) was 1.00 seconds. For the dE/dt scan rate, a value of 1.000 mV/s was utilized. The initial potential (Ei) was set at -0.300 volts, and a reference electrode potential of 0.250 volts indicated the end potential for this experiment. This same scan rate and voltage window were adopted in the study conducted by Sun et al. (2021). The investigation recorded the current (I) values and set the step percentage to 25, with a total of 5 steps. The E range for the Tafel plot is set to -2.50 V to 2.50 V, while the current range is set to auto with a minimum and maximum of 10 mA. An 8-bit bandwidth is employed for the experiment.

4.7.2 Tafel Test Results

Figure 4.23 represents the Tafel polarization curves obtained from the Tafel analysis test. The corrosion potential (Ecorr) and, corrosion current density (Icorr), polarization resistance (RP) extracted from the plots are reported in Table 4.14. Also, the polarization resistance (RP) of samples was determined by the Stern–Geary equation 4.1 (Angst and Büchler 2015; Verma et al. 2015):

$$Rp = \frac{\beta a * \beta c}{2.303 * Icorr(\beta a + \beta c)} \qquad \text{Equation 4. 1}$$

The Tafel slopes, βa (anodic Tafel slope) and βc (cathodic Tafel slope) provide information about the kinetics of the corrosion process. The βa value reflects the anodic reaction rate, while the βc value indicates the cathodic reaction rate. Steeper slopes, i.e., the higher value for both βa and βc, suggest faster reaction rates and a more active corrosion process.

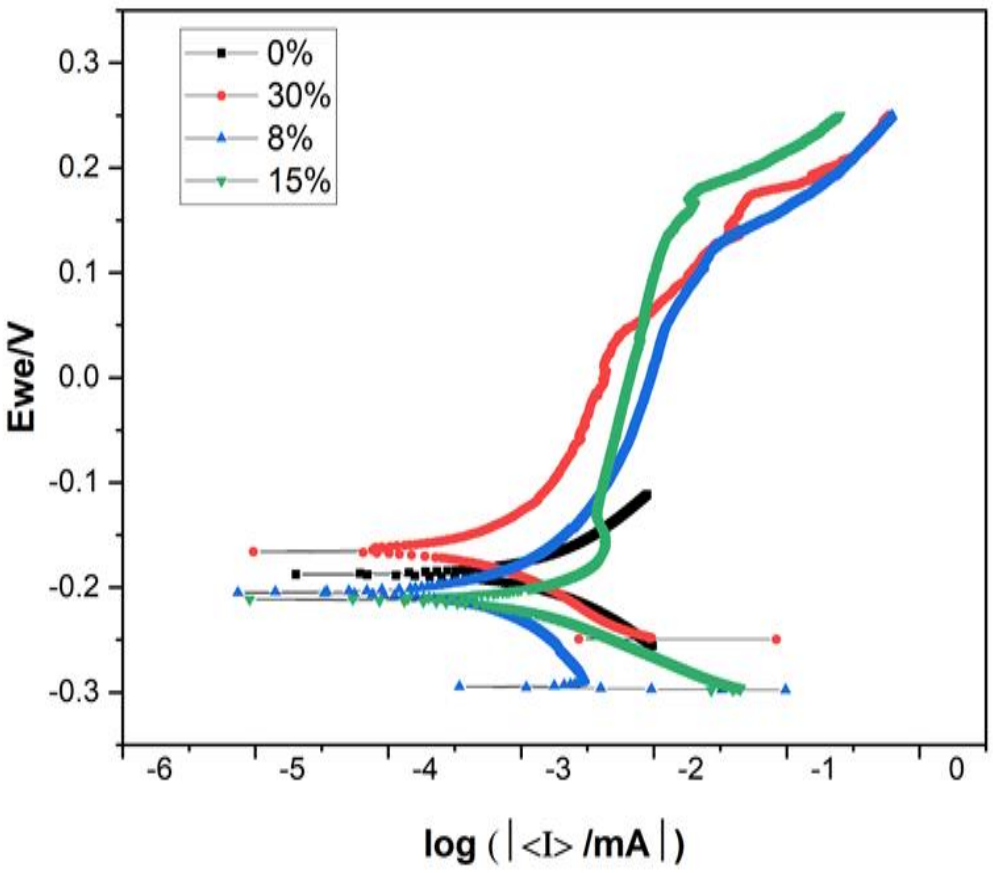

Figure 4.23 Tafel extrapolation plot of different Percentage addition of OFI concretes

The Tafel result in Table 4.18 shows the effect of adding opuntia ficus indica (OFI) as a corrosion inhibitor to a solution. There are five different parameters displayed: Ecorr (mV), βa

(mV), βc (mV), Icorr (μA), and Rp (Ω). Additionally, the corrosion inhibition efficiency (IE%) is calculated.

Table 4.18 Tafel analysis result

Samples	Ecorr (mV)	βa (mV)	βc (mV)	Icorr (μA)	Rp(Ω)	IE%
0% adtion of OFI	-187.265	121.2	101.6	2.195	10.93334	0.0000
8% adtion of OFI	-206.949	144.3	145.0	0.868	36.18031	0.6045
15% adtion of OFI	-214.282	48.1	39.9	0.736	12.86659	0.6646
30% addition of OFI	-166.503	107.5	63.0	0.430	40.11088	0.8041

4.7.2.1 Corrosion Current Density (Icorr)

As demonstrated by the results in Table 4.14, the value of Icorr decreases as the percentage of OFI addiction rises. This finding is directly related to the corrosion inhibition capacity of OFI in Concrete since (Berradja 2019) defines Icorr (μA) as a corrosion current that quantifies the rate at which corrosion occurs. An immense Icorr value implies a higher corrosion rate, signifying a less effective anti-corrosion protection capability. Due to this reason, Concrete with an addition of 30% OFI is the more corrosion resistance concrete mix since it has the least Icorr (μA) = 0.430 value. These findings have also been validated by (Díaz Blanco et al. 2019b) using similar measurements for determining Icorr. The addition of OFI affects both the anodic and cathodic Tafel slopes βa (mV) and βc (mV), suggesting that the inhibitor interacts with both the anodic and cathodic processes.

4.7.2.2 Tafel Slopes

The anodic and cathodic Tafel slopes, represented by βa and βc, respectively, provide insight into the kinetics of the corrosion process. The βa value reflects the anodic reaction rate, while the βc value indicates the cathodic reaction rate. A steeper slope for both βa and βc suggests that the reaction rates are faster with higher positive values of βa and βc and that the corrosion process is more active (Berradja 2019; Li et al. 2018). Tafel plot results show that for 15% and 30% OFI addition, the values of βa and βc are lower than 0% OFI. It indicates that adding OFI to the concrete mix affects the corrosion process in Concrete.

Additionally, it was observed that all samples had a higher βa than βc value, signifying that anodic dissolution of the rebar is the dominant factor underlying corrosion in all composition

percentages. It could be attributed to the aggressive environmental conditions where chloride content is high. On the other hand, there may be merit in using OFI (Cardoso et al. 2021) note that this cactus species has a wealth of bioactive phenolic compounds, including flavonoids, betalains, and phenolic acids – as its antioxidant properties can act as reprieve against oxidative stress in Concrete, hence reducing corrosion damage.

4.7.2.3 Corrosion Potential (Ecorr)

Corrosion potential (Ecorr) represents the electrode potential at which the anodic and cathodic reactions are balanced. A more negative Ecorr value indicates a higher tendency for corrosion, while a less negative or positive value suggests a more stable or passivated state (Berradja 2019).

4.7.2.4 Polarization Resistance (Rp) And Inhibition Efficiency (IE%)

According to Table 4.14, the inhibition efficiency of OFI increases as the percentage addition amount of OFI increases; however, it is unlikely that the resistance polarization increment from addition to addition occurs linearly. It may be related to the complex characteristics of the tafel test as the Icrro value obtained appears to fluctuate from 0% to 15% and decrease after storage. As a result, the two electrochemical tests of corrosion density (Icorr) were conducted.

A comparison is presented in Figure 4.24 between corrosion current densities calculated using the two electrochemical techniques. Both techniques were found to yield close agreement on the measured currents.

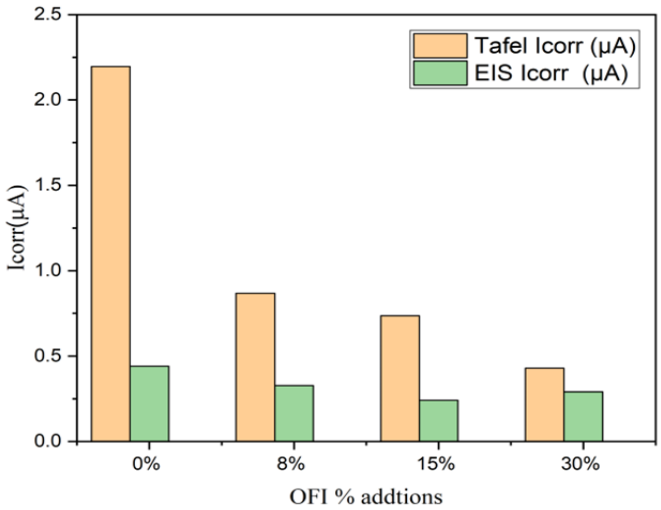

Figure 4.24 Comparison between current density obtained from the Tafel test and EIS test

According to the Sohail et al. (2020) study, the Stern and Geary constant B was recommended to be 26 mV and 52 mV for active and passive steel, respectively, to calculate Icorr using Icorr

= B/Rp. Since all steel rebars in this study were in an active corrosion state, the B was taken at 26 mV. For Icorr values to be approximately the same as those obtained from Tafel plots, B equal to 26 mV is used. For B to be similar to 26 mV, both ba and bc need to be significantly lower than observed in this study since it depends on ba and bc. A value of 42 mV to 53 mV would be obtained based on the obtained values. Other researchers (Martinez-Molina et al. 2016; Torres-Acosta and González-Calderón 2021)also reported higher values of anodic and cathodic Tafel slope constants (more than 120 mV/dec). For a better understanding of corrosion kinetics, further research on Tafel parameters for steel rebar in Concrete is needed.

After conducting electrochemical measurements on both the reinforcement samples and the concrete, it has been determined that adding 30% OFI (Opuntia ficus INdica) in concrete yields the most promising results. Therefore, further investigation will focus on studying the mass loss of the reinforcement after exposure to corrosion. This concrete composition with 30% OFI addition exhibits favorable properties for inhibiting corrosion and will be examined more closely in subsequent analyses.

4.8 Mass Loss Measurement

A mass loss measurement of reinforced concrete refers to quantifying the weight reduction in the material caused by factors such as corrosion and deterioration over time (Martinez-Molina et al. 2016). This is usually measured regarding the weight loss of the reinforcing steel bars (rebars) embedded within the concrete.

Following the accelerated corrosion test, the rebars from each sample are extracted and cleaned following ASTM G 01-03 standards. This standard suggests three cleaning methods: mechanical, chemical, and electrolytic. This study chose chemical cleaning due to its relative simplicity and lack of need for providing high current density, as required in electrolytic methods. ASTM G 01-03 outlines six potential solutions for washing and removing corrosion products from iron. A solution consisting of 200g NaOH, 20g zinc powder, and reagent water (deionized water) was selected for this study, as shown in Figure 25 because these chemicals are widely available. This solution requires immersing the rebars for 30-40 minutes at an 80-90°C temperature, as demonstrated in Figure 4.25. This temperature was achieved using a water bath.

Figure 4.25 A) string NaOH and Zinc, B) Bathtub washing, C) open-air oven dry

The results presented in Table 4.19 demonstrate a clear trend: as the addition of Opuntia Ficus indicia (OFI) in concrete increases, the corrosion rate and the mass loss decrease. This observation provides strong evidence of the corrosion inhibition capacity of OFI in concrete. The higher the proportion of OFI added, the greater the reduction in corrosion rate and mass loss, indicating the effectiveness of OFI in inhibiting corrosion processes.

Table 4.19 Mass loss reinforcement calculation

K= A CONSTANT	87600		
T= time of exposure in hours	504		
A= area in cm^2	175.84		CR= k(W1-W2)/A*T*D
D= density in g/cm^3	7.82		
W= mass loss in grams	260		
	Final mass W2	Initial mass W1	
0%	223	261	4.803222868
	226	260	0.047930469
	229	260.5	0.012216401
8%	234	260.5	1.58149E-05
	233	260	0.000608259
	237	261	0.000441933
15%	245	260	0.000271514
	248	261	0.000230387
	246	260	0.000242144

	258	260	3.23608E-05
30%	255	260	7.92803E-05
	257	261	6.22615E-05

This observation provides strong evidence of the corrosion inhibition capacity of OFI in concrete. The higher the proportion of OFI added, the greater the reduction in corrosion rate and mass loss, indicating the effectiveness of OFI in inhibiting corrosion processes. After determining the mass loss in the reinforcement, further analysis was conducted using an optical microscope to assess whether the reinforcement was susceptible to pit corrosion or uniform corrosion.

4.9 Optical Microscope Test Result

The optical microscope allows for a detailed examination of the surface morphology and characteristics of the reinforcement. By closely inspecting the surface, any signs of localized pit corrosion, characterized by small, deep pits or uniform corrosion, which results in a more evenly distributed corrosion pattern, can be identified. This analysis provides valuable insights into the corrosion behavior and damage mechanisms affecting the reinforcement. Based on the observation of Figure 4.26, this test method analyzes the most unfavorable condition of the reinforcement section for all concrete additions subjected to rebars.

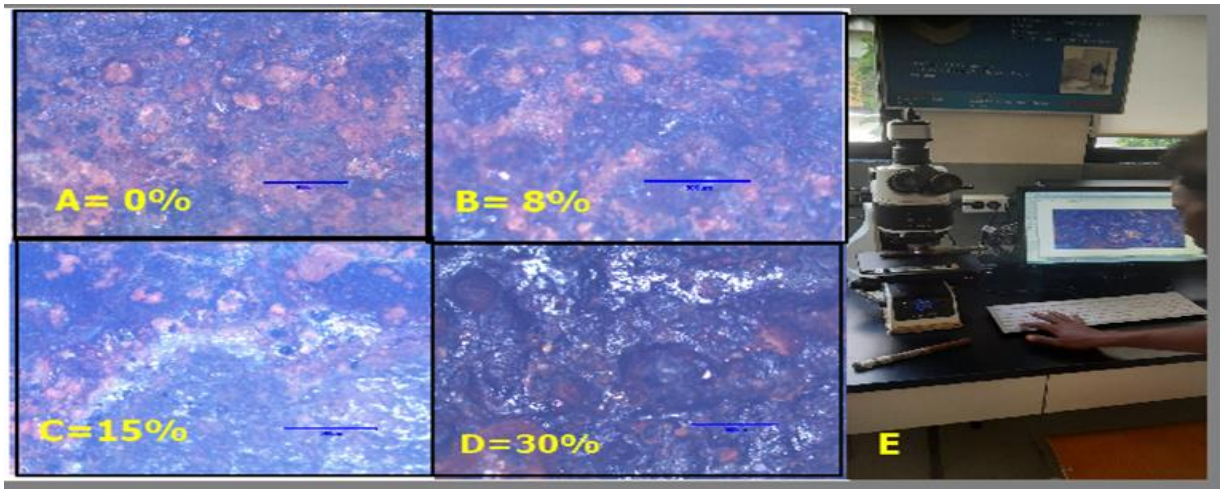

Figure 4.26 A, B, C, and D Optical microscope from reinforcement bar after different % addition of OFI and E) optical microscope measurement

This figure indicates that pitting corrosion is present in all the rebars examined in the current study. However, the severity of corrosion decreases as the percentage addition of OFI percentage in concrete increases. In other words, higher percentages of OFI additioned concrete

exhibit reduced pitting corrosion. This finding highlights the potential corrosion mitigation effect while increasing OFI addition percentages in concrete, inhibiting the formation and progression of pitting corrosion on the rebars.

The results confirm that chloride ions penetrate the concrete and reach the surface of the rebars, validating the effectiveness of the employed accelerated corrosion method, known as the impressed current method. Furthermore, the inhibitory effect of Opuntia ficus-indica (OFI) is not entirely protective. However, as the OFI addition increases, the level of inhibition also increases. This suggests a positive correlation between the concentration of OFI and its inhibitory impact on corrosion. While the protective nature of OFI may not be absolute, higher concentrations show enhanced corrosion inhibition properties.

After analyzing the type of corrosion present on the reinforcement, the study will proceed with the final test to assess the extent of corrosion in relation to the conductivity of the corroded area. To accomplish this, precise source measurements will be conducted.

4.10 Precision Source/Measure Unit

The precision source measurement unit was utilized to test the material's resistance by plotting the instantaneous applied voltage against the current reading for the samples. This method allows for the identification of the material's resistance. This method was chosen in this study based on the assumption that if materials are subjected to corrosion, their conductivity will be reduced. Therefore, by utilizing this method, any differences in conductivity can be observed in the reinforcement samples, indicating the extent of corrosion. A higher conductivity value would imply less corrosion in the material (Feliu et al. 1989). To perform this test, a reinforcement sample needs to be cut and extracted from the larger sample. To ensure minimal disturbance, an abrasive cutter machine is employed for precise cutting, as depicted in Figure 4.27a.

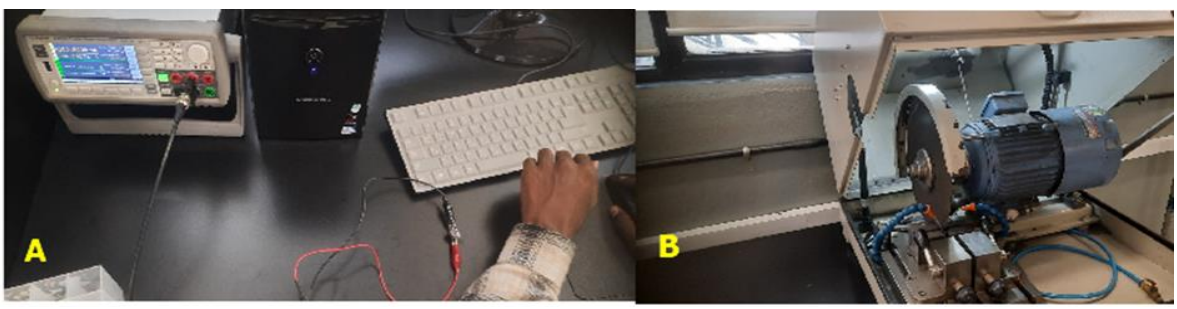

Figure 4.27 A) Precision unit measurement, B) Top met abrasive cutter

Once the sample is prepared, the precision unit measurement is conducted, as shown in Figure 4.27b. The measurement involves obtaining a graph with the slope representing the resistance (R) calculated using the equation R = V/I, as illustrated in Figure 4.28.

Figure 4.28 Iv curve

The above graph illustrates the relationship between the slope and the resistance of reinforcement bars extracted from concrete samples with varying OFI additions after undergoing corrosion. The slope value directly correlates with the resistance, with higher slope values indicating lower conductivity. Since resistance and conductivity are inversely proportional, decreasing slope values imply higher levels of corrosion and susceptibility in the reinforcement bars. Among the other OFI additions, it was observed that the 30% addition yielded the best corrosion inhibition performance for the reinforcement in concrete. This finding suggests that a higher percentage of OFI addition offers better protection against corrosion.

This study aimed to assess concrete's porosity, absorption, and total void characteristics by incorporating 5% FASG and 30% OFI in the mix. The study wanted to investigate the impact of OFI on these properties and evaluate its inhibitory capacity. So far, The results have

indicated that adding 30% OFI to the concrete mix exhibits significant inhibitory effects. In the next section of the study, the porosity, absorption, and total void aspects will be discussed, along with the specific durability tests and the contribution of OFI to these properties.

4.11 Total Void Percentage

ASTM C642 is a test method used to determine the total void percentage of hardened concrete. This test helps assess the porosity and density characteristics of the concrete, which can affect its strength, durability, and other mechanical properties. The aim was to assess concrete's porosity, absorption, and total void characteristics by incorporating 5% FASG and 30% OFI. Table 4.20 presents the results of evaluating the total void percentage in concrete mixes containing 30% OFI with 5% FASG and the control group comprising 5% FASG without OFI. The total void percentage values were obtained using equations 3.1-3.7, specified in the study. This analysis provides insights into the porosity and void characteristics of the concrete samples, allowing for a comparison between the two mix compositions.

Table 4.20 Total void percentage analysis result

Percentage addition of OFI and FASG	sample Name	Absorption after immersion %	Absorption after immersion and boiling	Bulk density, dry	Bulk density, after immersion	Bulk density, after immersion and boiling	volume of permeable void, %
5% FASG + 30% OFI	A-1	8.26	7.13	2.24	2.43	2.40	16.01
	A-2	6.74	5.91	2.07	2.20	2.19	12.22
	A-3	7.01	5.95	2.01	2.15	2.13	11.94
	A-4	7.04	6.40	2.02	2.16	2.15	12.93
	A-5	6.84	5.98	2.02	2.16	2.15	12.10
5% FASG + 0% OFI	O-1	8.31	6.67	2.17	2.35	2.32	14.51
	O-2	8.27	6.37	2.22	2.40	2.36	14.13
	O-3	8.46	6.37	2.01	2.18	2.14	12.80
	O-4	11.04	7.24	2.28	2.53	2.44	16.49
	O-5	8.11	7.12	2.27	2.45	2.43	16.16

In order to analyze the total void percentage, descriptive statistics have been performed in the following Table 4.21, and the full calculation data of the total void percentage is presented in Appendix A, Table A.11.

Table 4.21 Descriptive statistics for total void percentage calculation

Percentage addition of OFI and FASG	N total	Mean	Standard Deviation	Variance	Minimum	Maximum
5% FASG +30%OFI	5	13.04	1.70287	2.89975	11.94	16.01
5% FASG + 0% OFI	5	14.818	1.51963	2.30927	12.8	16.49

Based on the data presented in Table 4.16, the addition of 30% Optunia ficus indica (OFI) in the concrete mixture has significantly reduced the total void percentage, indicating improved durability. The total void percentage for the 30% OFI addition is 13.04 in Table 4.17. In contrast, the concrete mixture with only 5% fine aggregate scoria gravel (FASG) and no OFI shows a higher total void percentage of 14.18. This higher value can be attributed to the porous nature of FASG, which is known to be susceptible to corrosion, as discussed in Chapters 4.5-4.9. Comparing these results with other studies, it is observed that the total void percentage is lower in this study. This can be attributed to the internal curing capacity of FASG, which effectively hydrates the concrete and reduces surface voids. Furthermore, the addition of OFI contributes to filling voids due to its gel-like structure, further decreasing the voids in the concrete. Overall, the concrete mixtures containing FASG alone or combined with OFI did not significantly impact the total void percentage, but some improvement was observed compared to previous studies.

4.12 Summary

In this chapter, we have examined the results obtained by implementing the methods outlined in Chapter Three. The findings have revealed significant differences, enabling us to draw meaningful conclusions in line with the study's objectives. The conclusions and recommendations derived from these results will be presented in the subsequent chapter concisely and clearly, summarizing the key insights from this study.

CHAPTER FIVE

CONCLUSION AND RECCOMENDATION

5.1 Conclusion

The primary objective of this study is to investigate the optimal curing time and replacement ratio of scoria gravel for sand in concrete mixes to achieve the desired compressive strength of concrete with an effective internal curing effect. Observing the mix characteristics with 5%, 10%, and 15% FASG incorporation, it was observed that :-

- ✓ the concrete soaked for 0 days and left to cure for 28 days in open air exhibited significant compressive strength enhancement, with values of 21.69 N/mm2, 22.97 N/mm2, and 24.13 N/mm2
- ✓ the 5% FASG addition showed an increase in compressive strength till 14 days of soaking, reaching a maximum value of 30.58 N/mm2. The control group, soaked for 28 days, exhibited a compressive strength of 32.92 N/mm2. (see Appendix A, Table A.10).
- ✓ The 5% addition of FASG in the mix achieved the desired strength for this study (C-25 concrete mix)
- ✓ The 5% addition of FASG in the mix achieved the desired strength for this study (C-25 concrete mix). However, higher percentages of FASG led to a decline in compressive strength with an increasing soaking period. This can be attributed to the material's water desorption capacity, which increases the water/cement ratio and reduces compressive strength.

The second objective of this study was to explore the impact of replacing water with opuntia ficus-indica (OFI) on concrete's ability to resist corrosion. The findings revealed that:-

- ✓ as the percentage of OFI in the concrete increased from 8% to 15% to 30%, both the inhibition capacity and durability of the concrete improved. Consequently, it can be concluded that the highest level of corrosion inhibition and durability enhancement in concrete was achieved when 30% OFI was added instead of water, along with a 5% FASG addition as a replacement for sand in the concrete mix
- ✓ However, it is important to note that this conclusion does not establish the optimal replacement percentage of OFI for corrosion inhibition. While the study did not observe a decrease in inhibitory capacity as the percentage increased, this outcome is influenced by the presence of FASG in the concrete mix. FASG affects the hydration process and

enables OFI to fully utilize its potential in forming a protective film that hinders corrosion in the concrete.

- ✓ Based on these findings, the study suggests that incorporating OFI in concrete, coupled with continuous hydration from internal curing material, can lead to enhanced corrosion inhibition and improved durability, particularly at higher percentages of OFI addition.

The third aim of this study is to examine the formation of oxide and hydroxide at the interface between concrete and Opuntia ficus-indica (OFI)., this study utilized various analysis techniques, including macroscopic assessments, morphological tests, electrochemical measurements, and durability evaluations. The findings revealed:-

- ✓ the formation of a passive film layer at the concrete-steel interface facilitated by the thick mucilage characteristics of OFI. The natural composition of OFI, encompassing amines, polysaccharides, and aromatic ring chains (C-H, C-O), N-H, and O=C bonds, contributed to its effective corrosion inhibition properties.
- ✓ As the percentage of OFI addition increased, both corrosion inhibition and the durability of the concrete exhibited improvement. Moreover, the incorporation of 5% FASG as an internal curing material further enhanced these positive effects, highlighting the promising potential of OFI in enhancing corrosion resistance and durability when used in conjunction with internal curing materials.

This study contributes valuable insights into utilizing Opuntia Ficus Indica combined with internal curing in concrete. The advanced analytical techniques employed provide a reference for future research. Overall, this study serves as a benchmark for stakeholders in the construction industry interested in utilizing Opuntia Ficus Indica as a concrete corrosion protection method

5.2 Recommendation

Corrosion Resistant Concrete is a specially formulated concrete mix designed to provide enhanced durability and protection against various types of corrosion, including physical, chemical, and biological. This type of concrete is crucial for construction projects in aggressive environments, such as coastal areas, wastewater treatment plants, chemical processing plants, and regions with extreme weather conditions. This study found that incorporating 30% Opuntia ficus-indica in place of water in concrete mixes and substituting 5% fine aggregate scoria gravel for sand can effectively serve as corrosion inhibitors in concrete. This study recommends these two natural materials for their ability to prevent concrete corrosion. Implementing the findings

of this study can contribute to a greener environment worldwide by promoting corrosion prevention and using environmentally friendly materials. However, it should be noted that the scope of the current study is limited, as it does not include all durability tests for concrete and does not evaluate the mechanism of the internal curing effect of fine aggregate scoria gravel in terms of the amount of water desorption within the concrete.

For future investigation, this study recommends the following points

- ✓ Further research should investigate the water desorption capacity of fine aggregate scoria gravel.
- ✓ The test subject should be analyzed under natural corrosion conditions for more realistic results.
- ✓ The impact of Opuntia ficus-indica should be explored by incorporating more efficient internal curing materials.
- ✓ The life cycle cost of the investigated concrete should be assessed in comparison with conventional concrete to evaluate its economic feasibility.
- ✓ Determine the optimum value of Opuntia ficus-indica (OFI) inhibition efficiency by adding a percentage higher than 30% with 5% fine aggregate scoria gravel (FASG) incorporation as an internal curing enabler.

Special Acknowledgment

This research project is funded by Adama Science and Technology University under the grant number :

ASTU/SM-R/796/23

Adama Ethiopia

REFERENCES

Abd Elrehim, M. Z., M. A. Eid, and M. G. Sayed. 2019. “Structural optimization of concrete arch bridges using Genetic Algorithms.” Ain Shams Eng. J., 10 (3): 507–516. Elsevier. https://doi.org/10.1016/j.asej.2019.01.005.

Abdel-Gaber, A. M., B. A. Abd-El-Nabey, E. Khamis, and D. E. Abd-El-Khalek. 2011. “A natural extract as scale and corrosion inhibitor for steel surface in brine solution.” Desalination, 278 (1–3): 337–342. Elsevier B.V. https://doi.org/10.1016/j.desal.2011.05.048.

Abdulrahman, A. S., M. Ismail, and M. S. Hussain. 2011. “Corrosion inhibitors for steel reinforcement in concrete: A review.” Sci. Res. Essays. Academic Journals.

Ahmad, S. 2003. “Reinforcement corrosion in concrete structures, its monitoring and service life prediction - A review.” Cem. Concr. Compos., 25 (4-5 SPEC): 459–471. https://doi.org/10.1016/S0958-9465(02)00086-0.

Ahmadi Moghadam, H., A. Mirzaei, and Z. Abedi Dehghi. 2020. “The relation between porosity, hydration degree and compressive strength of Portland cement pastes in the presence of aluminum chloride additive.” Constr. Build. Mater., 250: 118884. Elsevier Ltd. https://doi.org/10.1016/j.conbuildmat.2020.118884.

Ahmed, A., S. Guo, Z. Zhang, C. Shi, and D. Zhu. 2020. “A review on durability of fiber reinforced polymer (FRP) bars reinforced seawater sea sand concrete.” Constr. Build. Mater., 256: 119484. Elsevier Ltd. https://doi.org/10.1016/j.conbuildmat.2020.119484.

Akhnoukh, A. K. 2018. “Internal curing of concrete using lightweight aggregates.” Part. Sci. Technol., 36 (3): 362–367. Taylor and Francis Inc.

AL-Lamei, A. J., N. K. Muftin, F. M. Hussein, and A. S. Mahdi. 2020. “Organic Compounds as Corrosion Inhibitors from Natural Products.” Int. J. Adv. Res. Phys. Sci., 7 (4): 25–35.

Al-Sabagh, A. M., M. A. Migahed, S. A. Sadeek, and N. M. El Basiony. 2018. “Inhibition of mild steel corrosion and calcium sulfate formation in highly saline synthetic water by a newly synthesized anionic carboxylated surfactant.” Egypt. J. Pet., 27 (4): 811–821. Egyptian Petroleum Research Institute. https://doi.org/10.1016/j.ejpe.2017.12.003.

Alaskar, A., M. Alshannag, and M. Higazey. 2021. “Mechanical properties and durability of high-performance concrete internally cured using lightweight aggregates.” Constr. Build. Mater., 288: 122998. Elsevier Ltd. https://doi.org/10.1016/j.conbuildmat.2021.122998.

Allahyarzadeh, M. H., M. Aliofkhazraei, A. S. Rouhaghdam, V. Torabinejad, H. Alimadadi, and A. Ashrafi. 2017. “Electrodeposition mechanism and corrosion behavior of multilayer nanocrystalline nickel-tungsten alloy.” Electrochim. Acta, 258: 883–899. Elsevier. https://doi.org/10.1016/j.electacta.2017.11.139.

Alrefaee, S. H., K. Y. Rhee, C. Verma, M. A. Quraishi, and E. E. Ebenso. 2021. “Challenges and advantages of using plant extract as inhibitors in modern corrosion inhibition systems: Recent advancements.” J. Mol. Liq., 321: 114666. Elsevier B.V. https://doi.org/10.1016/j.molliq.2020.114666.

Angst, U., and M. Büchler. 2015. “On the applicability of the Stern-Geary relationship to determine instantaneous corrosion rates in macro-cell corrosion.” Mater. Corros., 66 (10): 1017–1028. https://doi.org/10.1002/maco.201407997.

Angst, U. M. 2018. “Challenges and opportunities in corrosion of steel in concrete.” Mater. Struct., 51 (1): 4. Springer Netherlands. https://doi.org/10.1617/s11527-017-1131-6.

Apostolopoulos, C. A., and P. G. Koutsoukos. 2008. “Study of the corrosion of reinforcement in concrete elements used for the repair of monuments.” Constr. Build. Mater., 22 (7): 1583–1593. https://doi.org/10.1016/j.conbuildmat.2007.03.022.

Asaad, M. A. 2021. “Commercial and Green Corrosion Inhibitors for Reinforced Concrete Structures: A Review.” Int. J. Curr. Sci. Res. Rev., 04 (02). https://doi.org/10.47191/ijcsrr/V4-i2-04.

Ashebir, D. A., G. A. Mengesha, and D. K. Sinha. 2022. “The Role of Tetra Hybrid Reinforcements on the Behavior of Aluminum Metal Matrix Composites.” J. Nanomater., (M. Zarrelli, ed.), 2022: 1–18. Hindawi Limited. https://doi.org/10.1155/2022/1988293.

Aslam, J., R. Aslam, and A. Aslam. 2022. “Amino acids and their derivatives as corrosion inhibitor.” Eco-Friendly Corros. Inhib., 311–330. Elsevier.

ASTM C33/C33M. (2018). Standard Specification for Concrete Aggregates. West Conshohocken, PA: ASTM International.

ASTM C39. (2018). Standard Test Method for Compressive Strength of Cylindrical Concrete Specimens. West Conshohocken, PA: ASTM International.

ASTM C127. (2015). Standard Test Method for Relative Density (Specific Gravity) and Absorption of Coarse Aggregate. West Conshohocken, PA: ASTM International.

ASTM C128. (2015). Standard Test Method for Relative Density (Specific Gravity) and Absorption of Fine Aggregate. West Conshohocken, PA: ASTM international.

ASTM, C. (2006). 192. 2004. Standard Practice for Making and Curing Concrete Test Specimens in the Laboratory. Annual book of ASTM Standards, 4.

ASTM C136. (2006). Standard Test Method for Sieve Analysis of Fine and Coarse Aggregates. West Conshohocken, PA: ASTM International.

ASTM C143. (2012). Standard Test Method for Slump of Hydraulic-Cement Concrete. West Conshohocken, PA: ASTM International.

ASTM C150/C150M. (2012). Standard Specification for Portland Cement. West Conshohocken, PA: ASTM International.

ASTM C187. (2016). Standard Test Method for Amount of Water Required for Normal Consistency of Hydraulic Cement Paste. West Conshohocken, PA: ASTM International.

ASTM C192. (2000). Standard Practice for Making and Curing Concrete Test Specimens in the Laboratory. West Conshohocken, PA: ASTM International.

ASTM G1 (2015) Standard Test Method for preparation, cleaning and evaluation of corrosion test specimens. West Conshohocken, PA: ASTM international.

ASTM G31(2015) Standard Test Method for conducting laboratory immersion corrosion tests West Conshohocken, PA: ASTM international.

ASTM G3-89 (1989) Standard Practice for Conventions Applicable to Electrochemical Measurements in Corrosion Testing, ASTM International, PA West Conshohocken.Abd Elrehim, M. Z., M. A. Eid, and M. G. Sayed. 2019. “Structural optimization of concrete arch bridges using Genetic Algorithms.” Ain Shams Eng. J., 10 (3): 507–516. Elsevier. https://doi.org/10.1016/j.asej.2019.01.005.

Abdel-Gaber, A. M., B. A. Abd-El-Nabey, E. Khamis, and D. E. Abd-El-Khalek. 2011. “A natural extract as scale and corrosion inhibitor for steel surface in brine solution.” Desalination, 278 (1–3): 337–342. Elsevier B.V. https://doi.org/10.1016/j.desal.2011.05.048.

Abdulrahman, A. S., M. Ismail, and M. S. Hussain. 2011. “Corrosion inhibitors for steel reinforcement in concrete: A review.” Sci. Res. Essays. Academic Journals.

Ahmad, S. 2003. “Reinforcement corrosion in concrete structures, its monitoring and service life prediction - A review.” Cem. Concr. Compos., 25 (4-5 SPEC): 459–471. https://doi.org/10.1016/S0958-9465(02)00086-0.

Ahmadi Moghadam, H., A. Mirzaei, and Z. Abedi Dehghi. 2020. “The relation between porosity, hydration degree and compressive strength of Portland cement pastes in the presence of aluminum chloride additive.” Constr. Build. Mater., 250: 118884. Elsevier Ltd. https://doi.org/10.1016/j.conbuildmat.2020.118884.

Ahmed, A., S. Guo, Z. Zhang, C. Shi, and D. Zhu. 2020. “A review on durability of fiber reinforced polymer (FRP) bars reinforced seawater sea sand concrete.” Constr. Build. Mater., 256: 119484. Elsevier Ltd. https://doi.org/10.1016/j.conbuildmat.2020.119484.

Akhnoukh, A. K. 2018. “Internal curing of concrete using lightweight aggregates.” Part. Sci. Technol., 36 (3): 362–367. Taylor and Francis Inc. https://doi.org/10.1080/02726351.2016.1256360.

AL-Lamei, A. J., N. K. Muftin, F. M. Hussein, and A. S. Mahdi. 2020. “Organic Compounds as Corrosion Inhibitors from Natural Products.” Int. J. Adv. Res. Phys. Sci., 7 (4): 25–35.

Al-Sabagh, A. M., M. A. Migahed, S. A. Sadeek, and N. M. El Basiony. 2018. “Inhibition of mild steel corrosion and calcium sulfate formation in highly saline synthetic water by a newly synthesized anionic carboxylated surfactant.” Egypt. J. Pet., 27 (4): 811–821. Egyptian Petroleum Research Institute. https://doi.org/10.1016/j.ejpe.2017.12.003.

Alaskar, A., M. Alshannag, and M. Higazey. 2021. “Mechanical properties and durability of high-performance concrete internally cured using lightweight aggregates.” Constr. Build. Mater., 288: 122998. Elsevier Ltd. https://doi.org/10.1016/j.conbuildmat.2021.122998.

Allahyarzadeh, M. H., M. Aliofkhazraei, A. S. Rouhaghdam, V. Torabinejad, H. Alimadadi, and A. Ashrafi. 2017. “Electrodeposition mechanism and corrosion behavior of multilayer nanocrystalline nickel-tungsten alloy.” Electrochim. Acta, 258: 883–899. Elsevier. https://doi.org/10.1016/j.electacta.2017.11.139.

Alrefaee, S. H., K. Y. Rhee, C. Verma, M. A. Quraishi, and E. E. Ebenso. 2021. “Challenges and advantages of using plant extract as inhibitors in modern corrosion inhibition systems: Recent advancements.” J. Mol. Liq., 321: 114666. Elsevier B.V. https://doi.org/10.1016/j.molliq.2020.114666.

Angst, U., and M. Büchler. 2015. “On the applicability of the Stern-Geary relationship to determine instantaneous corrosion rates in macro-cell corrosion.” Mater. Corros., 66 (10): 1017–1028. https://doi.org/10.1002/maco.201407997.

Angst, U. M. 2018. “Challenges and opportunities in corrosion of steel in concrete.” Mater. Struct., 51 (1): 4. Springer Netherlands. https://doi.org/10.1617/s11527-017-1131-6.

Apostolopoulos, C. A., and P. G. Koutsoukos. 2008. “Study of the corrosion of reinforcement in concrete elements used for the repair of monuments.” Constr. Build. Mater., 22 (7): 1583–1593. https://doi.org/10.1016/j.conbuildmat.2007.03.022.

Asaad, M. A. 2021. “Commercial and Green Corrosion Inhibitors for Reinforced Concrete Structures: A Review.” Int. J. Curr. Sci. Res. Rev., 04 (02). https://doi.org/10.47191/ijcsrr/V4-i2-04.

Ashebir, D. A., G. A. Mengesha, and D. K. Sinha. 2022. “The Role of Tetra Hybrid Reinforcements on the Behavior of Aluminum Metal Matrix Composites.” J. Nanomater., (M. Zarrelli, ed.), 2022: 1–18. Hindawi Limited. https://doi.org/10.1155/2022/1988293.

Aslam, J., R. Aslam, and A. Aslam. 2022. “Amino acids and their derivatives as corrosion inhibitor.” Eco-Friendly Corros. Inhib., 311–330. Elsevier.

Backhouse, A., and N. Baddoo. 2021. “Recent developments of stainless steels in structural applications.” wileyonlinelibrary.com/journal/cepa, 4 (2–4): 2349–2355. https://doi.org/10.1002/cepa.1560.

Bahekar, P. V., and S. S. Gadve. 2017. “Impressed current cathodic protection of rebar in concrete using Carbon FRP laminate.” Constr. Build. Mater., 156: 242–251. Elsevier Ltd. https://doi.org/10.1016/j.conbuildmat.2017.08.145.

Bayar, N., M. Kriaa, and R. Kammoun. 2016. “Extraction and characterization of three polysaccharides extracted from Opuntia ficus indica cladodes.” Int. J. Biol. Macromol., 92: 441–450. Elsevier B.V. https://doi.org/10.1016/j.ijbiomac.2016.07.042.

Belay, T., and G. Gebreyohannes. 2010. Proceedings of the workshop on improved cactus pear (Opuntia ficus-indica (L.) Mill) utilization for food, feed and soil and water conservation and other products in Africa. Ethiop. Inst. Agric. Res. Ethiopian institute of agricultural research.

Belviranlı, B., F. Al-Juhaimi, M. M. Özcan, K. Ghafoor, E. E. Babiker, and O. N. Alsawmahi.

2019. “Effect of location on some physico-chemical properties of prickly pear (Opuntia ficus-indica L.) fruit and seeds.” J. Food Process. Preserv., 43 (3): e13896. https://doi.org/10.1111/jfpp.13896.

Bentz, D. P., and W. J. Weiss. 2011. Internal curing : Gaithersburg, MD.

Berradja, A. 2019. “Electrochemical Techniques for Corrosion and Tribocorrosion Monitoring: Methods for the Assessment of Corrosion Rates.” Corros. Inhib. IntechOpen.

Berrocal, C. G., K. Lundgren, and I. Löfgren. 2016. “Corrosion of steel bars embedded in fibre reinforced concrete under chloride attack: State of the art.” Cem. Concr. Res., 80: 69–85. Elsevier Ltd. https://doi.org/10.1016/j.cemconres.2015.10.006.

Bertolini, L., B. Elsener, P. Pedeferri, E. Redaelli, and R. B. Polder. 2013. Corrosion of steel in concrete: prevention, diagnosis, repair. John Wiley & Sons.

Broomfield, J. 2003. Corrosion of Steel in Concrete. London: CRC Press.

Bunaciu, A. A., E. gabriela Udriştioiu, and H. Y. Aboul-Enein. 2015. “X-Ray Diffraction: Instrumentation and Applications.” Crit. Rev. Anal. Chem., 45 (4): 289–299. https://doi.org/10.1080/10408347.2014.949616.

Byard, B. E., A. K. Schindler, and R. W. Barnes. 2012. “Early-Age Cracking Tendency and Ultimate Degree of Hydration of Internally Cured Concrete.” J. Mater. Civ. Eng., 24 (8): 1025–1033. American Society of Civil Engineers. https://doi.org/10.1061/(ASCE)MT.1943-5533.0000469.

Byrne, A., N. Holmes, and B. Norton. 2016. “State-of-the-art review of cathodic protection for reinforced concrete structures.” Mag. Concr. Res., 68 (13): 664–677. https://doi.org/10.1680/jmacr.15.00083.

Cárdenas, A., F. M. Goycoolea, and M. Rinaudo. 2008. “On the gelling behaviour of ‘nopal’ (Opuntia ficus indica) low methoxyl pectin.” Carbohydr. Polym., 73 (2): 212–222. https://doi.org/10.1016/j.carbpol.2007.11.017.

Cardoso, P. da S., I. N. B. da Silva, C. D. Ferreira-Ribeiro, and D. Murowaniecki Otero. 2021. “Nutritional and technological potential of cactus fruits for insertion in human food.” Crit. Rev. Food Sci. Nutr., 0 (0): 1–17. Taylor & Francis. https://doi.org/10.1080/10408398.2021.1997906.

Chen, X., X. G. Li, C. W. Du, and Y. F. Cheng. 2009. “Effect of cathodic protection on corrosion of pipeline steel under disbonded coating.” Corros. Sci., 51 (9): 2242–2245. Elsevier Ltd. https://doi.org/10.1016/j.corsci.2009.05.027.

Chen, Y. Y., H. J. Tzeng, L. I. Wei, L. H. Wang, J. C. Oung, and H. C. Shih. 2005. “Corrosion resistance and mechanical properties of low-alloy steels under atmospheric conditions.” Corros. Sci., 47 (4): 1001–1021. https://doi.org/10.1016/j.corsci.2004.04.009.

Chung, D. D. L. 2000. “Corrosion Control of Steel-Reinforced Concrete.” J. Mater. Eng. Perform., 9 (5): 585–588. https://doi.org/10.1361/105994900770345737.

Cicek, V. 2017. Corrosion Engineering and Cathodic Protection Handbook. Corros. Eng. Cathodic Prot. Handb.

Concrete Pavement Technology Center, N. 2017. Guide Specification for Internally Curing Concrete Sponsored by Federal Highway Administration Transportation Pooled Fund TPF-5(286) (Part of InTrans Project 13-482).

Contreras-Padilla, M., E. M. Rivera-Muñoz, E. Gutiérrez-Cortez, A. R. del López, and M. E. Rodríguez-García. 2015. “Characterization of crystalline structures in Opuntia ficus-indica.” J. Biol. Phys., 41 (1): 99–112. https://doi.org/10.1007/s10867-014-9368-6.

Van Damme, H. 2018. “Concrete material science: Past, present, and future innovations.” Cem. Concr. Res., 112: 5–24. Elsevier. https://doi.org/10.1016/j.cemconres.2018.05.002.

Daniyal, M., and S. Akhtar. 2020a. “Corrosion assessment and control techniques for reinforced concrete structures: a review.” J. Build. Pathol. Rehabil., 5 (1). Springer Science and Business Media B.V. https://doi.org/10.1007/s41024-019-0067-3.

Daniyal, M., and S. Akhtar. 2020b. “Corrosion assessment and control techniques for reinforced concrete structures: a review.” J. Build. Pathol. Rehabil., 5 (1): 1. Springer International Publishing. https://doi.org/10.1007/s41024-019-0067-3.

Daoud, D., T. Douadi, S. Issaadi, and S. Chafaa. 2014. “Adsorption and corrosion inhibition of new synthesized thiophene Schiff base on mild steel X52 in HCl and H2SO4 solutions.” Corros. Sci., 79: 50–58. Elsevier Ltd. https://doi.org/10.1016/j.corsci.2013.10.025.

Demissew, A. 2022. “Comparative Analysis of Selected Concrete Mix Design Methods Based on Cost-Effectiveness.” Adv. Civ. Eng., (A. C. Aydın, ed.), 2022: 1–8. https://doi.org/10.1155/2022/4240774.

Deshpande, P. P., N. G. Jadhav, V. J. Gelling, and D. Sazou. 2014. “Conducting polymers for corrosion protection: a review.” J. Coatings Technol. Res., 11 (4): 473–494. https://doi.org/10.1007/s11998-014-9586-7.

Dey, S., V. V. P. Kumar, K. R. Goud, and S. K. J. Basha. 2021. “State of art review on self compacting concrete using mineral admixtures.” J. Build. Pathol. Rehabil., 6 (1): 18. Springer International Publishing. https://doi.org/10.1007/s41024-021-00110-9.

Dhouibi, L., E. Triki, and A. Raharinaivo. 2002. “The application of electrochemical impedance spectroscopy to determine the long-term effectiveness of corrosion inhibitors for steel in concrete.” Cem. Concr. Compos., 24 (1): 35–43. https://doi.org/10.1016/S0958-9465(01)00062-2.

Díaz Blanco, Y., E. C. Menchaca Campos, C. I. Rocabruno Valdés, and J. Uruchurtu Chavarín. 2019a. “Natural additive (nopal mucilage) on the electrochemical properties of concrete reinforcing steel.” Rev. ALCONPAT, 9 (3): 260–276. Revista ALCONPAT. https://doi.org/10.21041/ra.v9i3.429.

Díaz Blanco, Y., E. C. Menchaca Campos, C. I. Rocabruno Valdés, and J. Uruchurtu Chavarín. 2019b. “Natural additive (nopal mucilage) on the electrochemical properties of concrete reinforcing steel.” Rev. ALCONPAT, 9 (3): 260–276. https://doi.org/10.21041/ra.v9i3.429.

Du, F., Z. Jin, W. She, C. Xiong, G. Feng, and J. Fan. 2020. “Chloride ions migration and induced reinforcement corrosion in concrete with cracks: a comparative study of current acceleration and natural marine exposure.” Constr. Build. Mater., 263: 120099. Elsevier.

Engels, H.-W., H.-G. Pirkl, R. Albers, R. W. Albach, J. Krause, A. Hoffmann, H. Casselmann, and J. Dormish. 2013. “Polyurethanes: Versatile Materials and Sustainable Problem Solvers for Today’s Challenges.” Angew. Chemie Int. Ed., 52 (36): 9422–9441. https://doi.org/10.1002/anie.201302766.

Feliu, S., J. A. González, S. Feliu, and C. Andrade. 1989. “Relationship between conductivity of concrete and corrosion of reinforcing bars.” Br. Corros. J., 24 (3): 195–198. Taylor & Francis.

Feng, W., A. Tarakbay, S. Ali Memon, W. Tang, and H. Cui. 2021a. “Methods of accelerating chloride-induced corrosion in steel-reinforced concrete: A comparative review.” Constr.

Build. Mater., 289: 123165. Elsevier Ltd. https://doi.org/10.1016/j.conbuildmat.2021.123165.

Feng, W., A. Tarakbay, S. Ali Memon, W. Tang, and H. Cui. 2021b. “Methods of accelerating chloride-induced corrosion in steel-reinforced concrete: A comparative review.” Constr. Build. Mater., 289: 123165. Elsevier Ltd. https://doi.org/10.1016/j.conbuildmat.2021.123165.

Gagg, C. R. 2014. “Cement and concrete as an engineering material: An historic appraisal and case study analysis.” Eng. Fail. Anal., 40: 114–140. Elsevier Ltd. https://doi.org/10.1016/j.engfailanal.2014.02.004.

García-Barradas, O., A. Esteban-Cortina, M. R. Mendoza-Lopez, R. I. Ortiz-Basurto, D. I. Díaz-Ramos, and M. Jiménez-Fernández. 2022. “Chemical modification of Opuntia ficus-indica mucilage: characterization, physicochemical, and functional properties.” Polym. Bull., (0123456789). Springer Berlin Heidelberg. https://doi.org/10.1007/s00289-022-04474-x.

Garnica-Rodríguez, A., and F. J. Rodriguez-Gomez. 2014. “Electrochemical Impedance Response of Zn Under Anodic Polarization in Simulated Concrete Solution.” ECS Meet. Abstr., MA2014-02 (13): 759–759. https://doi.org/10.1149/MA2014-02/13/759.

Gopi, D., K. Kanimozhi, and L. Kavitha. 2015. “Opuntia ficus indica peel derived pectin mediated hydroxyapatite nanoparticles: Synthesis, spectral characterization, biological and antimicrobial activities.” Spectrochim. Acta Part A Mol. Biomol. Spectrosc., 141: 135–143. Elsevier B.V. https://doi.org/10.1016/j.saa.2015.01.039.

Gopiraman, M., N. Selvakumaran, D. Kesavan, and R. Karvembu. 2012. “Adsorption and corrosion inhibition behaviour of N-(phenylcarbamothioyl) benzamide on mild steel in acidic medium.” Prog. Org. Coatings, 73 (1): 104–111. Elsevier B.V. https://doi.org/10.1016/j.porgcoat.2011.09.006.

Gowraraju, N. D., S. Jagadeesan, K. Ayyasamy, L. O. Olasunkanmi, E. E. Ebenso, and C. Subramanian. 2017. “Adsorption characteristics of Iota-carrageenan and Inulin biopolymers as potential corrosion inhibitors at mild steel/sulphuric acid interface.” J. Mol. Liq., 232: 9–19. Elsevier B.V. https://doi.org/10.1016/j.molliq.2017.02.054.

Goyal, A., H. S. Pouya, E. Ganjian, and P. Claisse. 2018a. “A Review of Corrosion and

Protection of Steel in Concrete." Arab. J. Sci. Eng., 43 (10): 5035–5055. Springer. https://doi.org/10.1007/s13369-018-3303-2.

Goyal, A., H. S. Pouya, E. Ganjian, and P. Claisse. 2018b. "A Review of Corrosion and Protection of Steel in Concrete." Arab. J. Sci. Eng., 43 (10): 5035–5055. Springer. https://doi.org/10.1007/s13369-018-3303-2.

Goyal, A., H. S. Pouya, E. Ganjian, and P. Claisse. 2018c. "A Review of Corrosion and Protection of Steel in Concrete." Arab. J. Sci. Eng., 43 (10): 5035–5055. Springer Verlag. https://doi.org/10.1007/s13369-018-3303-2.

Guo, Q., X. Li, Y. Song, and J. Liu. 2022. "Effect of rust inhibitor on the composition of steel passive film in carbonized concrete." Case Stud. Constr. Mater., 16 (October 2021): e00892. Elsevier Ltd. https://doi.org/10.1016/j.cscm.2022.e00892.

Hansson, C. M. 2016a. "An introduction to corrosion of engineering materials." Corros. Steel Concr. Struct., 3–18. Elsevier.

Hansson, C. M. 2016b. "An introduction to corrosion of engineering materials." Corros. Steel Concr. Struct., 3–18. Elsevier.

Harrington, D. A., and P. Van Den Driessche. 2011. "Mechanism and equivalent circuits in electrochemical impedance spectroscopy." Electrochim. Acta, 56 (23): 8005–8013. Elsevier Ltd. https://doi.org/10.1016/j.electacta.2011.01.067.

Hernández, E. F., P. F. D. J. Cano-Barrita, F. M. León-Martínez, and A. A. Torres-Acosta. 2017. "Performance of cactus mucilage and brown seaweed extract as a steel corrosion inhibitor in chloride contaminated alkaline media." Anti-Corrosion Methods Mater., 64 (5): 529–539. Emerald Group Publishing Ltd. https://doi.org/10.1108/ACMM-02-2016-1646.

Hong, S., F. Zheng, G. Shi, J. Li, X. Luo, F. Xing, L. Tang, and B. Dong. 2020a. "Determination of impressed current efficiency during accelerated corrosion of reinforcement." Cem. Concr. Compos., 108: 103536. Elsevier Ltd. https://doi.org/10.1016/j.cemconcomp.2020.103536.

Hong, S., F. Zheng, G. Shi, J. Li, X. Luo, F. Xing, L. Tang, and B. Dong. 2020b. "Determination of impressed current efficiency during accelerated corrosion of reinforcement." Cem. Concr. Compos., 108 (March): 103536. Elsevier Ltd.

https://doi.org/10.1016/j.cemconcomp.2020.103536.

Hossain, K. M. A., M. Lachemi, M. Sammour, and M. Sonebi. 2013. “Strength and fracture energy characteristics of self-consolidating concrete incorporating polyvinyl alcohol, steel and hybrid fibres.” Constr. Build. Mater., 45: 20–29. Elsevier. https://doi.org/10.1016/j.conbuildmat.2013.03.054.

Hossain, N., M. Asaduzzaman Chowdhury, and M. Kchaou. 2021. “An overview of green corrosion inhibitors for sustainable and environment friendly industrial development.” J. Adhes. Sci. Technol., 35 (7): 673–690. Taylor & Francis. https://doi.org/10.1080/01694243.2020.1816793.

Hu, J., S. A. Cao, and J. Xie. 2013. “EIS study on the corrosion behavior of rusted carbon steel in 3% NaCl solution.” Anti-Corrosion Methods Mater., 60 (2): 100–105. https://doi.org/10.1108/00035591311308074.

Hua, J., H. Fan, W. Yan, N. Wang, X. Xue, and L. Huang. 2022. “Seismic resistance of the corroded bimetallic steel bar under different strain amplitudes.” Constr. Build. Mater., 319: 126088. Elsevier. https://doi.org/10.1016/j.conbuildmat.2021.126088.

Hussain, R. R., T. Ishida, and M. Wasim. 2012. “Oxygen Transport and Corrosion of Steel in Concrete under Varying Concrete Cover, w/c, and Moisture.” ACI Mater. J., 109 (1): 3–10. https://doi.org/10.14359/51683565.

Juimo Tchamdjou, W. H., T. Cherradi, M. L. Abidi, and L. A. Pereira-de-Oliveira. 2020. “The use of volcanic scoria from ‘Djoungo’ (Cameroon) as cement replacement and fine aggregate by sand substitution in mortar for masonry.” Eur. J. Environ. Civ. Eng., 24 (1): 60–78. Taylor & Francis. https://doi.org/10.1080/19648189.2017.1364298.

Kazemian, M., and B. Shafei. 2022. “Internal curing capabilities of natural zeolite to improve the hydration of ultra-high performance concrete.” Constr. Build. Mater., 340: 127452. Elsevier. https://doi.org/10.1016/j.conbuildmat.2022.127452.

Kepler, J. L., and C. E. Locke. 2000. Evaluation of Corrosion Protection Methods for Reinforced Concrete Highway Structures. Corrosion. Lawrence, Kansas.

Kevern, J. T., and Q. C. Nowasell. 2018. “Internal curing of pervious concrete using lightweight aggregates.” Constr. Build. Mater., 161: 229–235. Elsevier Ltd. https://doi.org/10.1016/j.conbuildmat.2017.11.055.

Khaled, K. F., and N. Hackerman. 2003. “Investigation of the inhibitive effect of ortho-substituted anilines on corrosion of iron in 1 M HCl solutions.” Electrochim. Acta, 48 (19): 2715–2723. https://doi.org/10.1016/S0013-4686(03)00318-9.

Koch, G. 2017. “Cost of corrosion.” Trends Oil Gas Corros. Res. Technol., 3–30. Elsevier.

Koleva, D. A., J. H. W. de Wit, K. van Breugel, Z. F. Lodhi, and E. van Westing. 2007. “Investigation of Corrosion and Cathodic Protection in Reinforced Concrete.” J. Electrochem. Soc., 154 (4): P52. https://doi.org/10.1149/1.2436609.

Kumar, V. 1998. “Protection of Steel Reinforcement for Concrete- A Review.” Corros. Rev., 16 (4). https://doi.org/10.1515/CORRREV.1998.16.4.317.

Kwon, S.-J., H.-S. Lee, S. Karthick, V. Saraswathy, and H.-M. Yang. 2017. “Long-term corrosion performance of blended cement concrete in the marine environment – A real-time study.” Constr. Build. Mater., 154: 349–360. Elsevier Ltd. https://doi.org/10.1016/j.conbuildmat.2017.07.237.

Labiapari, W. S., R. J. Gonçalves, C. M. de Alcântara, V. Pagani, J. C. Di Cunto, and J. D. B. de Mello. 2021. “Understanding abrasion-corrosion to improve concrete mixer drum performance: A laboratory and field approach.” Wear, 477 (September 2020). https://doi.org/10.1016/j.wear.2021.203830.

Lefsih, K., C. Delattre, G. Pierre, P. Michaud, T. M. Aminabhavi, F. Dahmoune, and K. Madani. 2016. “Extraction, characterization and gelling behavior enhancement of pectins from the cladodes of Opuntia ficus indica.” Int. J. Biol. Macromol., 82: 645–652. Elsevier B.V. https://doi.org/10.1016/j.ijbiomac.2015.10.046.

Li, D., C. Lin, C. Batchelor-McAuley, L. Chen, and R. G. Compton. 2018. “Tafel analysis in practice.” J. Electroanal. Chem., 826: 117–124. Elsevier B.V. https://doi.org/10.1016/j.jelechem.2018.08.018.

Li, Z., Z. Jin, P. Wang, and T. Zhao. 2021. “Corrosion mechanism of reinforced bars inside concrete and relevant monitoring or detection apparatus: A review.” Constr. Build. Mater., 279: 122432. Elsevier Ltd. https://doi.org/10.1016/j.conbuildmat.2021.122432.

Liang, C., Z. Cai, H. Wu, J. Xiao, Y. Zhang, and Z. Ma. 2021. “Chloride transport and induced steel corrosion in recycled aggregate concrete: A review.” Constr. Build. Mater., 282: 122547. Elsevier.

Liu, L., Z. Fang, Z. Huang, and Y. Wu. 2022. “Solving shrinkage problem of ultra-high-performance concrete by a combined use of expansive agent, super absorbent polymer, and shrinkage-reducing agent.” Compos. Part B Eng., 230: 109503. Elsevier. https://doi.org/10.1016/j.compositesb.2021.109503.

Liu, M., X. Cheng, X. Li, P. Yue, and J. Li. 2016a. “Corrosion Behavior and Durability of Low-Alloy Steel Rebars in Marine Environment.” J. Mater. Eng. Perform., 25 (11): 4967–4979. Springer US. https://doi.org/10.1007/s11665-016-2342-7.

Liu, W., H. Cui, Z. Dong, F. Xing, H. Zhang, and T. Y. Lo. 2016b. “Carbonation of concrete made with dredged marine sand and its effect on chloride binding.” Constr. Build. Mater., 120: 1–9. Elsevier Ltd. https://doi.org/10.1016/j.conbuildmat.2016.05.011.

Luo, Q., D. Liang, T. Wang, L. Zhang, and L. Jiang. 2020. “Application of High-Vesicularity Cinder Gravels to Railway Earth Structure in Ethiopia.” J. Mater. Civ. Eng., 32 (11): 1–13. https://doi.org/10.1061/(asce)mt.1943-5533.0003432.

Ma, I. A. W., S. Ammar, S. S. A. Kumar, K. Ramesh, and S. Ramesh. 2022. “A concise review on corrosion inhibitors: types, mechanisms and electrochemical evaluation studies.” J. Coatings Technol. Res., 19 (1): 241–268. Springer US. https://doi.org/10.1007/s11998-021-00547-0.

Ma, X., J. Liu, and C. Shi. 2019. “A review on the use of LWA as an internal curing agent of high performance cement-based materials.” Constr. Build. Mater., 218: 385–393. Elsevier Ltd. https://doi.org/10.1016/j.conbuildmat.2019.05.126.

Maldonado, S., and A. G. L. Borthwick. 2018. “Quasi-two-layer morphodynamic model for bedload-dominated problems: Bed slope-induced morphological diffusion.” R. Soc. Open Sci., 5 (2). https://doi.org/10.1098/rsos.172018.

Mannai, F., M. Ammar, J. G. Yanez, E. Elaloui, and Y. Moussaoui. 2016. “Cellulose fiber from Tunisian Barbary Fig ‘Opuntia ficus-indica’ for papermaking.” Cellulose, 23 (3): 2061–2072. https://doi.org/10.1007/s10570-016-0899-9.

“Map of Opuntia ficus-indica -- Discover Life.” n.d. Accessed December 23, 2022. https://www.discoverlife.org/mp/20m?kind=Opuntia+ficus-indica&guide=Opuntia.

Martínez-Molina, W., A. A. Torres-Acosta, C. E. Celis-Mendoza, and E. Alonso-Guzman. 2015. “Physical properties of cement-based paste and mortar with dehydrated cacti

additions.” Int. J. Archit. Herit., 9 (4): 443–452. Taylor and Francis Inc. https://doi.org/10.1080/15583058.2013.800919.

Martinez-Molina, W., A. A. Torres-Acosta, G. E. I. Martínez-Peña, E. A. Guzmán, and I. N. Mendoza-Pérez. 2015. “Cement-Based Materials Enhanced Durability from Opuntia Ficus Indica Mucilage Additions.” ACI Mater. J., 112 (1): 165–172. American Concrete Institute. https://doi.org/10.14359/51687225.

Martinez-Molina, W., A. Torres-Acosta, R. Hernández-Leos, E. Alonso-Guzman, I. Mendoza-Pérez, and I. Martinez-Peña. 2016. “The inhibitive properties of Nopal slime on the corrosion of steel in chloride-contaminated mortar.” Anti-Corrosion Methods Mater., 63 (1): 65–71. Emerald Group Publishing Ltd. https://doi.org/10.1108/ACMM-05-2014-1381.

Matsuhiro, B., L. E. Lillo, C. Sáenz, C. C. Urzúa, and O. Zárate. 2006. “Chemical characterization of the mucilage from fruits of Opuntia ficus indica.” Carbohydr. Polym., 63 (2): 263–267. https://doi.org/10.1016/j.carbpol.2005.08.062.

Mehta, P. K., and P. J. M. Monteiro. 2014. Concrete: microstructure, properties, and materials. McGraw-Hill Education.

Mohamed, N., M. Boulfiza, and R. Evitts. 2013. “Corrosion of Carbon Steel and Corrosion-Resistant Rebars in Concrete Structures Under Chloride Ion Attack.” J. Mater. Eng. Perform., 22 (3): 787–795. https://doi.org/10.1007/s11665-012-0314-0.

Møller, V. B., K. Dam-Johansen, S. M. Frankær, and S. Kiil. 2017. “Acid-resistant organic coatings for the chemical industry: a review.” J. Coatings Technol. Res., 14 (2): 279–306. Springer US. https://doi.org/10.1007/s11998-016-9905-2.

Mugahed Amran, Y. H., R. Alyousef, R. S. M. Rashid, H. Alabduljabbar, and C. C. Hung. 2018. “Properties and applications of FRP in strengthening RC structures: A review.” Structures, 16: 208–238. Elsevier Ltd on behalf of Institution of Structural Engineers. https://doi.org/10.1016/j.istruc.2018.09.008.

Nie, S., S. Hu, F. Wang, P. Yuan, Y. Zhu, J. Ye, and Y. Liu. 2016. “Internal curing – A suitable method for improving the performance of heat-cured concrete.” Constr. Build. Mater., 122: 294–301. Elsevier. https://doi.org/10.1016/j.conbuildmat.2016.05.159.

Otálora, M. C., J. G. Carriazo, L. Iturriaga, M. A. Nazareno, and C. Osorio. 2015.

"Microencapsulation of betalains obtained from cactus fruit (Opuntia ficus-indica) by spray drying using cactus cladode mucilage and maltodextrin as encapsulating agents." Food Chem., 187: 174–181. https://doi.org/10.1016/j.foodchem.2015.04.090.

Ouglova, A., Y. Berthaud, M. François, and F. Foct. 2006. "Mechanical properties of an iron oxide formed by corrosion in reinforced concrete structures." Corros. Sci., 48 (12): 3988–4000. https://doi.org/10.1016/j.corsci.2006.03.007.

Özcan, M. 2008. "AC impedance measurement of cystine adsorption at mild steel/sulfuric acid interface as corrosion inhibitor." J. Solid State Electrochem., 12 (12): 1653–1661. https://doi.org/10.1007/s10008-008-0551-1.

Park, S.-M., and J.-S. Yoo. 2003. "Peer Reviewed: Electrochemical Impedance Spectroscopy for Better Electrochemical Measurements." Anal. Chem., 75 (21): 455 A-461 A. https://doi.org/10.1021/ac0313973.

Patel, J., J. M. Patel, C. N. Patel, and H. S. Patel. 2014. "Critical Review of the Literature on Self Curing Concrete Critical Review on Lime Mortar View project INVESTIGATIONS ON FLEXURAL CAPACITY OF STEEL CONCRETE COMPOSITE DECK WITH DIVERSE BOND PATTERNS View project Critical Review of the Literature on Self Cu."

Poupard, O., A. Aït-Mokhtar, and P. Dumargue. 2004. "Corrosion by chlorides in reinforced concrete: Determination of chloride concentration threshold by impedance spectroscopy." Cem. Concr. Res., 34 (6): 991–1000. https://doi.org/10.1016/j.cemconres.2003.11.009.

Poursaee, A. 2016. "Corrosion protection methods of steel in concrete." Corros. Steel Concr. Struct., 241–248. Elsevier.

Prasad, N. K., A. S. Pathak, S. Kundu, P. Panchal, and K. Mondal. 2021. "On the novel approach of sacrificial cathodic protection of mild steel in simulated concrete pore solution and concrete mortar by high phosphorus pig iron anodes." J. Mater. Res. Technol., 14: 582–608. Elsevier Ltd. https://doi.org/10.1016/j.jmrt.2021.06.070.

Prof. Luca Bertolin. 2011. Corrosion of Steel in Concrete. Wiley-VCH.

Qiao, G., B. Guo, Z. Li, J. Ou, and Z. He. 2017. "Corrosion behavior of a steel bar embedded in a cement-based conductive composite." Constr. Build. Mater., 134: 388–396. Elsevier.

Quraishi, M., D. Nayak, R. Kumar, and V. Kumar. 2017. "Corrosion of Reinforced Steel in

Concrete and Its Control: An overview." J. Steel Struct. Constr., 03 (01): 1–6. https://doi.org/10.4172/2472-0437.1000124.

Rahman, A., M. Sam, G. F. Huseien, and U. Memon. 2018. A review: Mechanism, materials and properties of self-curing concrete.

Raja, P. B., M. Ismail, S. Ghoreishiamiri, J. Mirza, M. C. Ismail, S. Kakooei, and A. A. Rahim. 2016. "Reviews on Corrosion Inhibitors: A Short View." Chem. Eng. Commun., 203 (9): 1145–1156. Taylor and Francis Ltd. https://doi.org/10.1080/00986445.2016.1172485.

Rani, B. E. A., and B. B. J. Basu. 2012. "Green Inhibitors for Corrosion Protection of Metals and Alloys: An Overview." Int. J. Corros., 2012: 1–15. https://doi.org/10.1155/2012/380217.

Reda, T. H., and M. K. Atsbha. 2019. "Nutritional composition, antinutritional factors, antioxidant activities, functional properties, and sensory evaluation of cactus pear (Opuntia ficus-indica) seeds grown in Tigray Region, Ethiopia." Int. J. Food Sci., 2019. Hindawi Limited. https://doi.org/10.1155/2019/5697052.

Regina, C., M. Engineer, M. Gerais, S. Stephany, M. Engineer, M. Gerais, R. L. Perez, R. De Janeiro, R. De Janeiro, U. Feder-, B. Horizonte, C. A. De Souza, and B. Horizonte. n.d. "ACCELERATED CORROSION TEST FOR THE QUALITATIVE."

Revert, A. B., K. De Weerdt, K. Hornbostel, and M. R. Geiker. 2018. "Carbonation-induced corrosion: Investigation of the corrosion onset." Constr. Build. Mater., 162: 847–856. Elsevier.

Rodrigues, R., S. Gaboreau, J. Gance, I. Ignatiadis, and S. Betelu. 2021. "Reinforced concrete structures: A review of corrosion mechanisms and advances in electrical methods for corrosion monitoring." Constr. Build. Mater., 269 (xxxx): 121240. Elsevier Ltd. https://doi.org/10.1016/j.conbuildmat.2020.121240.

Rodríguez-González, S., H. E. Martínez-Flores, C. K. Chávez-Moreno, L. I. Macías-Rodríguez, E. Zavala-Mendoza, M. G. Garnica-Romo, and L. Chacón-García. 2014. "Extraction and Characterization of Mucilage From Wild Species of O puntia." J. Food Process Eng., 37 (3): 285–292. https://doi.org/10.1111/jfpe.12084.

Ruiz-Garcia, A., V. Esquivel-Peña, J. Genesca, and R. Montoya. 2023. "Advances in galvanic corrosion of aluminum alloys." Electrochim. Acta, 449: 142227. Elsevier.

https://doi.org/10.1016/j.electacta.2023.142227.

Sáenz, C., E. Sepúlveda, and B. Matsuhiro. 2004. “Opuntia spp mucilage’s: a functional component with industrial perspectives.” J. Arid Environ., 57 (3): 275–290. https://doi.org/10.1016/S0140-1963(03)00106-X.

Salasi, M., G. Stachowiak, and G. Stachowiak. 2015. “Tribo-electrochemical behaviour of 316L stainless steel: The effects of contact configuration, tangential speed, and wear mechanism.” Corros. Sci., 98: 20–32. Elsevier. https://doi.org/10.1016/j.corsci.2015.05.009.

Salehi, E., Z. Emam-Djomeh, G. Askari, and M. Fathi. 2019. “Opuntia ficus indica fruit gum: Extraction, characterization, antioxidant activity and functional properties.” Carbohydr. Polym., 206: 565–572. Elsevier Ltd. https://doi.org/10.1016/j.carbpol.2018.11.035.

Salehi, E., R. Naderi, and B. Ramezanzadeh. 2017. “Synthesis and characterization of an effective organic/inorganic hybrid green corrosion inhibitive complex based on zinc acetate/Urtica Dioica.” Appl. Surf. Sci., 396: 1499–1514. Elsevier B.V. https://doi.org/10.1016/j.apsusc.2016.11.198.

Saravanan, M., R. Gopi, and M. Harihanandh. 2021. “Durability properties of self compacting self curing concrete with presaturated light weight aggregates.” Mater. Today Proc., 7805–7809. Elsevier Ltd.

Sawant, P., S. Sawant, and S. S. Mutagekar. 2020. “Experimental Study on Different Tests of Self Curing Concrete by Using Polyethylene Glycol (PEG-400) As Self Curing Agent.” Int. J. Innov. Res. Sci. Eng. Technol.

Siddika, A., M. A. Al Mamun, W. Ferdous, and R. Alyousef. 2020. “Performances, challenges and opportunities in strengthening reinforced concrete structures by using FRPs – A state-of-the-art review.” Eng. Fail. Anal., 111: 104480. Elsevier Ltd. https://doi.org/10.1016/j.engfailanal.2020.104480.

Singh, D. D. N., and T. Venugopalan. 2013. “Understanding the Corrosion and Remedial Measures to Control the Deterioration of Reinforcement Steel Bars by Modification in Their Chemistry and Application of Surface Coatings.” Trans. Indian Inst. Met., 66 (5–6): 677–687. https://doi.org/10.1007/s12666-013-0335-x.

Sohail, M. G., R. Kahraman, N. A. Alnuaimi, B. Gencturk, W. Alnahhal, M. Dawood, and A.

Belarbi. 2020. “Electrochemical behavior of mild and corrosion resistant concrete reinforcing steels.” Constr. Build. Mater., 232: 117205. https://doi.org/10.1016/j.conbuildmat.2019.117205.

Song, G. 2000. “Equivalent circuit model for AC electrochemical impedance spectroscopy of concrete.” Cem. Concr. Res., 30 (11): 1723–1730. https://doi.org/10.1016/S0008-8846(00)00400-2.

Söylev, T. A., and M. G. Richardson. 2008. “Corrosion inhibitors for steel in concrete: State-of-the-art report.” Constr. Build. Mater., 22 (4): 609–622. https://doi.org/10.1016/j.conbuildmat.2006.10.013.

Srinivasan, R., and R. Punathil Meethal. 2022. “EIS Technique for Corrosion Study and Analysis.” 3–20. Springer Nature Singapore.

Sun, M., C. Du, Z. Liu, C. Liu, X. Li, and Y. Wu. 2021. “Fundamental understanding on the effect of Cr on corrosion resistance of weathering steel in simulated tropical marine atmosphere.” Corros. Sci., 186 (January): 109427. Elsevier Ltd. https://doi.org/10.1016/j.corsci.2021.109427.

Tchamdjou, W. H. J., S. Grigoletto, F. Michel, L. Courard, M. L. Abidi, and T. Cherradi. 2017. “An investigation on the use of coarse volcanic scoria as sand in Portland cement mortar.” Case Stud. Constr. Mater., 7 (July): 191–206. Elsevier Ltd. https://doi.org/10.1016/j.cscm.2017.07.005.

Torres-Acosta, A. A. 2007. “Opuntia-Ficus-Indica (Nopal) mucilage as a steel corrosion inhibitor in alkaline media.” J. Appl. Electrochem., 37 (7): 835–841. https://doi.org/10.1007/s10800-007-9319-z.

Torres-Acosta, A. A. 2019. “Water and chloride permeability of cement-based mortar with additions of dehydrated cacti.” J. Chem. Technol. Biotechnol., 94 (11): 3488–3494. John Wiley and Sons Ltd. https://doi.org/10.1002/jctb.5938.

Torres-Acosta, A. A., and L. Alejandra Díaz-Cruz. 2020. “Concrete durability enhancement from nopal (opuntia ficus-indica) additions.” Constr. Build. Mater., 243: 118170. Elsevier Ltd. https://doi.org/10.1016/j.conbuildmat.2020.118170.

Torres-Acosta, A. A., and P. Y. González-Calderón. 2021. “Opuntia Ficus-Indica (OFI) Mucilage as Corrosion Inhibitor of Steel in CO2-Contaminated Mortar.” Materials

(Basel)., 14 (5): 1316. MDPI AG. https://doi.org/10.3390/ma14051316.

Umoren, S. A., M. M. Solomon, I. B. Obot, and R. K. Suleiman. 2019. “A critical review on the recent studies on plant biomaterials as corrosion inhibitors for industrial metals.” J. Ind. Eng. Chem., 76: 91–115. The Korean Society of Industrial and Engineering Chemistry. https://doi.org/10.1016/j.jiec.2019.03.057.

Venkatesh, C., S. K. Mohiddin, and N. Ruben. 2019a. “Corrosion Inhibitors Behaviour on Reinforced Concrete—A Review.” Lect. Notes Civ. Eng., 127–134. Springer Singapore.

Venkatesh, C., S. K. Mohiddin, and N. Ruben. 2019b. Corrosion inhibitors behaviour on reinforced concrete—A Review. Lect. Notes Civ. Eng. Springer Singapore.

Venkatesh, G., C. Kamal, P. Vennila, S. Kaya, M. G. L. Annaamalai, and B. El Ibrahimi. 2022. “Sustainable corrosion inhibitor for steel embedded in concrete by Guar Gum: Electrochemical and theoretical analyses.” Appl. Surf. Sci. Adv., 12 (September): 100328. Elsevier B.V. https://doi.org/10.1016/j.apsadv.2022.100328.

Verma, A. S., Sumankant, N. M. Suri, and Yashpal. 2015. “Corrosion Behavior of Aluminum Base Particulate Metal Matrix Composites: A Review.” Mater. Today Proc., 2 (4–5): 2840–2851. Elsevier Ltd. https://doi.org/10.1016/j.matpr.2015.07.299.

Verma, C., E. E. Ebenso, and M. A. Quraishi. 2017. “Corrosion inhibitors for ferrous and non-ferrous metals and alloys in ionic sodium chloride solutions: A review.” J. Mol. Liq., 248: 927–942. Elsevier B.V. https://doi.org/10.1016/j.molliq.2017.10.094.

Waghmare, R., P. R, J. A. Moses, and C. Anandharamakrishnan. 2022. “Mucilages: sources, extraction methods, and characteristics for their use as encapsulation agents.” Crit. Rev. Food Sci. Nutr., 62 (15): 4186–4207. Taylor & Francis. https://doi.org/10.1080/10408398.2021.1873730.

Wang, R., S. Luo, M. Liu, and Y. Xue. 2014. “Electrochemical corrosion performance of Cr and Al alloy steels using a J55 carbon steel as base alloy.” Corros. Sci., 85: 270–279. Elsevier Ltd. https://doi.org/10.1016/j.corsci.2014.04.023.

Wei, J., X. X. Fu, J. H. Dong, and W. Ke. 2012. “Corrosion Evolution of Reinforcing Steel in Concrete under Dry/Wet Cyclic Conditions Contaminated with Chloride.” J. Mater. Sci. Technol., 28 (10): 905–912. Elsevier. https://doi.org/10.1016/S1005-0302(12)60149-2.

Wilby, C. B. 2013. Structural Concrete: Materials; Mix Design; Plain, Reinforced and

Prestressed Concrete; Design Tables. London: Elsevier.

Witkowski, H., and M. Koniorczyk. 2018. “New sampling method to improve the reliability of FTIR analysis for Self-Compacting Concrete.” Constr. Build. Mater., 172: 196–203. Elsevier Ltd. https://doi.org/10.1016/j.conbuildmat.2018.03.216.

Wong, K., and P. C. Cheung. 2001. “Influence of drying treatment on three Sargassum species: 1. Proximate composition, amino acid profile and some physico-chemical properties.” J. Appl. Phycol., 13 (1): 43–50. https://doi.org/10.1023/A:1008149215156.

Xhanari, K., and M. Finšgar. 2019. “Organic corrosion inhibitors for aluminum and its alloys in chloride and alkaline solutions: A review.” Arab. J. Chem., 12 (8): 4646–4663. https://doi.org/10.1016/j.arabjc.2016.08.009.

Yadav, M., D. Behera, and U. Sharma. 2016. “Nontoxic corrosion inhibitors for N80 steel in hydrochloric acid.” Arab. J. Chem., 9: S1487–S1495. King Saud University. https://doi.org/10.1016/j.arabjc.2012.03.011.

Ye, C.-Q., R.-G. Hu, S.-G. Dong, X.-J. Zhang, R.-Q. Hou, R.-G. Du, C.-J. Lin, and J.-S. Pan. 2013. “EIS analysis on chloride-induced corrosion behavior of reinforcement steel in simulated carbonated concrete pore solutions.” J. Electroanal. Chem., 688: 275–281. https://doi.org/10.1016/j.jelechem.2012.09.012.

Yeomans, S. R. 2016. “Galvanized steel reinforcement.” Corros. Steel Concr. Struct., 111–129. Elsevier.

Yifru, B. W., and B. B. Mitikie. 2020. “Partial replacement of sand with marble waste and scoria for normal strength concrete production.” SN Appl. Sci., 2 (12): 1938. Springer International Publishing. https://doi.org/10.1007/s42452-020-03716-9.

Yuan, Y., Y. Ji, and S. P. Shah. 2007a. “Comparison of two accelerated corrosion techniques for concrete structures.” ACI Struct. J., 104 (3): 344. American Concrete Institute.

Yuan, Y., Y. Ji, and S. P. Shah. 2007b. “Comparison of Two Accelerated Corrosion Techniques for Concrete Structures.” ACI Struct. J., 104 (3): 344–347. https://doi.org/10.14359/18624.

Zafeiropoulou, T., E. Rakanta, and G. Batis. 2011. “Performance evaluation of organic coatings against corrosion in reinforced cement mortars.” Prog. Org. Coatings, 72 (1–2): 175–180. Elsevier B.V. https://doi.org/10.1016/j.porgcoat.2011.04.005.

Zarazúa-Villalobos, L., N. Mary, J. Soo-Hyun, K. Ogawa, H. Kato, and Y. Ichikawa. 2021. "Microstructure and corrosion study of Fe-based bulk metallic glass obtained by spark plasma sintering." J. Alloys Compd., 880: 160399. Elsevier. https://doi.org/10.1016/j.jallcom.2021.160399.

Zengin, E., H. Ahlatci, and H. Zengin. 2021. "Investigation of microstructure, tribological and corrosion properties of AISI 316 L stainless steel matrix composites reinforced by carbon nanotubes." Mater. Today Commun., 29 (August): 102758. Elsevier Ltd. https://doi.org/10.1016/j.mtcomm.2021.102758.

Zhang, D., H. Qian, L. Wang, and X. Li. 2016. "Comparison of barrier properties for a superhydrophobic epoxy coating under different simulated corrosion environments." Corros. Sci., 103: 230–241. Elsevier Ltd. https://doi.org/10.1016/j.corsci.2015.11.023.

Zheng, H., W. Li, F. Ma, and Q. Kong. 2012. "The effect of a surface-applied corrosion inhibitor on the durability of concrete." Constr. Build. Mater., 37: 36–40. Elsevier Ltd. https://doi.org/10.1016/j.conbuildmat.2012.07.007.

Zhou, Y., B. Gencturk, K. Willam, and A. Attar. 2015. "Carbonation-induced and chloride-induced corrosion in reinforced concrete structures." J. Mater. Civ. Eng., 27 (9): 4014245. American Society of Civil Engineers.

APPENDIX A

A1: Mix design of conducted c-25 concrete according to ACI 211

Step 1: Calculating the required mean compressive strength based on the characteristic strength of 25 Mpa, which gives; fck = f'ck + 8.5 = 25 + 8.5 = 33.5 Mpa

Table A.1 Average Compressive Strength Conversion

Characteristics strength (f'ck, Mpa)	Mean strength (fck, Mpa)
<21	F'ck + 7
21-35 F'ck +8.5	
>35	1.1 x F'ck + 5

Step 2: Determining the minimum cement content

From a durability point of view, the minimum cement content was taken as 300 Kg/m^3.

Step 3: Choose a slump Value

It is recommended to use concrete with a slump of 2-10 cm for C-25

Step 4: Choose the maximum aggregate size.

For higher compressive strength, a reduced maximum size aggregate was selected; in this case, the maximum size aggregate was 20mm, and the nominal size aggregate was 19 mm.

Step 5: Mixing water and air content determination

The Amount of Water per unit volume of Concrete required for the required slump value depends on aggregate grading, amount of entrained air, and maximum size aggregate.

Table A.2 Mixing water for different slumps and Maximum size aggregate

Slump (cm)	Water (**Kg/m^3**) of concrete for indicated maximum size aggregate in mm							
	10	12.5	20	25	40	50	70	150
	Non-air entrained Concrete							

2-10	205	200	185	180	160	155	145	125
8-10	225	215	200	195	175	170	160	140
15-18	240	230	210	205	205	185	180	170
Amount of entrapped Air (%)	3	25	2	15	1	0.5	0.3	0.2

In Table 3.2 above, with a slump of 2-10 cm and a maximum size aggregate of 20 mm, the water content becomes 185 Kg/$\boldsymbol{m^3}$ And 2%, or 20 liters, and entrapped air.

Step 6: Determine the water-cement ratio

In a concrete mix, the water-cement ratio is the Weight of Water to the Weight of cement.

Table A.3 Average Compressive Strength with Water Cement Ratio

Compressive strength at 28 days (Mpa)	Water cement ratio (by mass)
45	0.38
40	0.42
35	0.47
30	0.54
25	0.61
20	0.69
15	0.79

In the case of concrete with a mean strength of 33.5 MPa, the ACI table above cannot provide a precise water-cement ratio. It can be calculated by interpolating the above and below values: 33.5 MPa.

35	0.47	by interpolation, $\frac{33.5-35}{30-35} = \frac{x-0.47}{0.54-0.47}$
33.5	x	by solving the above equation, x=0.491
30	0.54	Hence, the minimum water-cement ratio is 0.491

Step 7: Determination of mix cement content

$$\text{cement content} = \frac{\text{water content}}{\text{water cement ratio}}$$

$$= \frac{185}{0.491}$$

$$= 376.78 \text{ Kg}/\boldsymbol{m^3}$$

Since the mix cement content is higher than the minimum cement use.

Step 8: Estimating the Bulk volume per unit volume of Concrete

Concrete's bulk volume per unit volume depends on the fineness modulus, which is 2.98, and the maximum size aggregate of 20 mm.

Table A.4 Volume of coarse aggregate per unit volume of Concrete

Maximum size of aggregate	The volume of coarse aggregate per volume of Concrete for different fitness modules			
	2.4	2.6	2.8	3.0
10	0.50		0.46	0.44
12.5	0.59		0.55	0.53
20	0.66		0.62	0.60
25	0.71		0.67	0.65
40	0.76		0.72	0.70
50	0.78		0.74	0.72
70	0.81		0.77	0.75
150	0.87		0.83	0.81

In the above table, it was not possible to determine the bulk volume of dry-rodded aggregate directly. In the case of a 20 mm aggregate with a fitness modulus of 2.98, it is possible to calculate the fitness modulus by interpolation since it lies between 2.8 and 3.

2.8 0.62 by interpolation, $\frac{2.8-2.98}{0.62-x} = \frac{2.98-3}{x-0.6}$

2.98 x by solving the above equation, x=0.602

3.0 0.6 Hence, the dry volume of aggregate per volume of concrete is 0.602

Step 9: Calculate the Weight of coarse aggregate (WCA) per $\boldsymbol{m^3}$ Of Concrete.

WCA= bulk volume x bulk density of coarse aggregate

WCA= 0.602*1681

= 1011.962

Step 10: Determine the solid volume of coarse aggregate

The solid volume of coarse aggregate = WCA/Specific gravity

= 1011.962/2.854

= 354.576 Kg/m^3

Step 11: Calculating the solid volume of cement, Water, and air

The volume of cement (VC) = Weight of cement / Specific gravity of cement

= 376.78/3.15

= 119.612 Kg/m^3

Volume of Water (VW) = 185 Kg/m^3

Volume of Air (VA) = 20 Kg/m^3

Step 12: Calculating the Volume of Sand

Solid volume of Sand = 1000 - (VCA + VC + VW + VA)

= 1000 – (354.576 +119.612 + 185 + 20)

= 1000 – 679.188

=320.812 Kg/m^3

Solid Weight of Sand = dry volume * specific gravity

= 320.812 * 2.76

= 885.4412 Kg/m^3

Step 13: Adjustment for moisture taken together

The actual moisture content of fine aggregate (Am) = 0.02

Fine aggregate water absorption (WA) = 2.08

Correction factor = $\frac{100+Am}{100+WA} = \frac{100+0.02}{100+2.08}$ = 0.97942

The actual moisture content of coarse aggregate (Am) = 0

Coarse aggregate water absorption (WA) = 1.6

Correction factor = $\frac{100+Am}{100+WA} = \frac{100+0.00}{100+1.6}$ = 0.98425

Table A.5 Moisture adjustment in the aggregate's calculation

Mixture design	Batch Weight SSD (kg/ m^3)	Moisture correction Factor	Moisture corrected Batch Weight (kg/ m^3)	Change in Weight (kg/ m^3)
Cement	376.78		376.78	
Fine aggregate	885.4412	0.97942	867.2188	-18.22245
Coarse aggregate	1011.962	0.98425	996.0235	-15.93840
Water	185		219.1608	34.1608515
Total	2459.183		2459.183	

The Amount of Water needed to be added = 18.22245+ 15.78660

= 34.1608515 kg/ m^3

Fine aggregate = 867.2188 Kg/m^3

Coarse aggregate= 996.0235 kg/ m^3

Amount of water added = 219.1608 kg/ m^3

Table A.6 Calculated Batch for 1 m^3 of concrete

Water	219.1608 Kg/$\boldsymbol{m^3}$
Cement	376.78 Kg/$\boldsymbol{m^3}$
Fine aggregate	867.2188 Kg/$\boldsymbol{m^3}$
Coarse aggregate	996.0235Kg/$\boldsymbol{m^3}$

The above result in the mix design ratio can be expressed in Table 3.7 below.

Table A.7 Mix Ratio for C-25 Concrete Grade

Ingredients	Cement	Fine aggregate	coarse aggregate
Amount/$\boldsymbol{m^3}$	376.78/376.78	867.2188/376.78	996.0235/376.78
Ratio	1	2.30165	2.64351

Based on the mix proportion presented above, the quantity of each concrete ingredient can be calculated for a standard mold of one cube.

Wet volume for one mold = length x width x height

= 0.15 x 0.15 x 0.15

= 0.003375 m^3

Dry volume = wet volume x 1.55

= 0.003375 m^3 x 1.55

= 0.00523125 m^3

Sum of ratio = 1 +2.30165 + 2.643514 = 5.9451m^3

Weight of the cement = $\frac{1}{sum\ of\ ratio}$ x dry volume x unit weight of the cement

= $\frac{1}{5.9451}$ x 0.00523125 x 1440

= 1.2670 kg

Weight of Fine aggregate = $\frac{2.301}{sum\ of\ ratio}$ x dry volume x unit weight of FA

= $\frac{2.301}{5.9451}$ x 0.00523125 x 1515.5

= 3.0684 kg

Weight of Coarse aggregate = $\frac{2.6435}{sum\ of\ ratio}$ x dry volume x unit weight of GA

= $\frac{2.6435}{5.9451}$ x 0.00523125 x 1681

= 3.9101 kg

Weight of water = amount of water needed x dry volume

= 219.1608 x 0.0058125

= 1.274 kg (L)

A2: Slump value of sample for concrete with and without FASG

Table A.8 Slump value of sample for concrete with and without FASG

No	Addition of FASG in percentage	Trial	Slump value in (mm)	Average slump value (mm)
	0%	1	45.4	
1	0%	2	46.5	45.63
	0%	3	45	
	5%	1	47.6	
2	5%	2	47.5	47.2
	5%	3	46.5	
	10%	1	48.8	
3	10%	2	49.2	48.8
	10%	3	48.6	
	15%	1	49	
4	15%	2	50	49.5
	15%	3	49.5	

A3: Tukey HSD sample for slump value interaction with and without FASG

Table A.9 Tukey HSD sample for slump value interaction with and without FASG

	MeanDiff	SEM	q Value	Prob	Alpha	Sig	LCL	UCL
5%OFI 0%OFI	1.56667	0.46845	4.72965	0.04096	0.05	1	0.06653	3.0668
10%OFI 0%OFI	3.23333	0.46845	9.7612	5.6634E-4	0.05	1	1.7332	4.73347
10%OFI 5%OFI	1.66667	0.46845	5.03155	0.03043	0.05	1	0.16653	3.1668
15%OFI 0%OFI	3.86667	0.46845	11.67319	1.60871E-4	0.05	1	2.36653	5.3668
15%OFI 5%OFI	2.3	0.46845	6.94353	0.00516	0.05	1	0.79986	3.80014
15%OFI 10%OFI	0.63333	0.46845	1.91199	0.55903	0.05	0	-0.8668	2.13347

A4: 28 days compressive strength for different % replacement and Soaking days

Table A.10 28 days compressive strength for different % replacement and Soaking days

Soaking day	Addtion of FASG	N total	Compressive strength	Standard Deviation	Variance	Sum	Minimum	Maximum
Day 0	0%FASG	3	16.64	1.90	3.61	49.91	14.44	17.78
Day 0	5%FASG	3	21.69	0.44	0.20	65.07	21.24	22.13
Day 0	10%FASG	3	22.97	0.45	0.20	68.90	22.50	23.40
Day 0	15%FASG	3	24.13	0.32	0.10	72.40	23.90	24.50
Day 3	0%FASG	3	17.85	0.14	0.02	53.56	17.73	18.00
Day 3	5%FASG	3	23.05	1.40	1.96	69.16	22.22	24.67
Day 3	10%FASG	3	23.91	0.51	0.26	71.73	23.51	24.49
Day 3	15%FASG	3	25.87	0.15	0.02	77.60	25.70	26.00
Day 7	0%FASG	3	22.70	1.35	1.83	68.09	21.64	24.22
Day 7	5%FASG	3	24.96	0.80	0.64	74.89	24.04	25.51
Day 7	10%FASG	3	24.34	0.31	0.09	73.02	24.11	24.69
Day 7	15%FASG	3	22.47	1.13	1.27	67.42	21.56	23.73
Day 14	0%FASG	3	30.65	0.48	0.23	91.96	30.13	31.07
Day 14	5%FASG	3	30.58	0.16	0.03	91.73	30.40	30.71
Day 14	10%FASG	3	22.93	0.55	0.30	68.80	22.31	23.33
Day 14	15%FASG	3	20.37	0.99	0.98	61.11	19.78	21.51
Day 21	0%FASG	3	31.76	0.53	0.28	95.29	31.16	32.09
Day 21	5%FASG	3	27.79	0.65	0.42	83.38	27.20	28.49
Day 21	10%FASG	3	21.88	0.56	0.31	65.64	21.24	22.27
Day 21	15%FASG	3	19.88	0.45	0.21	59.64	19.56	20.40
Day 28	0%FASG	3	32.92	0.24	0.06	98.76	32.67	33.16
Day 28	5%FASG	3	25.73	0.58	0.34	77.20	25.07	26.13
Day 28	10%FASG	3	21.01	0.83	0.68	63.02	20.09	21.69
Day 28	15%FASG	3	19.87	0.89	0.79	59.60	18.89	20.62

Table A.11 Total void percentage calculation

Percentage addtion of OFI and FASG	sample Name	Mass of Oven-dried sample (A)	Mass of Surface dry samle in the air after	Mass of surface-dry sample in the air after	Apparent mass of sample in water after immersion	Absoption after immersion % = ((B-	Absorption after immersion and boiling %=((C_A)/A)*100	Bulk density , dry =(A/(C-D))*p	Bulk density , after immersion =(B/(C-D))*p	Bulk density , after immersion and boiling	volume of permable void, % =((C-A)/(C-D))*100
5% FASG + 30% OFI	A-1	1598	1730	1712	1000	8.26	7.13	2.24	2.43	2.40	16.01
	A-2	1826	1949	1934	1050	6.74	5.91	2.07	2.20	2.19	12.22
	A-3	1782	1907	1888	1000	7.01	5.95	2.01	2.15	2.13	11.94
	A-4	1406	1505	1496	800	7.04	6.40	2.02	2.16	2.15	12.93
	A-5	1856	1983	1967	1050	6.84	5.98	2.02	2.16	2.15	12.10
5% FASG + 0% OFI	O-1	1648	1785	1758	1000	8.31	6.67	2.17	2.35	2.32	14.51
	O-2	1632	1767	1736	1000	8.27	6.37	2.22	2.40	2.36	14.13
	O-3	1679	1821	1786	950	8.46	6.37	2.01	2.18	2.14	12.80
	O-4	1105	1227	1185	700	11.04	7.24	2.28	2.53	2.44	16.49
	O-5	1110	1200	1189	700	8.11	7.12	2.27	2.45	2.43	16.16

APPENDIX B

PROCEDURES

Tests on Fine Aggregate

Fine Aggregate gradation test for sand and scoria

The test procedure was in accordance with (ASTM C136). The range of fineness modulus is between 2.3-3.1 (ASTM C33).

Procedure for Grading Fine Aggregate

1. The researcher weighted a sample of 2 kg of fine aggregates.
2. The sample was quartered.
3. From the quartered sample, weighing 500 g,
4. The empty sieves were weighted, and the data was recorded properly.
5. The pan was placed on the bottom and the other sieves were put on the pan with increasing opening sizes of the sieves.
6. Placed the 500 g of sample on the top of the sieves (having a larger opening size).
7. Smashed the sample for about 10 minutes in a sieve shaker.
8. Each sieve, together with the aggregate retained on it, was measured and the weight retained on each sieve was calculated.
9. The gradation chart was filled in and the fineness modulus was computed.

$$Fineness\ modulus = \sum_{n=1}^{7} \left({}^{commulative\ retained\ by\ mass}/_{100} \right)$$

Gradation test for Fine aggregates sand(A) and scoria(B)

Unit Weight of Fine Aggregate test for (sand and scoria)

To comply with ASTM C29, this study followed the following the same procedures.

1. Fill the measure one-third full and level the surface with your fingers. Rod the layer of aggregate with 25 strokes with the tamping rod evenly distributed over the surface. Then fill the measure to two-thirds capacity, level and rod as before. Finally, fill the measuring cup to overflowing and rod as above.

2. Level the surface of the aggregate with your fingers in such a way that any slight projections of the large pieces of the coarse aggregate approximately balance the larger voids in the surface below the top of the measure.
3. When roding the first layer, do not allow the rod to strike the bottom of the measure forcibly. In roding, the second and third layers use only enough force to cause the taping rodto penetrate the previous layers of aggregate.
4. The fine aggregate was weighed and the data were recorded as follow:
   X: Fine aggregate plus cylinder weight = 6,674 g.

   Y: Weight of empty cylinder = 4,734 g

   V: Cylinder volume = 0.001375 m3

$$UWFA = \frac{X - Y}{V}$$

A) unit weight of coarse aggregate, B) specific gravity of coarse aggregate

Specific Gravity and Water Absorption of Fine Aggregate

In this experiment, the specific gravity and water absorption capacity of a fine aggregate were determined using the ASTM C128 standard.

Preparation of The Test Specimen:

1. Approximately 1 kg of the fine aggregate was prepared.
2. At 110°C, the sample was dried to a constant weight in a suitable pan. Allow it to cool for 24 hours and then make it saturated.
3. The excess water was decanted with care to avoid loss of fines, spreading the sample on a flat, non-absorbent surface exposed to a gently moving current of warm air.
4. The sample was stirred frequently to get homogeneous drying until achieving the saturated surface dry condition by using the cone test for surface moisture.
5. Hold the mold firmly on a smooth, non-absorbent surface with a large diameter. Placed a portion of partially dried fine aggregate loosely in the mold by filling it to the brim and heaping additional materials above the top of the mold.
6. Lightly tamp the sand into the mold with 25 light drops of the tamper about 5 mm above the top surface of the sand.

7. The surface was adjusted by removing loose sand from the base and lifting the mold vertically. If surface moisture was still present, the sand would retain the molded shape. When the sand slumped slightly, it indicated that it had reached S.S.D. condition.

Procedure:

1. The S.S.D sample was weighted at 500 g.
2. Partially fill the Pycnometer with water and put 500 g of saturated surface dry aggregates into the Pycnometer.
3. Then they filled the pycnometer with additional water to fill it to 90% of its capacity.
4. The pycnometer was rolled and inverted to eliminate all air bubbles.
5. Place the Pycnometer in a water bath at 23 °C for an hour.
6. Brought the water level in the pycnometer to its calibrated capacity.
7. Then, the total weight of the pycnometer, specimen, and water was measured.
8. The researcher removed the fine aggregate from the pycnometer, dried it to a constant weight at 105 °C, cooled it in room temperature air for one hour, and measured it.
9. The weight of the pycnometer filled to capacity with water was determined at 23°C, and the following data were recorded:
   X: Weight of oven-dry specimen in air = 482 g

   Y: Weight of water-filled pycnometer = 1460 g

   Z: Weight of the saturated surface-dry specimen = 500 g

   W: Pycnometer weight with specimen and water to calibration mark = 1,767 g

$$Bsg = \frac{Z}{Y + Z - W}$$

$$Asg \frac{X}{Y + X - W}$$

$$Water\ absorption = \frac{Z - X}{X} x\ 100\%$$

Scoria sample(A) and sand sample(B) on determination of specific gravity

Silt content for fine aggregate (sand and scoria)

The following are detailed procedures that were followed based on ASTM C 117.

Test Procedure for Silt Content

1. The researcher took a graduated cylinder having a capacity of 1000 ml.

2. 300 ml of sand was poured into the cylinder.
3. Approximately 3/4 of the jar was filled with water.
4. The jar was shaken vigorously for about a minute.
5. The jar was left for an hour to allow the silt to settle on the layer of sand.
6. The amount of fine forming a separate layer on the top was measured.
7. The silt content was calculated based on following Equation.

$$\text{Silt content} = \frac{Silt\ deposited\ above\ the\ sand\ (A)}{Amount\ of\ clean\ sand\ (B)} x\ 100$$

A)Scoria sample

B) sand sample

Tests on Coarse Aggregate

Coarse Aggregate gradation test

The test procedure followed was in accordance with (ASTM C136).

Sieve Analysis for Coarse Aggregate

1. 20 kg of coarse aggregates were weighed.
2. A representative sample was selected by quartering.
3. From the quartered sample, 2 kg was taken.
4. The empty sieves were weighted and the data was recorded properly.
5. 5. Placed the 2 kg of sample on the top sieves (which have a large opening size).
6. 6. smashed the sample for about 10 minutes in a sieve shaker.
7. 7. Each sieve, together with the aggregate retained on it, was measured and the weight retained on each sieve was calculated.
8. The gradation chart was filled in and the fineness modulus was computed. The range of fineness modulus of coarse aggregate according to ASTM C33 is 5.5-8.

$$Fineness\ modulus = \sum_{n=1}^{7} \left({}^{commulative\ retained\ by\ mass}/_{100} \right)$$

Gradation of coarse aggregate

Unit Weight of Coarse Aggregate

The unit weight of aggregate ranges from 1200 to 1750 kg/m3 (ASTM C29). the following procedure was used to determine the unit weight of coarse aggregate based on ASTM C29.

1. Fill the measure one-third full and level the surface with your fingers. Rod the layer of aggregate with 25 strokes with the tamping rod evenly distributed over the surface. Then fill the measure to two-thirds capacity, level and rod as before. Finally, fill the measuring cup to overflowing and rod as above.
2. Level the surface of the aggregate with your fingers in such a way that any slight projections of the large pieces of the coarse aggregate approximately balance the larger voids in the surface below the top of the measure.
3. When roding the first layer, do not allow the rod to strike the bottom of the measure forcibly. In roding, the second and third layers use only enough force to cause the taping rod to penetrate the previous layers of aggregate.
4. The coarse aggregate was weighted, and the data was recorded as follows.
   X = aggregate plus cylinder weight = 6.977 kg

   Y = Weight of the empty cylinder = 4.734 kg.

   V = Volume of the cylinder (m^3) = 0.001375 m^3

   The unit weight of coarse aggregate can be computed by using below Equation:

$$UWCA = \frac{X - Y}{V}$$

Specific Gravity and Water Absorption Capacity of Coarse Aggregate

ASTM C127 was used for this experiment. bulk specific gravity, saturated-surface-dry bulk specific gravity (SSD), or apparent specific gravity, shown in the following procedures:

Test Procedures

1. The researcher took the sample of coarse aggregate by using the sample splitter.
2. The sample was sieved with a 4.75 mm sieve, and the sample passing through the 4.75 mm sieve was ignored.
3. The sample was washed to remove dust.
4. Put the sample in the oven at 105°C for 24 hours.
5. The sample was taken out of the oven, left to cool, and then the weight was measured.
6. The sample was submerged in water for 24 hours.
7. The researcher removed the sample from the water and rolled it in a large absorbent cloth until all visible films of water were removed.
8. The required weight of the sample in its (S.S.D) condition was taken.
9. The researcher immediately placed the S.S.D sample in the sample container, determined the weight in water at 23 °C, and recorded the data.
   H: Weight of air-dried oven-dried specimen = 2,950 g

G: Weight of the saturated surface-dry specimen = 3000 g

F: Pycnometer weight with specimen and water to calibration mark = 1,848 g

The Bsg,Asg,and water absorption of coarse aggregate can be computed based on the following Equation:

$$Bsg = \frac{G}{G - F}$$

$$Asg = \frac{H}{H - F}$$

$$Water\ absorption = \frac{G - H}{H} x\ 100\%$$

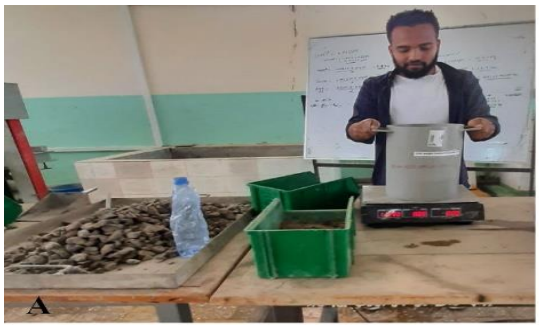

A) unit weight of coarse aggregate, B) specific gravity of coarse aggregate

Water Test

The pH of water can impact concrete, and to determine the pH of the mixing and curing water, a pH meter was employed. The process involved preparing a water sample, immersing the electrode in a buffer, submerging the electrode into the prepared sample, and recording the resulting pH reading.

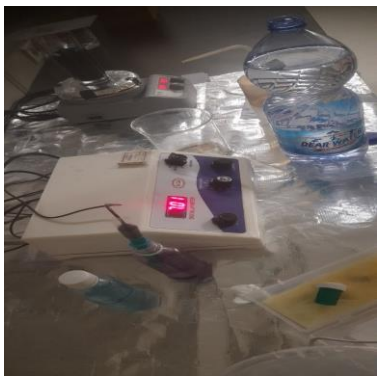

Water PH test

Slump test

A slump test was conducted to determine the degree of workability and mix quality of the concrete based on the (ASTM C143) standard.

Procedure:

1. First, the slump cone was placed on a smooth metal plate.
2. The slump cone was filled with freshly mixed concrete in three different layers.
3. Each layer of the concrete mix was tapped 25 times with a 600 mm long metal rod that was 16 mm in diameter.
4. Extra concrete was removed after filling the last layer from the top of the cone.
5. The slump cone was then quickly lifted upward with two hands. The concrete is then free to fall.
6. After free fall, the remaining height is known as a slump (the difference between the height of the mold and the height of the vertical axis) and was measured.

Slump Test

Compressive Strength Test

A compressive test is conducted to determine the compressive strength of concrete based on the (ASTM C39) standard.

Procedure:

1. The cast cubes were taken out of the curing water after 7, 14, and 28 curing periods
2. wipe out excess water from the surface.
3. Clean the test machine and place the sample in the test machine.
4. Apply the load at a rate of 14 N/mm^2/minute, having a load capacity of 3000 KN.
5. When the specimens fail, record the maximum load.

The compressive strength is calculated:

$$Compressive\ strength = \frac{Load}{cross - sectional\ area\ of\ the\ sample}$$

Automatic Compressive Test Machine (a), Compressive Strength Test (b)

RESEARCH OUT PUT

This thesis work has been prepared in manuscript form with the following titles, and we anticipate its acceptance for future publication.this thesis work is presented in manuscript form with the following titles:

1. "Microstructural Analysis of Optunia Ficus Indica as a Corrosion Inhibitor with Incorporation of Internal Curing Effect"
2. "Electro Impedance Spectroscopy and Tafel Analysis of Internally Cured Concrete with the Addition of Optunia Ficus Indica as a Corrosion Inhibitor."